Supporting Information for:

Towards Sustainable Biogas Upgrading: MIL-120(Al) as a Cost-Effective Water Stable MOF for CO_2/CH_4 Separation

Marta Bordonhos,[a,b] Rosana V. Pinto,[c] Tânia Frade,[a] Bingbing Chen,[c] Farid Nouar,[c] Georges Mouchaham,[c] José R. B. Gomes,[b] Christian Serre,[c] Moisés L. Pinto,[a,*]

[a] *CERENA, Departamento de Engenharia Química, Instituto Superior Técnico, Universidade de Lisboa, Av. Rovisco Pais, N.° 1, 1049-001 Lisboa, Portugal*

[b] *CICECO – Aveiro Institute of Materials, Department of Chemistry, University of Aveiro, Campus Universitário de Santiago, 3810-193 Aveiro, Portugal*

[c] *Institut des Matériaux Poreux de Paris (IMAP), ESPCI Paris, École Normale Supérieure de Paris, CNRS, PSL University, 75005 Paris, France*

** Corresponding author: moises.pinto@tecnico.ulisboa.pt*

Table of Contents

Section S1. Synthesis, shaping and characterisation of MIL-120(Al)

S1.A. Synthesis and shaping of MIL-120(Al)

Figure S1. MIL-120(Al) large-scale reaction using a 30-litre reactor.

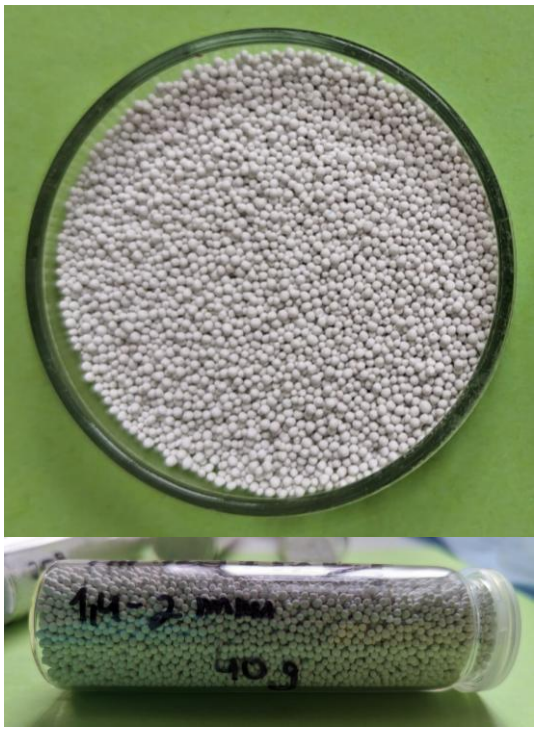

Figure S2. Photographs of the MIL-120(Al) beads (d_p [1.4–2[mm) used in this work.

S1.B. Characterisation of MIL-120(Al) powder and beads

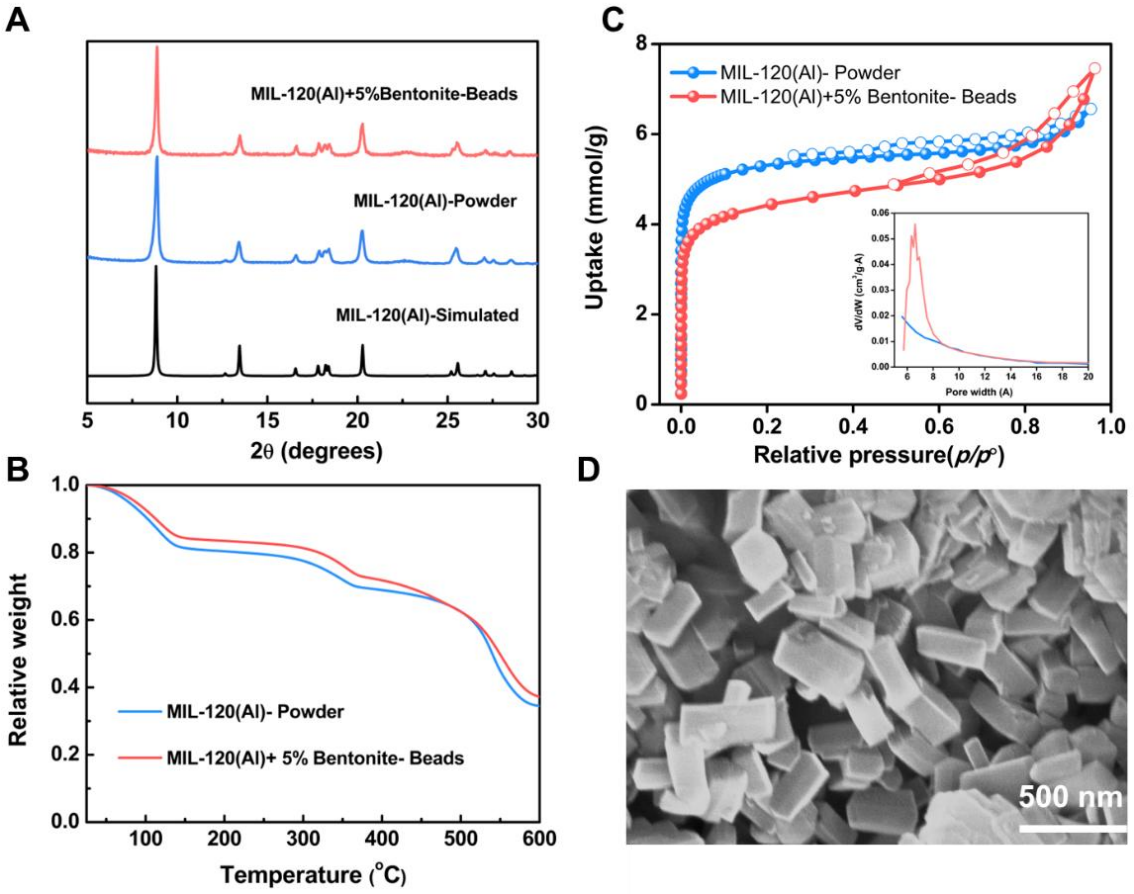

Figure S3. Characterisation of the MIL-120(Al) powder and shaped beads. **A**) PXRD patterns (Cu K_α radiation, λ = 1.5418 Å) showing the obtained pure phase of the MIL-120(Al) powder and after shaping. **B**) TGA results showing similar composition between the powder and shaped MIL-120(Al). **C**) N_2 adsorption isotherms (77 K) of the MIL-120(Al) powder and beads; the slight difference might be caused by the partial pore blocking due to the presence of bentonite. The inset shows the pore size distribution determined from the Horvath-Kawazoe method as implemented in MicroActive[S1] (additional details in footnote [d] in Table S1). **D**) SEM image of the MIL-120(Al) powder showing a particle size around 300 nm. All data is in accordance with a previously reported work.[S2]

Table S1. Textural properties of MIL-120(Al) in powder and shaped forms determined from N_2 adsorption at 77 K.

MIL-120(Al)	S_{BET} ($m^2 \cdot g^{-1}$)	V_{micro} [a] ($cm^3 \cdot g^{-1}$)	V_{pore} ($cm^3 \cdot g^{-1}$)	$\overline{W}_{micro}$ [d] (Å)
Powder	456 ± 2	0.169	0.212 [b]	5.61
Beads	365 ± 2	0.126	0.168 [c]	6.89

[a] Determined from the *t*-plot method for 0.4 ≤ *t* ≤ 0.8 nm.

[b] Determined from single-point analysis at $p/p° \approx 0.85$.

[c] Determined from single-point analysis at $p/p° \approx 0.50$.

[d] Determined from the Horvath-Kawazoe model as implemented in MicroActive[S1] Version 7.00, with:

- Pore geometry: *Cylinder (Saito-Foley)*
- Adsorbent: *Other*
- Adsorptive: *N2*

Section S2. Extended experimental and simulation results

S2.A. Experimental single-component adsorption studies

The experimental single-component adsorption isotherms have been fit using the Virial isotherm model[S3–S6] in (S1):

$$p = \frac{n_a^*}{K} \cdot \exp\left(\sum_{i=1}^{\infty} C_i \cdot n_a^{*\,i}\right) \tag{S1}$$

in which p is the pressure, n_a^* is the absolute adsorbed amount, K is the Henry constant and C_i is the i-th coefficient of the Virial series expansion.[S7] The excess adsorbed amounts (n_e^*) measured by the volumetric method have been converted into absolute adsorbed amounts by taking into account the pore volume of the material (V_{pore}, *cf.* Table S1) and the molar density of the gas phase (ρ_g),[S8] according to:

$$n_a^* = n_e^* + \rho_g \cdot V_{pore} = n_e^* + \frac{p \cdot V_{pore}}{z \cdot R \cdot T} \tag{S2}$$

where p is the pressure, z is the compressibility factor, R is the universal gas constant and T is the temperature. The non-ideality of the gas phase has been considered with the second and third virial coefficients for CO_2[S9] and for CH_4[S10] as reported by Dymond *et al.*[S11]. Using data from the single-component adsorption isotherms, the mean selectivity and phase diagrams of the separation of binary CO_2/CH_4 mixtures have been estimated based on the Ideal Adsorbed Solution Theory (IAST)[S12], following a method proposed by Myers[S7] and described in detail in previous works[S13,S14]. The effect of the presence of a small amount of pre-adsorbed water (H_2O) vapour (*ca.* 0.16 mmol·g^{-1}) on the adsorption of CO_2 and CH_4 at 25 °C in MIL-120(Al) (powder form) has been studied as described in a previous work[S15]. The non-ideality of H_2O vapour has been considered with the second and third virial coefficients as reported by Hyland and Mason[S16] from the correlations reported by Keyes[S17]. The isosteric enthalpies of adsorption for CO_2 and CH_4 for the powder form of MIL-120(Al) have been determined using the Clausius-Clapeyron equation.[S18] The experimental adsorption isotherm data is reported in Table S2 and the corresponding fitting parameters are reported in Table S3. All isotherms are reported in absolute adsorbed amounts, n_a^*.

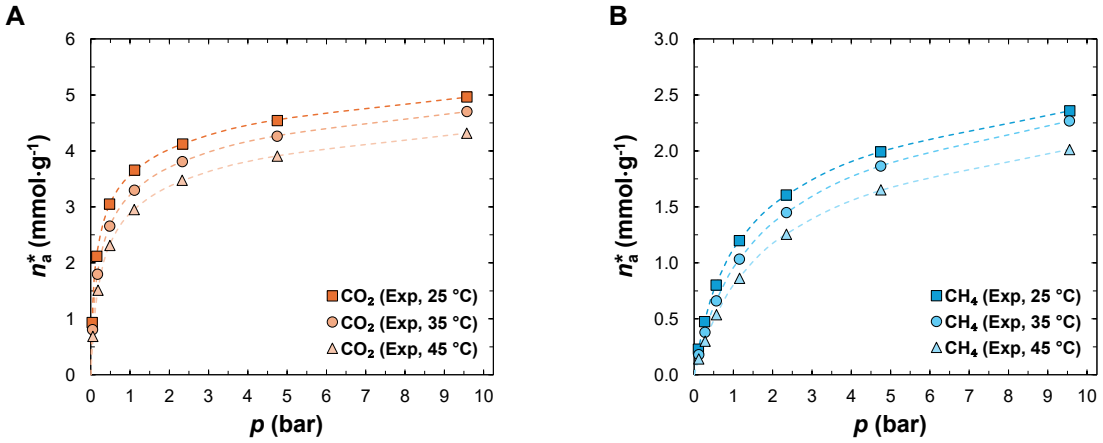

Figure S4. Experimental **A**) CO_2 and **B**) CH_4 single-component isotherms measured at 25 (squares), 35 (diamonds) and 45 (triangles) °C on the powder form of MIL-120(Al) and corresponding non-linear least squares fit of the Virial isotherm model (dashed lines) (*cf.* Table S2 and Table S3).

Table S2. Experimental data for the single-component adsorption isotherms of CO_2 and CH_4 measured for MIL-120(Al). All isotherms are reported in absolute adsorbed amounts, n_a^*.

Powder, dry, T = 25 °C				Powder, with 0.16 mmol·g^{-1} of pre-adsorbed H_2O vapour, T = 25 °C			
CO_2		CH_4		CO_2		CH_4	
p (bar)	n_a^* (mmol·g^{-1})	p (bar)	n_a^* (mmol·g^{-1})	p (bar)	n_a^* (mmol·g^{-1})	p (bar)	n_a^* (mmol·g^{-1})
0.0352	0.9342	0.1109	0.2283	0.0373	0.9383	0.1125	0.2211
0.1536	2.1168	0.2677	0.4750	0.1563	2.1161	0.2677	0.4665
0.4773	3.0520	0.5600	0.8015	0.4800	3.0356	0.5616	0.7962
1.1146	3.6554	1.1508	1.1988	2.1662	4.0389	2.2100	1.5360
2.3390	4.1233	2.3475	1.6060	9.0830	4.8965	9.0569	2.2938
4.7500	4.5433	4.7489	1.9924	–	–	–	–
9.5736	4.9624	9.5603	2.3584	–	–	–	–

Powder, dry, T = 35 °C				Powder, dry, T = 45 °C			
CO_2		CH_4		CO_2		CH_4	
p (bar)	n_a^* (mmol·g^{-1})	p (bar)	n_a^* (mmol·g^{-1})	p (bar)	n_a^* (mmol·g^{-1})	p (bar)	n_a^* (mmol·g^{-1})
0.0464	0.8058	0.1163	0.1795	0.0560	0.6874	0.1200	0.1418
0.1728	1.7964	0.2746	0.3795	0.1877	1.5114	0.2794	0.3000
0.4826	2.6580	0.5674	0.6603	0.4885	2.3102	0.5706	0.5366
1.1098	3.2975	1.1540	1.0330	1.1071	2.9517	1.1578	0.8617
2.3321	3.8088	2.3497	1.4497	2.3257	3.4743	2.3502	1.2558
4.7468	4.2614	4.7484	1.8649	4.7473	3.9083	4.7527	1.6523
9.5736	4.7021	9.5533	2.2677	9.5704	4.3163	9.5576	2.0118

Shaped beads, d_p [1.4–2[mm, dry, T = 25 °C			
CO_2		CH_4	
p (bar)	n_a^* (mmol·g^{-1})	p (bar)	n_a^* (mmol·g^{-1})
0.0341	0.8685	0.1147	0.1960
0.1477	1.9854	0.2688	0.4155
0.4709	2.8582	0.5568	0.7342
1.1130	3.4179	1.1439	1.1483
2.3374	3.8446	2.3411	1.5738
4.7489	4.2392	4.7420	1.9726
9.5731	4.6333	9.5560	2.3022

Table S3. Parameters of the Virial isotherm model and adjusted correlation coefficients (R^2_{adj}) obtained from the non-linear least-squares fit of the isotherm model to the experimental data for the single-component adsorption of CO_2 and CH_4 on MIL-120(Al).

MIL-120(Al) (dry)	Powder						Shaped	
T (°C)	25		35		45		25	
Gas	CO_2	CH_4	CO_2	CH_4	CO_2	CH_4	CO_2	CH_4
K (mmol·g^{-1}·bar^{-1})	36.270	2.174	21.762	1.636	11.834	1.168	39.995	1.573
C_1 (g·mmol^{-1})	0.127	0.294	0.144	0.362	–0.045	0.234	0.217	–0.072
C_2 (g^2·mmol^{-2})	0.147	0.267	0.141	0.216	0.186	0.306	0.159	0.384
R^2_{adj} (–)	0.99966	0.99998	0.99987	0.99999	0.99983	0.99984	0.99951	0.99951

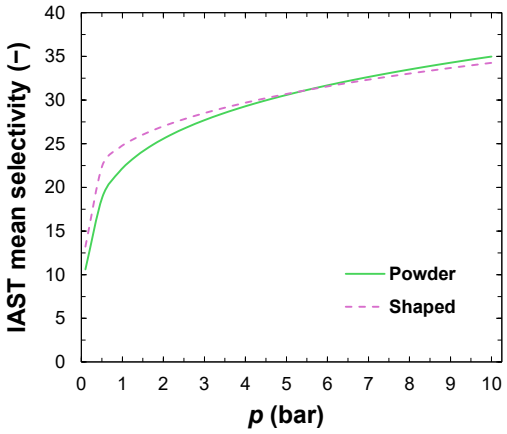

Figure S5. IAST-predicted mean selectivity at 25 °C for the separation of CO_2/CH_4 on the powder and the shaped forms of MIL-120(Al) (beads, d_p [1.4–2[mm).

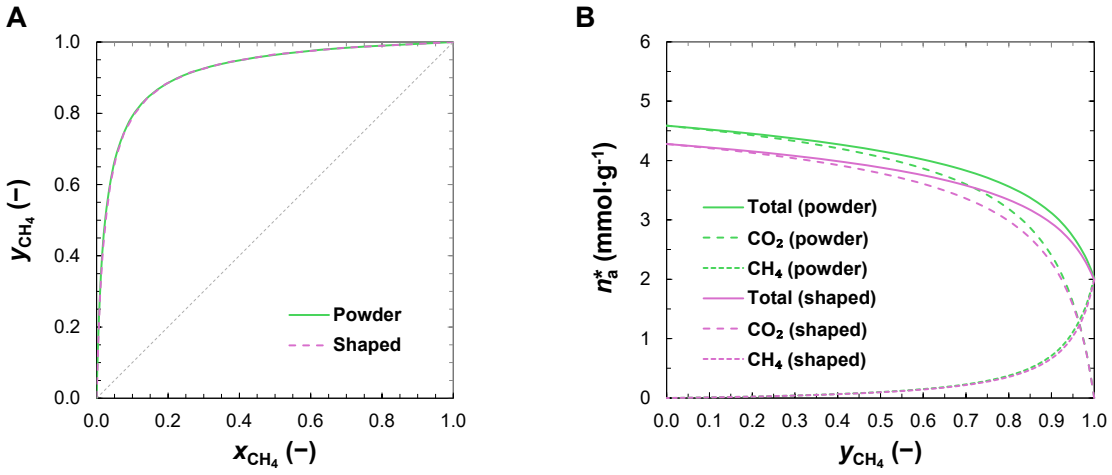

Figure S6. IAST-predicted isothermal (25 °C), isobaric (5 bar) phase diagrams of the adsorption of CO_2/CH_4 mixtures on the powder and shaped forms of MIL-120(Al) (beads, d_p [1.4–2[mm), shown in the form of **A**) *xy* phase diagrams and **B**) n_a^* (total, CO_2 and CH_4) as a function of y_{CH_4}. y_{CH_4} and x_{CH_4} represent the molar fractions of CH_4 in the gas and in the adsorbed phases, respectively.

S2.B. Molecular simulation studies

Two crystalline structures, the Str1 and Str2 models, have been considered for MIL-120(Al), following the approach and nomenclature given by our colleagues in a previous work[S2]. The structures have been optimised by density functional theory (DFT) calculations with the Vienna Ab initio Simulation Package (VASP)[S19–S22], version 6.1.2. The starting point for both structures has been the original MIL-120(Al) crystallographic information file (.cif extension) made available by Volkringer *et al*.[S23], after removing the water moieties present in the original .cif file by hand. Structure Str2 has the same pore configuration as the original (published) MIL-120(Al) structure[S23], whereas in structure Str1 the pore configuration differs in the position of some of the hydrogen (H) atoms of the μ_2-OH groups[S2]. In this work, the structure of Str1 has been constructed as follows:

1. Identification of the H atoms that are different in both structures in the central pore of the unit cell (UC) of the original MIL-120(Al) .cif[S23] (H7, H8, H19 and H20, *cf*. Table S4 and Figure S7 for Str2, and Table S5 and Figure S8 for Str1);
2. Manipulation of the position of the four identified H atoms in Avogadro[S24,S25];
3. Initial optimisation of the position of the four identified H atoms in Avogadro[S24,S25] with the following options:
    - *Force Field: UFF*
    - *Steps per Update: 4*
    - *Algorithm: Steepest Descent*
4. Identification of the remaining H atoms in the UC to be changed (H11, H12, H15 and H16). The relative position of these atoms to the centre of the corresponding pore is the same as the atoms identified in step 1, so that there are four pairs of alike H atoms (H7 and H11; H8 and H12; H19 and H15; H20 and H16);
5. Modification of the H atoms identified in step 4 by subtracting the same distance between each pair in the original MIL-120(Al) .cif file[S23] for all coordinates, *e.g*.:

Original MIL-120(Al) structure[S23]:

	x	*y*	*z*
H7	0.67000	0.32400	0.68400
H11	0.17000	0.82400	0.68400
$\Delta_{H7\text{-}H11}$	0.5	−0.5	0

Modified MIL-120(Al) structure (future Str1):

	x	*y*	*z*	
H7	0.77124	0.25793	0.83943	← From Avogadro (step 3)
H11	0.27124	0.75793	0.83943	← From subtraction of $\Delta_{H7\text{-}H11}$ in [S23]
$\Delta_{H7\text{-}H11}$	0.5	−0.5	0	

6. Optimisation of the modified structure from step 5 by DFT in VASP ← Final optimised Str1 structure (*cf*. Table S5).

The DFT calculations have been run within the generalised gradient approximation (GGA) of Perdew, Burke, and Ernzerhof (PBE) as implemented in VASP[S19–S22]. The D3 dispersion correction method with Becke-Johnson damping function proposed by Grimme *et al*.[S26] has been used, and the electron-ionic core interaction has been described with projector augmented wave (PAW) potentials[S27,S28]. The Brillouin zone integration has been sampled using the Monkhorst-Pack method and a 2×1×3 k-grid mesh. Plane-wave basis sets have been employed with a cut-off energy (ENCUT) of 550 eV for the valence electron density, and the convergence criteria for the electronic self-consistency loop (EDIFF) and for the ionic relaxation loop (EDIFFG) have been set to 1×10^{-7} eV and to -5×10^{-3} eV/Å, respectively. The structure has been optimised at fixed volume and shape (ISIF = 2). A typical DFT optimisation run in VASP in the scope of this work has included the following keywords in the INCAR input file:

1) Generic parameters:
   NWRITE = 2
   ISTART = 1
   GGA = PE
   IVDW = 12
   PREC = accurate
   ENCUT = 550.0
   ISPIN = 1
   NPAR = 2
   ADDGRID = .TRUE.

2) Electronic relaxation:
   EDIFF = 0.1E-06
   EDIFFG = -0.005
   LREAL = AUTO
   ALGO = FAST
   ISMEAR = 0
   SIGMA = 0.05

3) Ionic relaxation:
   ISIF = 2
   IBRION = 2
   POTIM = 0.25
   NSW = 500
   LORBIT = .FALSE.

Electrostatic potential (ESP)-derived partial atomic charges have been calculated using the Repeating Electrostatic Potential Extracted Atomic (REPEAT) method[S29], from the electrostatic potential generated in VASP for the optimised structures of MIL-120(Al).

The lattice parameters, fractional coordinates and partial atomic charges of the UC of the optimised MIL-120(Al) structures are listed in Table S4 for Str2 and Table S5 for Str1, respectively, and the optimised structures are illustrated in Figure S7 (Str2) and Figure S8 (Str1).

Table S4. Lattice parameters, fractional coordinates and partial atomic charges of the UC of the optimised structure Str2 of MIL-120(Al) (*cf.* Figure S7).

MIL-120(Al) Str2										
Lattice length (Å)		***a***	***b***	***c***	**Lattice angle (°)**		***α***	***β***	***γ***	
		9.748	20.048	7.489			90.00	134.42	90.00	
Atom		**Fractional coordinates**			**Charge**	**Atom**		**Fractional coordinates**		**Charge**
#	**Label**	***x***	***y***	***z***	**(e^-)**	**#**	**Label**	***x***	***y***	***z***	**(e^-)**
1	C1	0.95355	0.37564	0.64769	0.647	41	O1	0.27002	0.29146	0.28741	-0.760
2	C2	0.04645	0.62436	0.35231	0.647	42	O2	0.72998	0.70854	0.71259	-0.760 [a]
3	C3	0.04645	0.37564	0.35231	0.647	43	O3	0.72998	0.29146	0.71259	-0.760
4	C4	0.95355	0.62436	0.64769	0.647	44	O4	0.27002	0.70854	0.28741	-0.760 [a]
5	C5	0.45355	0.87564	0.64769	0.647	45	O5	0.77002	0.79146	0.28741	-0.760
6	C6	0.54645	0.12436	0.35231	0.647	46	O6	0.22998	0.20854	0.71259	-0.760
7	C7	0.54645	0.87564	0.35231	0.647	47	O7	0.22998	0.79146	0.71259	-0.760
8	C8	0.45355	0.12436	0.64769	0.647	48	O8	0.77002	0.20854	0.28741	-0.760
9	C9	0.98612	0.43963	0.58002	0.036	49	O9	0.99692	0.23323	0.80679	-0.931
10	C10	0.01388	0.56037	0.41998	0.036	50	O10	0.00308	0.76677	0.19321	-0.931
11	C11	0.01388	0.43963	0.41998	0.036	51	O11	0.00308	0.23323	0.19321	-0.931
12	C12	0.98612	0.56037	0.58002	0.036	52	O12	0.99692	0.76677	0.80679	-0.931
13	C13	0.48612	0.93963	0.58002	0.036	53	O13	0.49692	0.73323	0.80679	-0.931
14	C14	0.51388	0.06037	0.41998	0.036	54	O14	0.50308	0.26677	0.19321	-0.931
15	C15	0.51388	0.93963	0.41998	0.036	55	O15	0.50308	0.73323	0.19321	-0.931
16	C16	0.48612	0.06037	0.58002	0.036	56	O16	0.49692	0.26677	0.80679	-0.931
17	C17	0.97439	0.50000	0.66169	-0.242	57	O17	0.04179	0.36792	0.87558	-0.667
18	C18	0.02561	0.50000	0.33831	-0.242	58	O18	0.95821	0.63208	0.12442	-0.667
19	C19	0.47439	0.00000	0.66169	-0.242	59	O19	0.95821	0.36792	0.12442	-0.667
20	C20	0.52561	0.00000	0.33831	-0.242	60	O20	0.04179	0.63208	0.87558	-0.667
21	H1	0.95112	0.50000	0.78444	0.162	61	O21	0.54179	0.86792	0.87558	-0.667
22	H2	0.04888	0.50000	0.21556	0.162	62	O22	0.45821	0.13208	0.12442	-0.667
23	H3	0.45112	0.00000	0.78444	0.162	63	O23	0.45821	0.86792	0.12442	-0.667
24	H4	0.54888	0.00000	0.21556	0.162	64	O24	0.54179	0.13208	0.87558	-0.667
25	H5	0.32391	0.33607	0.33457	0.334	65	O25	0.83267	0.33508	0.47064	-0.677
26	H6	0.67609	0.66393	0.66543	0.334	66	O26	0.16733	0.66492	0.52936	-0.677
27	H7	0.67609	0.33607	0.66543	0.334	67	O27	0.16733	0.33508	0.52936	-0.677
28	H8	0.32391	0.66393	0.33457	0.334	68	O28	0.83267	0.66492	0.47064	-0.677
29	H9	0.82391	0.83607	0.33457	0.334	69	O29	0.33267	0.83508	0.47064	-0.677
30	H10	0.17609	0.16393	0.66543	0.334	70	O30	0.66733	0.16492	0.52936	-0.677
31	H11	0.17609	0.83607	0.66543	0.334	71	O31	0.66733	0.83508	0.52936	-0.677
32	H12	0.82391	0.16393	0.33457	0.334	72	O32	0.33267	0.16492	0.47064	-0.677
33	H13	0.09679	0.23162	0.80536	0.362	73	Al1	0.00000	0.29365	0.00000	1.783
34	H14	0.90321	0.76838	0.19464	0.362	74	Al2	0.00000	0.70635	0.00000	1.783
35	H15	0.90321	0.23162	0.19464	0.362	75	Al3	0.50000	0.79365	0.00000	1.783
36	H16	0.09679	0.76838	0.80536	0.362	76	Al4	0.50000	0.20635	0.00000	1.783
37	H17	0.59679	0.73162	0.80536	0.362	77	Al5	0.75000	0.25000	0.50000	1.609
38	H18	0.40321	0.26838	0.19464	0.362	78	Al6	0.25000	0.75000	0.50000	1.609
39	H19	0.40321	0.73162	0.19464	0.362	79	Al7	0.25000	0.25000	0.50000	1.609
40	H20	0.59679	0.26838	0.80536	0.362	80	Al8	0.75000	0.75000	0.50000	1.609

[a] Partial atomic charge adjusted by 0.001 due to rounding errors to achieve framework charge neutrality[S30].

Table S5. Lattice parameters, fractional coordinates and partial atomic charges of the UC of the optimised structure Str1 of MIL-120(Al) (*cf.* Figure S8).

MIL-120(Al) Str1										
Lattice length (Å)		***a***	***b***	***c***	Lattice angle (°)		***α***	***β***	***γ***	
		9.748	20.048	7.489			90.00	134.42	90.00	
Atom		Fractional coordinates			Charge	Atom		Fractional coordinates		Charge
#	Label	***x***	***y***	***z***	(e^-)	#	Label	***x***	***y***	***z***	(e^-)
1	C1	0.94499	0.37809	0.64709	0.684	41	O1	0.26452	0.29448	0.28895	-0.784
2	C2	0.05792	0.62152	0.35494	0.683	42	O2	0.73839	0.70511	0.71309	-0.785
3	C3	0.04208	0.37310	0.35765	0.664	43	O3	0.73133	0.29015	0.70785	-0.974
4	C4	0.96083	0.62651	0.64436	0.665	44	O4	0.27162	0.70947	0.29420	-0.974
5	C5	0.44499	0.87809	0.64709	0.684	45	O5	0.76452	0.79448	0.28895	-0.784
6	C6	0.55792	0.12152	0.35494	0.683	46	O6	0.23839	0.20511	0.71309	-0.785
7	C7	0.54208	0.87310	0.35765	0.664	47	O7	0.23133	0.79015	0.70785	-0.974
8	C8	0.46083	0.12651	0.64436	0.665	48	O8	0.77162	0.20947	0.29420	-0.974
9	C9	0.98160	0.44090	0.58006	0.009	49	O9	0.00358	0.23583	0.81278	-1.006
10	C10	0.02132	0.55871	0.42197	0.009	50	O10	0.99935	0.76379	0.18927	-1.006
11	C11	0.01473	0.43829	0.42587	0.027	51	O11	0.99983	0.23104	0.19048	-0.854
12	C12	0.98819	0.56132	0.57616	0.026	52	O12	0.00302	0.76859	0.81152	-0.856
13	C13	0.48160	0.94090	0.58006	0.009	53	O13	0.50358	0.73583	0.81278	-1.006
14	C14	0.52132	0.05871	0.42197	0.009	54	O14	0.49935	0.26379	0.18927	-1.006
15	C15	0.51473	0.93829	0.42587	0.027	55	O15	0.49983	0.73104	0.19048	-0.854
16	C16	0.48819	0.06132	0.57616	0.026	56	O16	0.50302	0.26859	0.81152	-0.856
17	C17	0.97057	0.50226	0.65740	-0.231	57	O17	0.03078	0.37160	0.87444	-0.625
18	C18	0.03234	0.49735	0.34461	-0.231	58	O18	0.97221	0.62801	0.12760	-0.625
19	C19	0.47057	0.00226	0.65740	-0.231	59	O19	0.94753	0.36441	0.12880	-0.586
20	C20	0.53234	0.99735	0.34461	-0.231	60	O20	0.05547	0.63524	0.87322	-0.587
21	H1	0.94368	0.50394	0.77622	0.164	61	O21	0.53078	0.87160	0.87444	-0.625
22	H2	0.05917	0.49568	0.22572	0.165	62	O22	0.47221	0.12801	0.12760	-0.625
23	H3	0.44368	0.00394	0.77622	0.164	63	O23	0.44753	0.86441	0.12880	-0.586
24	H4	0.55917	0.99568	0.22572	0.165	64	O24	0.55547	0.13524	0.87322	-0.587
25	H5	0.33862	0.33527	0.34493	0.341	65	O25	0.82857	0.33677	0.47160	-0.680
26	H6	0.66420	0.66434	0.65703	0.341	66	O26	0.17425	0.66287	0.53041	-0.680
27	H7	0.64917	0.27589	0.73251	0.415	67	O27	0.16457	0.33216	0.53376	-0.714
28	H8	0.35375	0.72375	0.26950	0.414	68	O28	0.83824	0.66742	0.46821	-0.714
29	H9	0.83862	0.83527	0.34493	0.341	69	O29	0.32857	0.83677	0.47160	-0.680
30	H10	0.16420	0.16434	0.65703	0.341	70	O30	0.67425	0.16287	0.53041	-0.680
31	H11	0.14917	0.77589	0.73251	0.415	71	O31	0.66457	0.83216	0.53376	-0.714
32	H12	0.85375	0.22375	0.26950	0.414	72	O32	0.33824	0.16742	0.46821	-0.714
33	H13	0.10480	0.23305	0.81470	0.409	73	Al1	0.99347	0.29671	0.99402	1.601
34	H14	0.89814	0.76656	0.18737	0.409	74	Al2	0.00944	0.70291	0.00800	1.603
35	H15	0.98329	0.18673	0.12433	0.391	75	Al3	0.49347	0.79671	0.99402	1.601
36	H16	0.01937	0.81289	0.87755	0.391	76	Al4	0.50944	0.20291	0.00800	1.603
37	H17	0.60480	0.73305	0.81470	0.409	77	Al5	0.75149	0.24981	0.50105	1.914 [a]
38	H18	0.39814	0.26656	0.18737	0.409	78	Al6	0.25149	0.74981	0.50105	1.914 [a]
39	H19	0.48329	0.68673	0.12433	0.391	79	Al7	0.25145	0.24979	0.50101	1.587
40	H20	0.51937	0.31289	0.87755	0.391	80	Al8	0.75145	0.74979	0.50101	1.587

[a] Partial atomic charge adjusted by -0.001 due to rounding errors to achieve framework charge neutrality[S30].

Grand-canonical Monte Carlo (GCMC) calculations[S31] have been run in RASPA[S30] 2.0 to estimate CO_2 and CH_4 single-component isotherms, and the adsorption isotherms of a binary CO_2/CH_4 mixture with (50:50) %(*V*/*V*) in the optimised MIL-120(Al) Str1 and Str2 structures. The simulations have been run at 25 °C for pressures up to 10 bar, considering a 4×2×5 simulation box (SB), obtained by repetition of the *a*, *b* and *c* vectors of the UC by 4, 2 and 5, respectively.

RASPA runs have been computed with 1×10^5 cycles for production, preceded by 2×10^4 cycles for initialisation (each cycle in RASPA corresponds to max(20,*N*) steps, where *N* represents the number of molecules in the system)[S30]. The probabilities (*P*) of attempting specific types of moves in random positions that have been considered to compute the single-component and binary mixture isotherms are listed in Table S6.

Table S6. Types of moves and respective probabilities (*P*) considered in the GCMC simulations.

Type of move	Single-component		Multi-component	
	$P(CO_2)$	$P(CH_4)$	$P(CO_2)$ [a]	$P(CH_4)$ [a]
Translation	0.5	0.5	0.5	0.5
Rotation	0.5	–	–	–
Reinsertion	0.5	0.5	–	–
Swap [b]	1.0	1.0	1.0	1.0
Regrowth	–	–	0.5	0.5
Identity change [c]	–	–	1.0	1.0

[a] Following an example provided in RASPA's manual.[S30]

[b] A *Swap* move corresponds to attempting an insertion or deletion.[S30]

[c] An *Identity change* move corresponds to changing the identity of a molecule (*e.g.*, from CH_4 to CO_2) at a given position.[S30]

The frameworks of both MIL-120(Al) structures have been considered rigid and the total interaction energy between any two atoms *i* and *j* of the framework (host) and gas (guest) (U_{ij}) has been described by non-bonded interactions using the classical 12–6 Lennard-Jones (LJ) potential ($U_{LJ,ij}$), and by electrostatic interactions (where applicable) represented by a Coulomb potential ($U_{C,ij}$), as given in (S3).[S31,S32] The Ewald summation technique has been used with a relative precision of 1×10^{-6} as implemented in RASPA[S30] 2.0, to compute long-distance electrostatics.

$$U_{ij} = U_{LJ,ij} + U_{C,ij} = 4\cdot\varepsilon_{ij}\cdot\left[\left(\frac{\sigma_{ij}}{r_{ij}}\right)^{12} - \left(\frac{\sigma_{ij}}{r_{ij}}\right)^{6}\right] + \frac{1}{4\cdot\pi\cdot\varepsilon_0}\cdot\frac{q_i\cdot q_j}{r_{ij}} \quad \text{(S3)}$$

where ε_{ij} is the well depth of the potential, σ_{ij} is the distance at which the potential energy between particles *i* and *j* is zero, r_{ij} is the distance between atoms *i* and *j*, ε_0 is the vacuum permittivity, and q_i and q_j are the partial charges of atoms *i* and *j*, respectively.[S31,S32] The Lennard-Jones potential has been considered shifted and with a cut-off of 12 Å. Following the approach used by our colleagues in a previous work[S2], the UFF[S33] force field has been used to describe the framework atoms, with the dispersion energies of aluminium (Al) and the H atoms of the μ_2-OH groups not being considered. The TraPPE force field has been used to describe CO_2[S34] and CH_4[S35], with CH_4 following the united atoms (UA) approach. The interactions between each atom pair have been calculated with the general Lorentz-Berthelot mixing rules[S31], *cf.* equations (S4A-B). The atom assignment and LJ parameters are listed in Table S7 for Str2 and Table S8 for Str1.

$$\varepsilon_{ij} = \sqrt{\varepsilon_i \cdot \varepsilon_j} \quad \text{(S4A)}$$

$$\sigma_{ij} = \frac{\sigma_i + \sigma_j}{2} \quad \text{(S4B)}$$

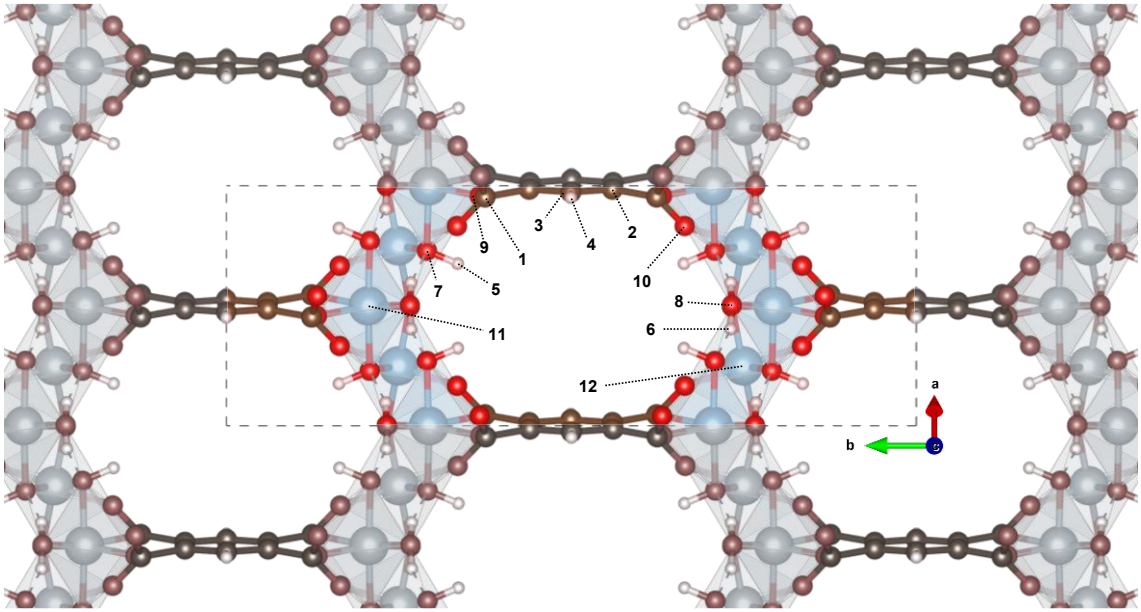

Figure S7. Assignment of the atom-types used to describe structure Str2 of MIL-120(Al) in the GCMC adsorption studies (*cf.* Table S4 and Table S7). The black dashed line delimits the UC. Colour code: aluminium (Al, blue); oxygen (O, red); carbon (C, brown); hydrogen (H, white). Structure drawing produced by VESTA 3[S36].

Table S7. Assignment of the atom-types (*cf.* Figure S7) and LJ parameters used to describe structure Str2 of MIL-120(Al) in the GCMC adsorption studies.

Assignment			LJ parameter	
Label	**Atom**	**Description**	ε/k_B **(K)**	σ **(Å)**
1	C	C-DiCarb (C1-C8)	52.84 [a]	3.431 [a]
2		C-AroRing (C9-C16)		
3		C-AroRing with H (C17-C20)		
4	H	H-AroRing (H1-H4)	22.14 [a]	2.571 [a]
5		H from μ_2-OH_1 (H5-H12)	0.00 [b]	
6		H from μ_2-OH_2 (H13-H20)		
7	O	O from μ_2-OH_1 (O1-O8)	30.19 [a]	3.118 [a]
8		O from μ_2-OH_2 (O9-O16)		
9		O-DiCarb-Al_1 (O17-O24)		
10		O-DiCarb-Al_2 (O25-O32)		
11	Al	Al_1 (Al1-Al4)	0.00 [b]	4.008 [a]
12		Al_2 (Al5-Al8)		

[a] Converted from data reported for the UFF[S33] force field, with:

$$\varepsilon/k_B\ (\mathrm{K}) = \frac{D_I\ (\mathrm{kcal \cdot mol^{-1}})}{R\ (\mathrm{kcal \cdot K^{-1} \cdot mol^{-1}})}\ ;\ \sigma\ (\text{Å}) = \frac{1}{2^{1/6}} \cdot x_I\ (\text{Å})$$

[b] Following the approach used by our colleagues in a previous work.[S2]

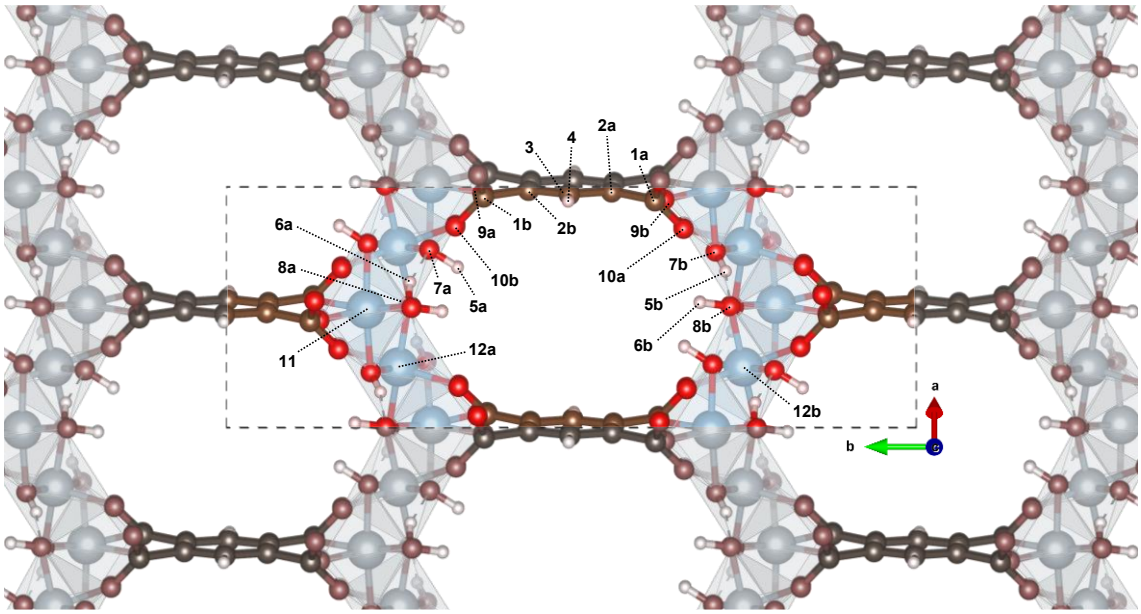

Figure S8. Assignment of the atom-types used to describe structure Str1 of MIL-120(Al) in the GCMC adsorption studies (*cf*. Table S5 and Table S8). The black dashed line delimits the UC. Colour code: Al (blue); O (red); C (brown); H (white). Structure drawing produced by VESTA 3[S36].

Table S8. Assignment of the atom-types (*cf*. Figure S8) and LJ parameters used to describe structure Str1 of MIL-120(Al) in the GCMC adsorption studies.

Assignment			LJ parameter	
Label	**Atom**	**Description**	**ε/k_B (K)**	**σ (Å)**
1a	C	C-DiCarb_a (C1, C2, C5, C6)	52.84 [a]	3.431 [a]
1b		C-DiCarb_b (C3, C4, C7, C8)		
2a		C-AroRing_a (C9, C10, C13, C14)		
2b		C-AroRing_b (C11, C12, C15, C16)		
3		C-AroRing with H (C17-C20)		
4	H	H-AroRing (H1-H4)	22.14 [a]	2.571 [a]
5a		H from μ_2-OH_1a (H5, H6, H9, H10)	0.00 [b]	
5b		H from μ_2-OH_1b (H7, H8, H11, H12)		
6a		H from μ_2-OH_2a (H13, H14, H17, H18)		
6b		H from μ_2-OH_2b (H15, H16, H19, H20)		
7a	O	O from μ_2-OH_1a (O1, O2, O5, O6)	30.19 [a]	3.118 [a]
7b		O from μ_2-OH_1b (O3, O4, O7, O8)		
8a		O from μ_2-OH_2a (O9, O10, O13, O14)		
8b		O from μ_2-OH_2b (O11, O12, O15, O16)		
9a		O-DiCarb-Al_1a (O17, O18, O21, O22)		
9b		O-DiCarb-Al_1b (O19, O20, O23, O24)		
10a		O-DiCarb-Al_2a (O25, O26, O29, O30)		
10b		O-DiCarb-Al_2b (O27, O28, O31, O32)		
11	Al	Al_1 (Al1-Al4)	0.00 [b]	4.008 [a]
12a		Al_2a (Al5, Al6)		
12b		Al_2b (Al7, Al8)		

[a] Converted from data reported for the UFF[S33] force field, with:

$$\varepsilon/k_B\ (\mathrm{K}) = \frac{D_i\ (\mathrm{kcal\cdot mol^{-1}})}{R\ (\mathrm{kcal\cdot K^{-1}\cdot mol^{-1}})}\ ;\ \sigma\ (\text{Å}) = \frac{1}{2^{1/6}}\cdot x_i\ (\text{Å})$$

[b] Following the approach used by our colleagues in a previous work.[S2]

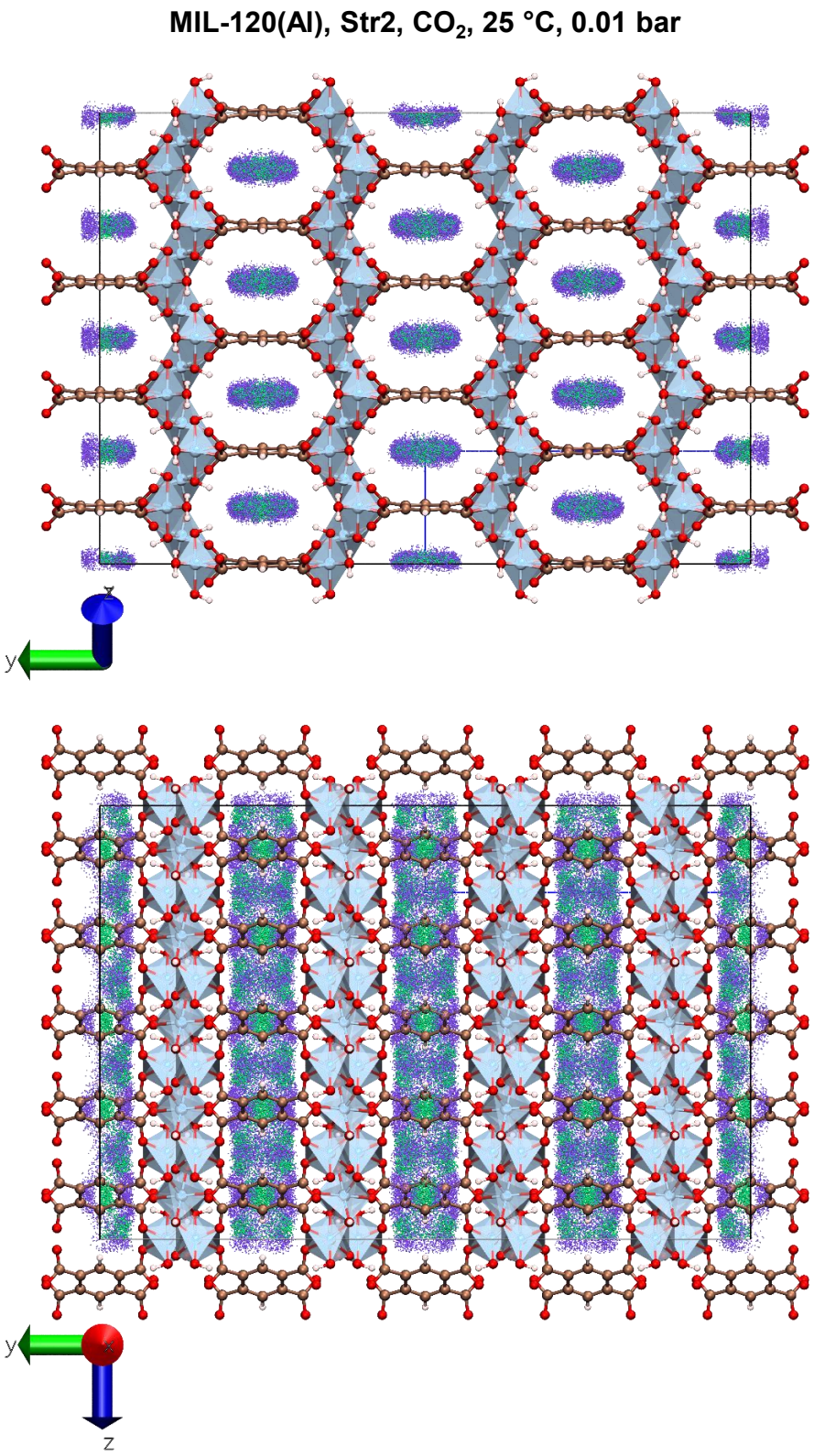

Figure S9. Density map of the single-component adsorption of CO_2 at 0.01 bar and 25 °C obtained for Str2 of MIL-120(Al) from GCMC calculations, as viewed from two directions. The black outer box delimits the SB (4×2×5) and the blue-dashed inner box delimits the UC. The framework atoms outside the SB are only drawn for visual completion of the periodic structure. Colour code for framework atoms: Al (blue); O (red); C (brown); H (white). Colour code for CO_2 atoms: C (green); O (violet). CO_2 atoms are drawn without bonds and on a 1:8 radii scale relative to framework atoms. Density map generated from the combined snapshots of GCMC simulations collected every 100 cycles of the production run. Structure drawing and density maps produced by VMD 1.9.4[S37].

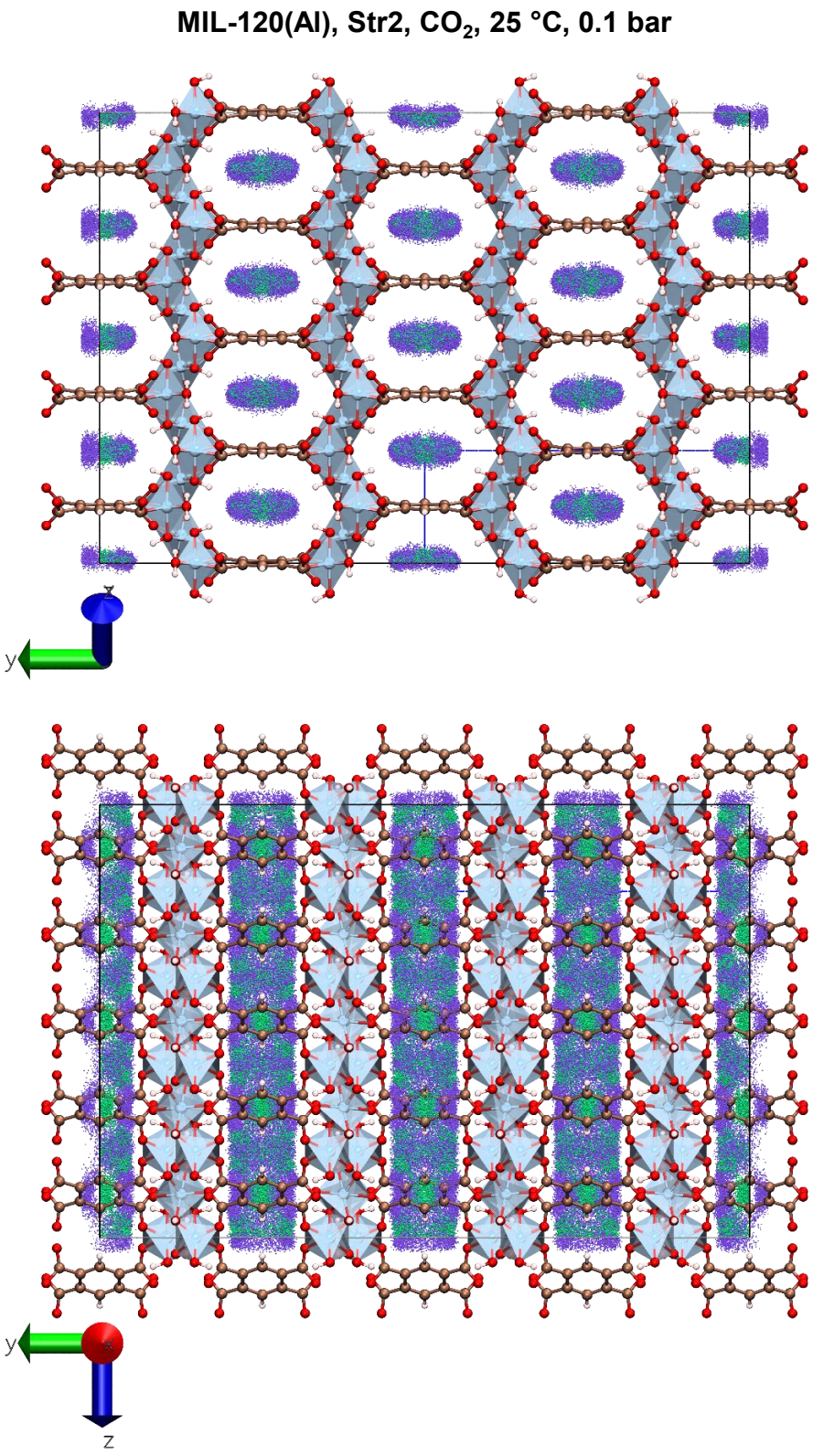

Figure S10. Density map of the single-component adsorption of CO_2 at 0.1 bar and 25 °C obtained for Str2 of MIL-120(Al) from GCMC calculations, as viewed from two directions. The black outer box delimits the SB (4×2×5) and the blue-dashed inner box delimits the UC. The framework atoms outside the SB are only drawn for visual completion of the periodic structure. Colour code for framework atoms: Al (blue); O (red); C (brown); H (white). Colour code for CO_2 atoms: C (green); O (violet). CO_2 atoms are drawn without bonds and on a 1:8 radii scale relative to framework atoms. Density map generated from the combined snapshots of GCMC simulations collected every 100 cycles of the production run. Structure drawing and density maps produced by VMD 1.9.4[S37].

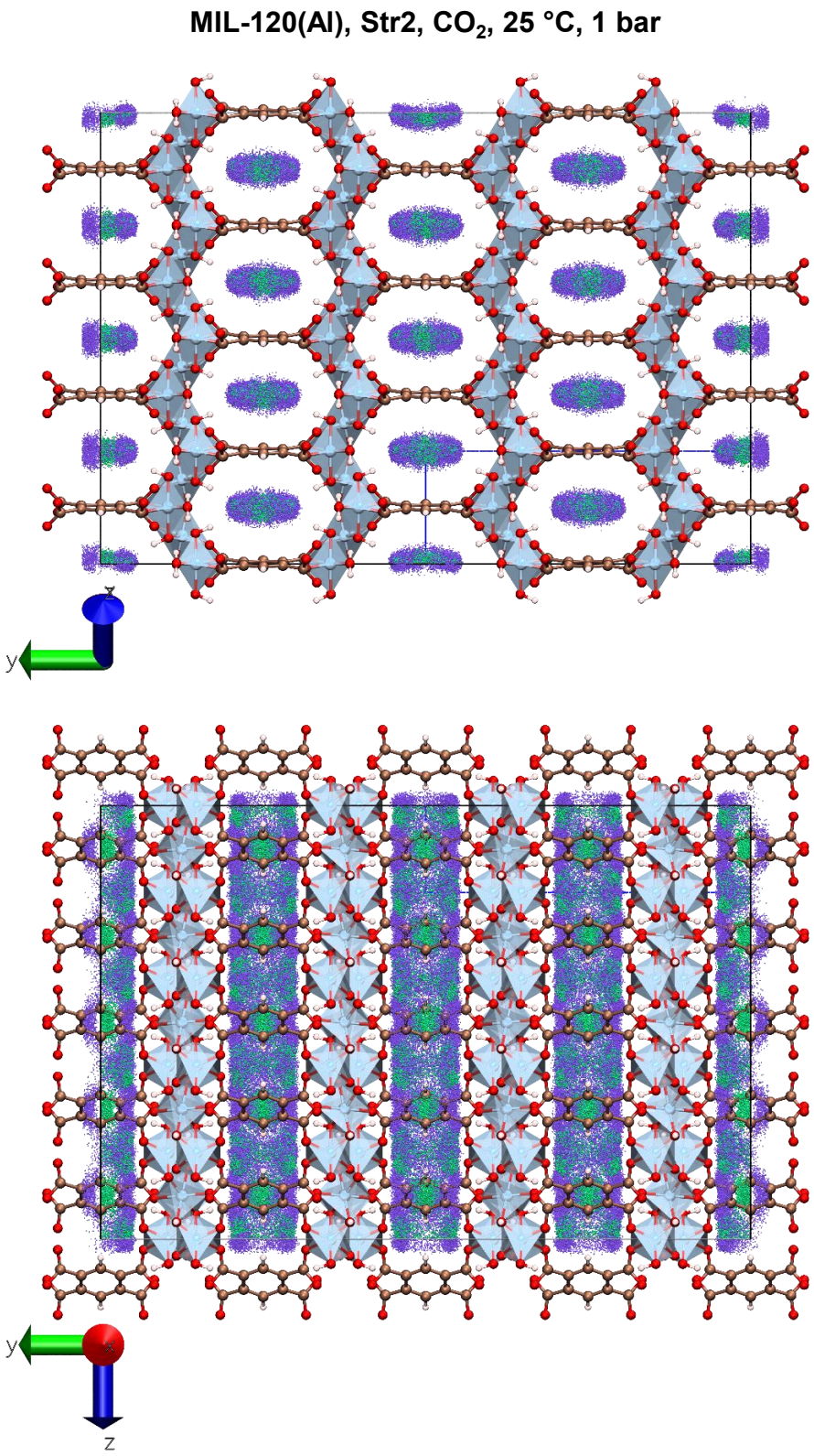

Figure S11. Density map of the single-component adsorption of CO_2 at 1 bar and 25 °C obtained for Str2 of MIL-120(Al) from GCMC calculations, as viewed from two directions. The black outer box delimits the SB (4×2×5) and the blue-dashed inner box delimits the UC. The framework atoms outside the SB are only drawn for visual completion of the periodic structure. Colour code for framework atoms: Al (blue); O (red); C (brown); H (white). Colour code for CO_2 atoms: C (green); O (violet). CO_2 atoms are drawn without bonds and on a 1:8 radii scale relative to framework atoms. Density map generated from the combined snapshots of GCMC simulations collected every 100 cycles of the production run. Structure drawing and density maps produced by VMD 1.9.4[S37].

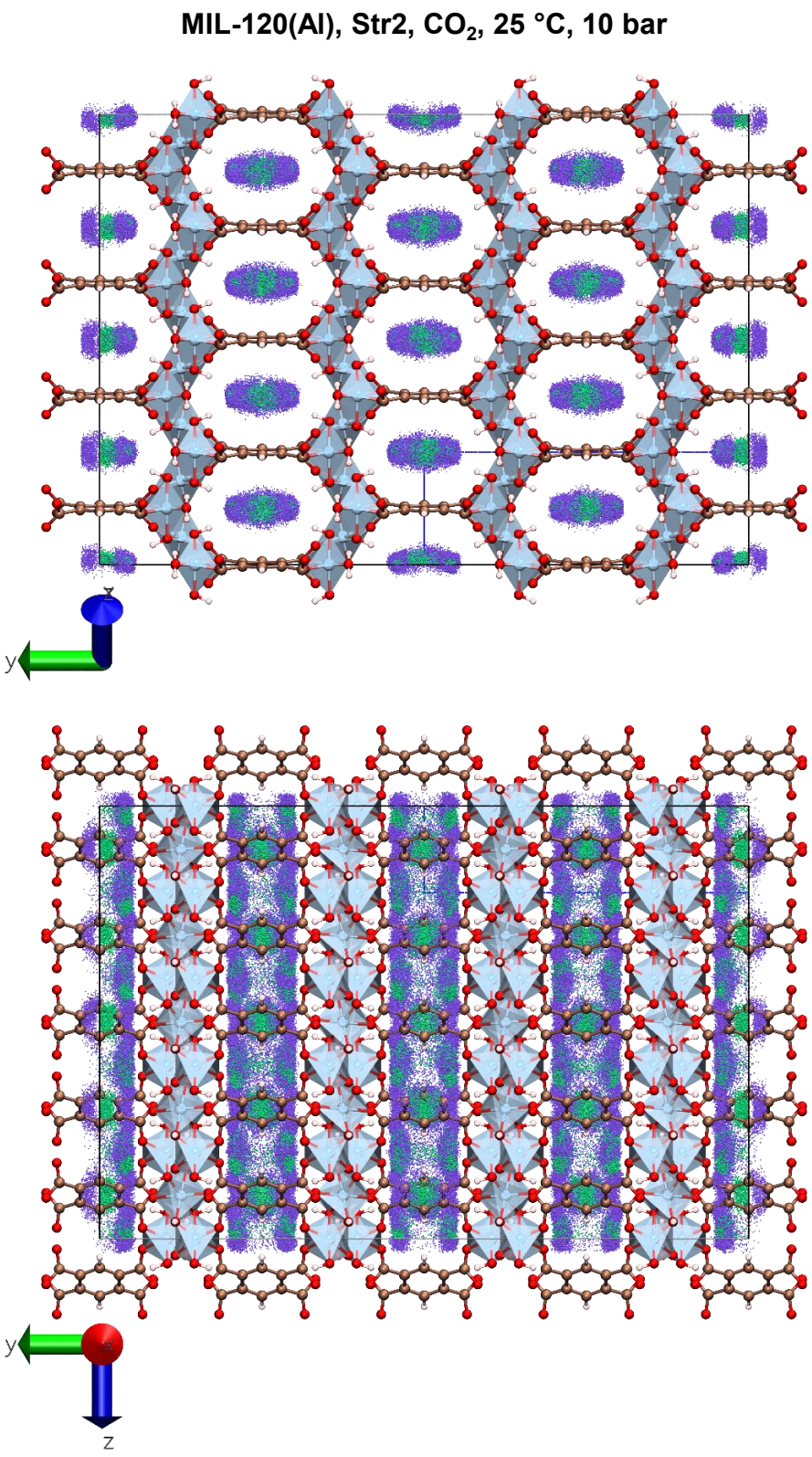

Figure S12. Density map of the single-component adsorption of CO_2 at 10 bar and 25 °C obtained for Str2 of MIL-120(Al) from GCMC calculations, as viewed from two directions. The black outer box delimits the SB (4×2×5) and the blue-dashed inner box delimits the UC. The framework atoms outside the SB are only drawn for visual completion of the periodic structure. Colour code for framework atoms: Al (blue); O (red); C (brown); H (white). Colour code for CO_2 atoms: C (green); O (violet). CO_2 atoms are drawn without bonds and on a 1:8 radii scale relative to framework atoms. Density map generated from the combined snapshots of GCMC simulations collected every 100 cycles of the production run. Structure drawing and density maps produced by VMD 1.9.4[S37].

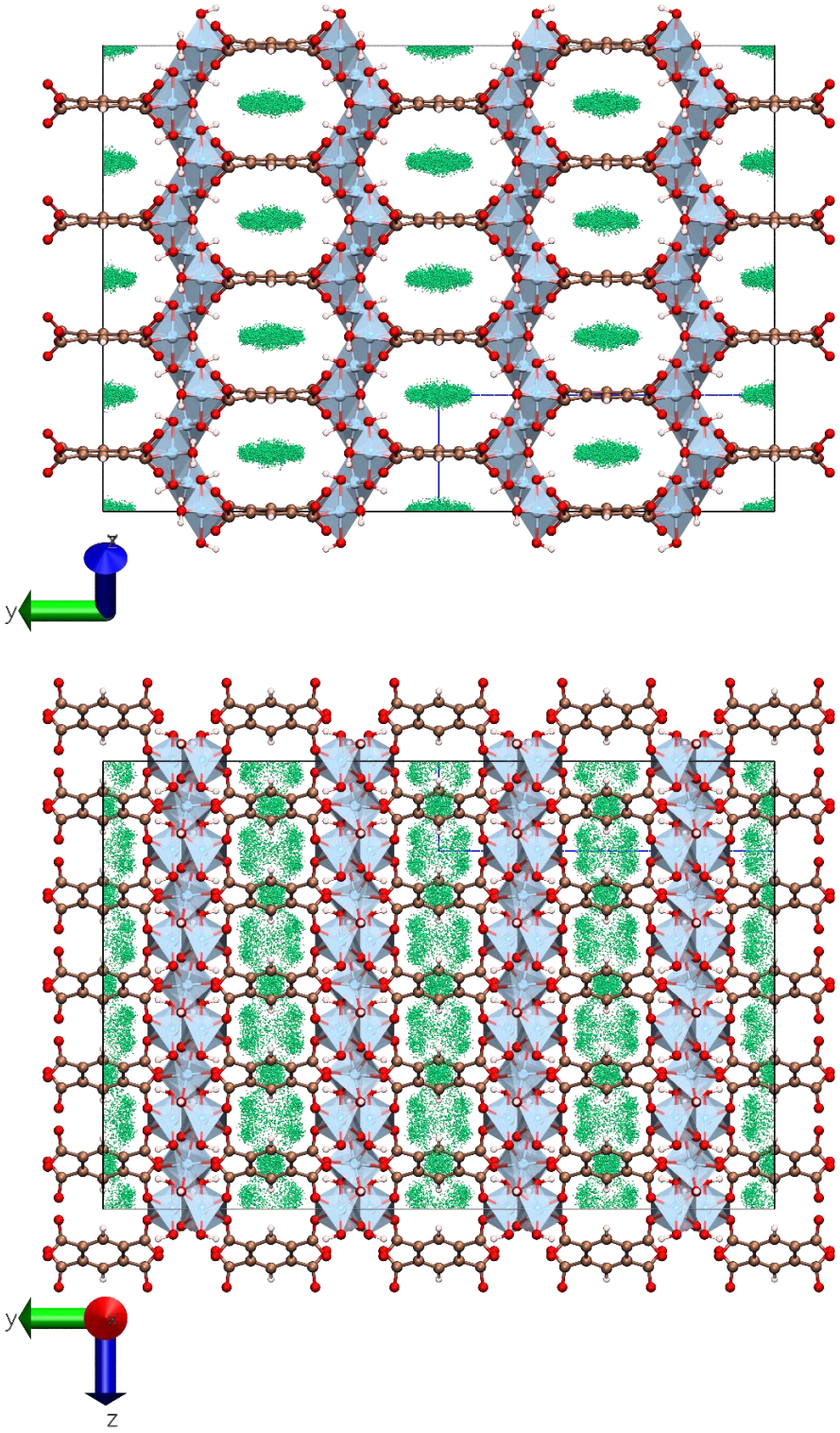

Figure S13. Density map of the single-component adsorption of CO_2 at 0.01 bar and 25 °C obtained for Str2 of MIL-120(Al) from GCMC calculations, showing only the C atoms of CO_2, as viewed from two directions. The black outer box delimits the SB (4×2×5) and the blue-dashed inner box delimits the UC. The framework atoms outside the SB are only drawn for visual completion of the periodic structure. Colour code for framework atoms: Al (blue); O (red); C (brown); H (white). Colour code for the C atoms from CO_2: C (green). C atoms from CO_2 are drawn on a 1:8 radii scale relative to framework atoms. Density map generated from the combined snapshots of GCMC simulations collected every 100 cycles of the production run. Structure drawing and density maps produced by VMD 1.9.4[S37].

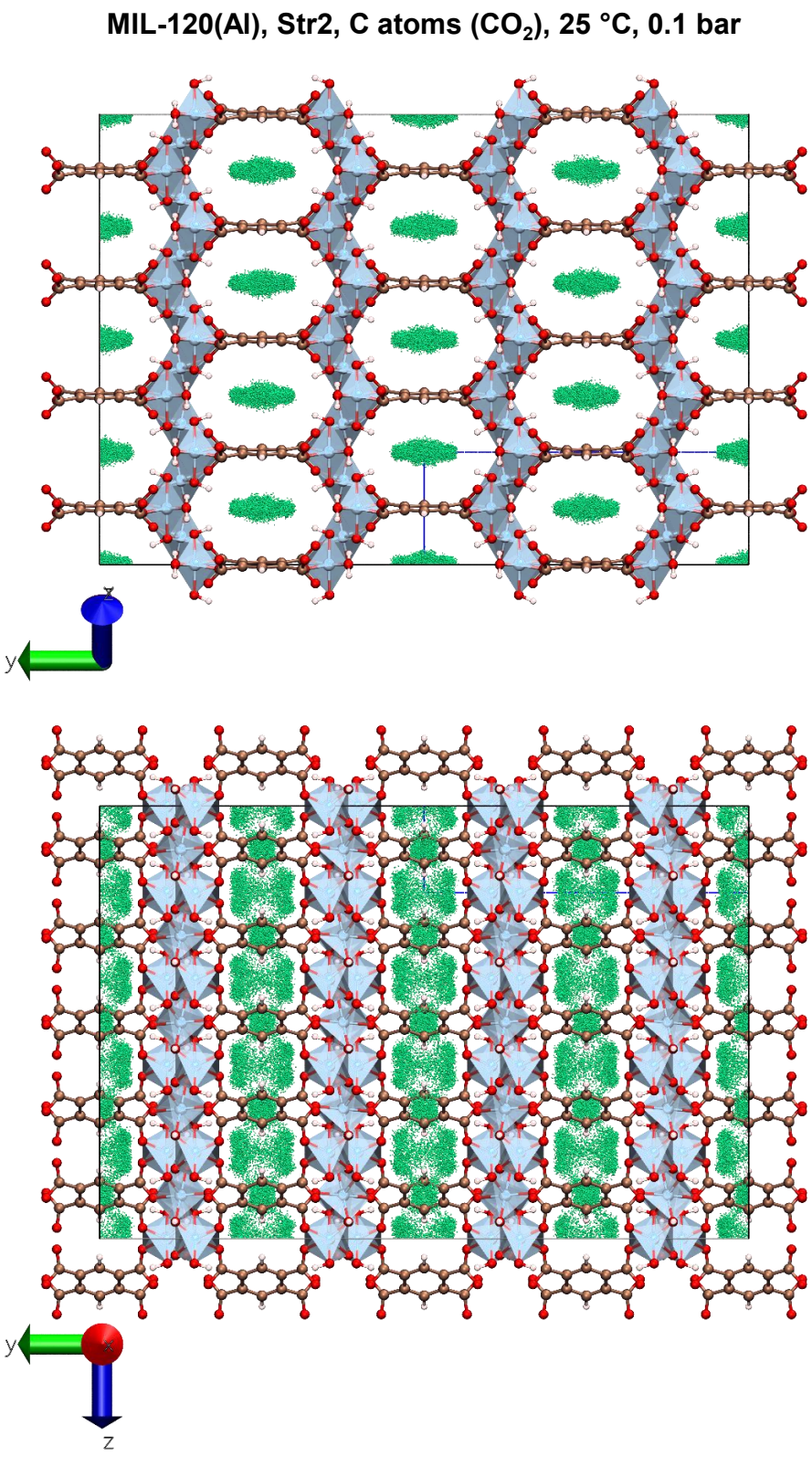

Figure S14. Density map of the single-component adsorption of CO_2 at 0.1 bar and 25 °C obtained for Str2 of MIL-120(Al) from GCMC calculations, showing only the C atoms of CO_2, as viewed from two directions. The black outer box delimits the SB (4×2×5) and the blue-dashed inner box delimits the UC. The framework atoms outside the SB are only drawn for visual completion of the periodic structure. Colour code for framework atoms: Al (blue); O (red); C (brown); H (white). Colour code for the C atoms from CO_2: C (green). C atoms from CO_2 are drawn on a 1:8 radii scale relative to framework atoms. Density map generated from the combined snapshots of GCMC simulations collected every 100 cycles of the production run. Structure drawing and density maps produced by VMD 1.9.4[S37].

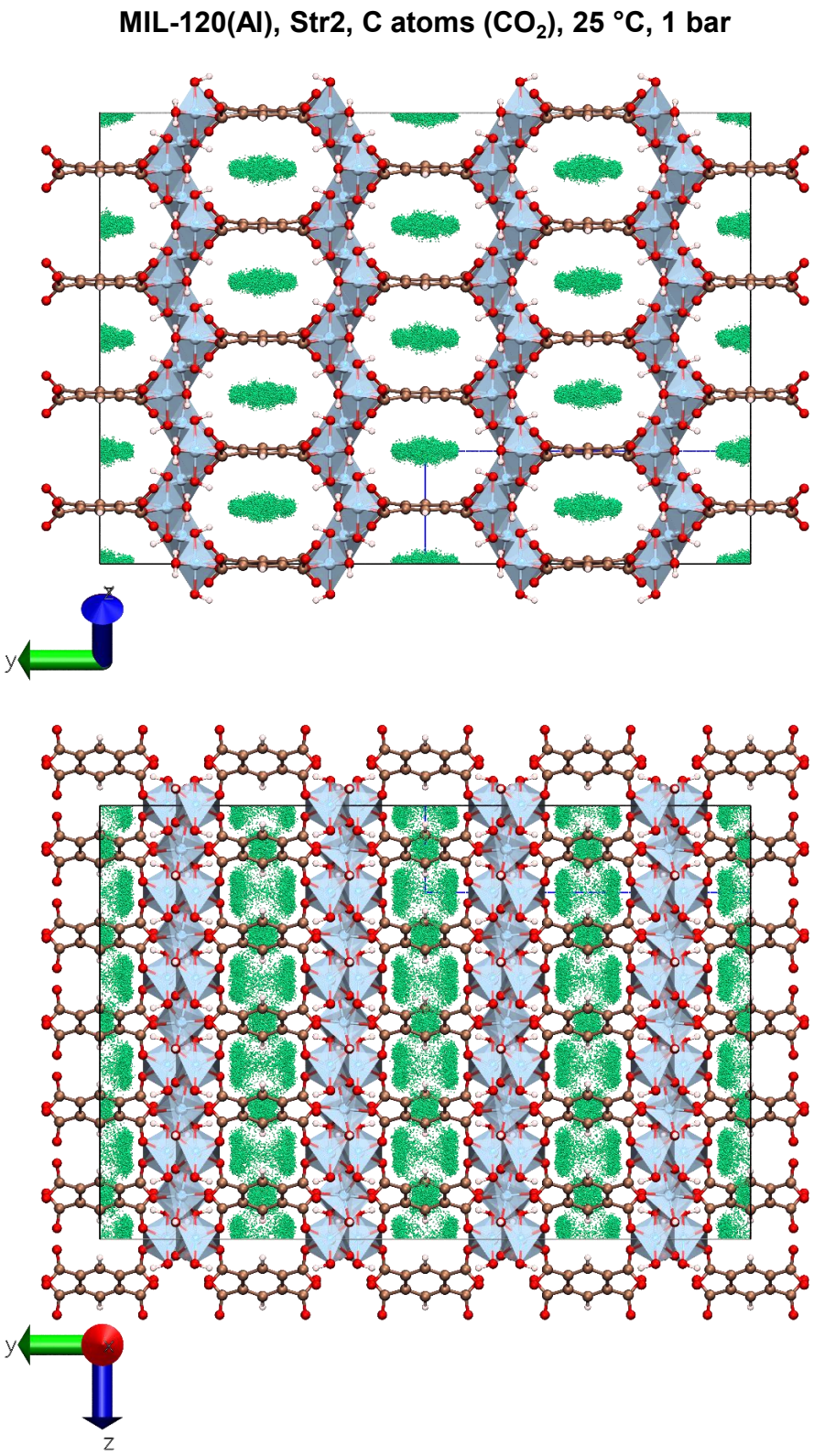

Figure S15. Density map of the single-component adsorption of CO_2 at 1 bar and 25 °C obtained for Str2 of MIL-120(Al) from GCMC calculations, showing only the C atoms of CO_2, as viewed from two directions. The black outer box delimits the SB (4×2×5) and the blue-dashed inner box delimits the UC. The framework atoms outside the SB are only drawn for visual completion of the periodic structure. Colour code for framework atoms: Al (blue); O (red); C (brown); H (white). Colour code for the C atoms from CO_2: C (green). C atoms from CO_2 are drawn on a 1:8 radii scale relative to framework atoms. Density map generated from the combined snapshots of GCMC simulations collected every 100 cycles of the production run. Structure drawing and density maps produced by VMD 1.9.4[S37].

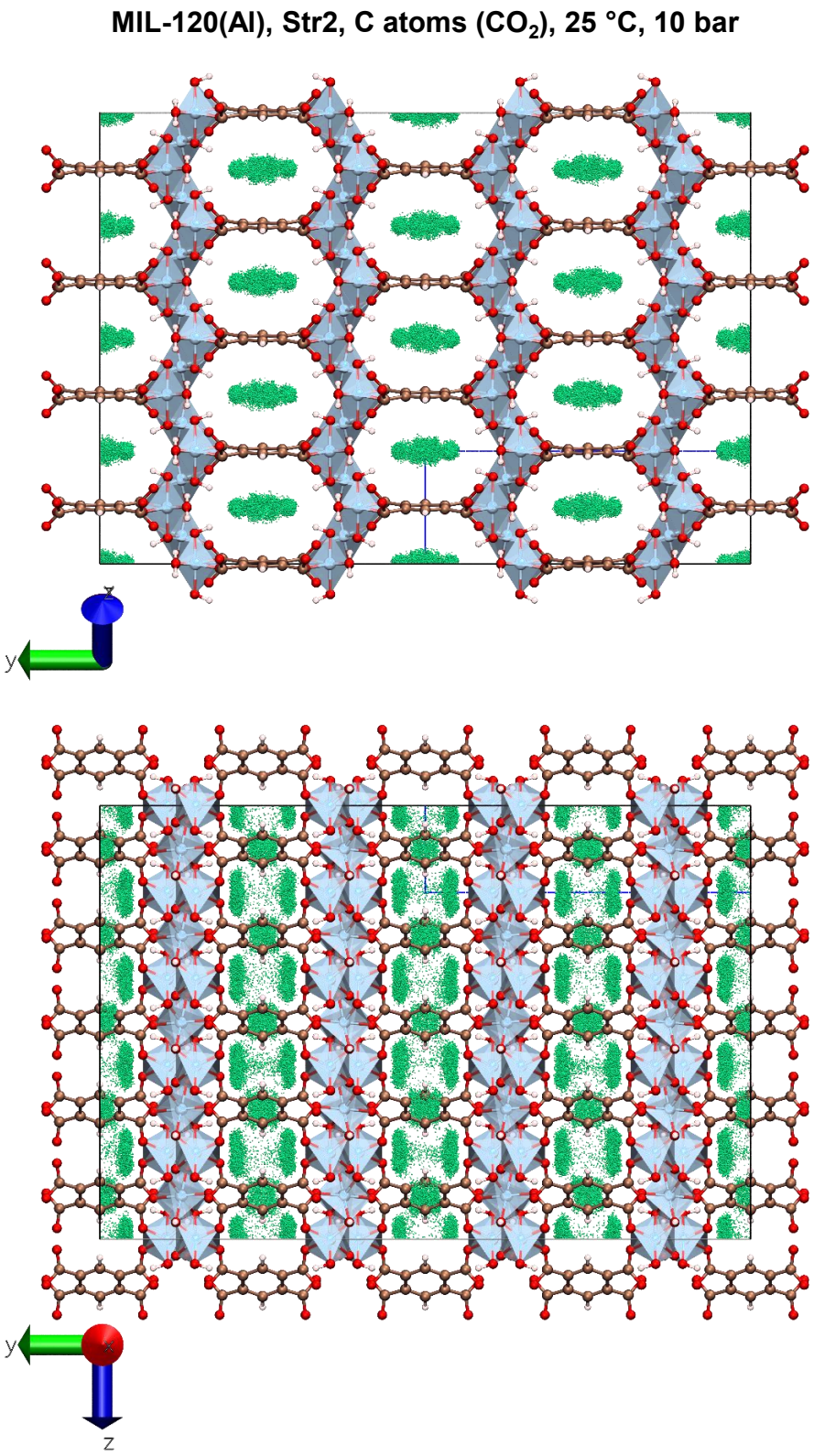

Figure S16. Density map of the single-component adsorption of CO_2 at 10 bar and 25 °C obtained for Str2 of MIL-120(Al) from GCMC calculations, showing only the C atoms of CO_2, as viewed from two directions. The black outer box delimits the SB (4×2×5) and the blue-dashed inner box delimits the UC. The framework atoms outside the SB are only drawn for visual completion of the periodic structure. Colour code for framework atoms: Al (blue); O (red); C (brown); H (white). Colour code for the C atoms from CO_2: C (green). C atoms from CO_2 are drawn on a 1:8 radii scale relative to framework atoms. Density map generated from the combined snapshots of GCMC simulations collected every 100 cycles of the production run. Structure drawing and density maps produced by VMD 1.9.4[S37].

MIL-120(Al), Str2, C atoms (CH_4 – UA), 25 °C, 0.01 bar

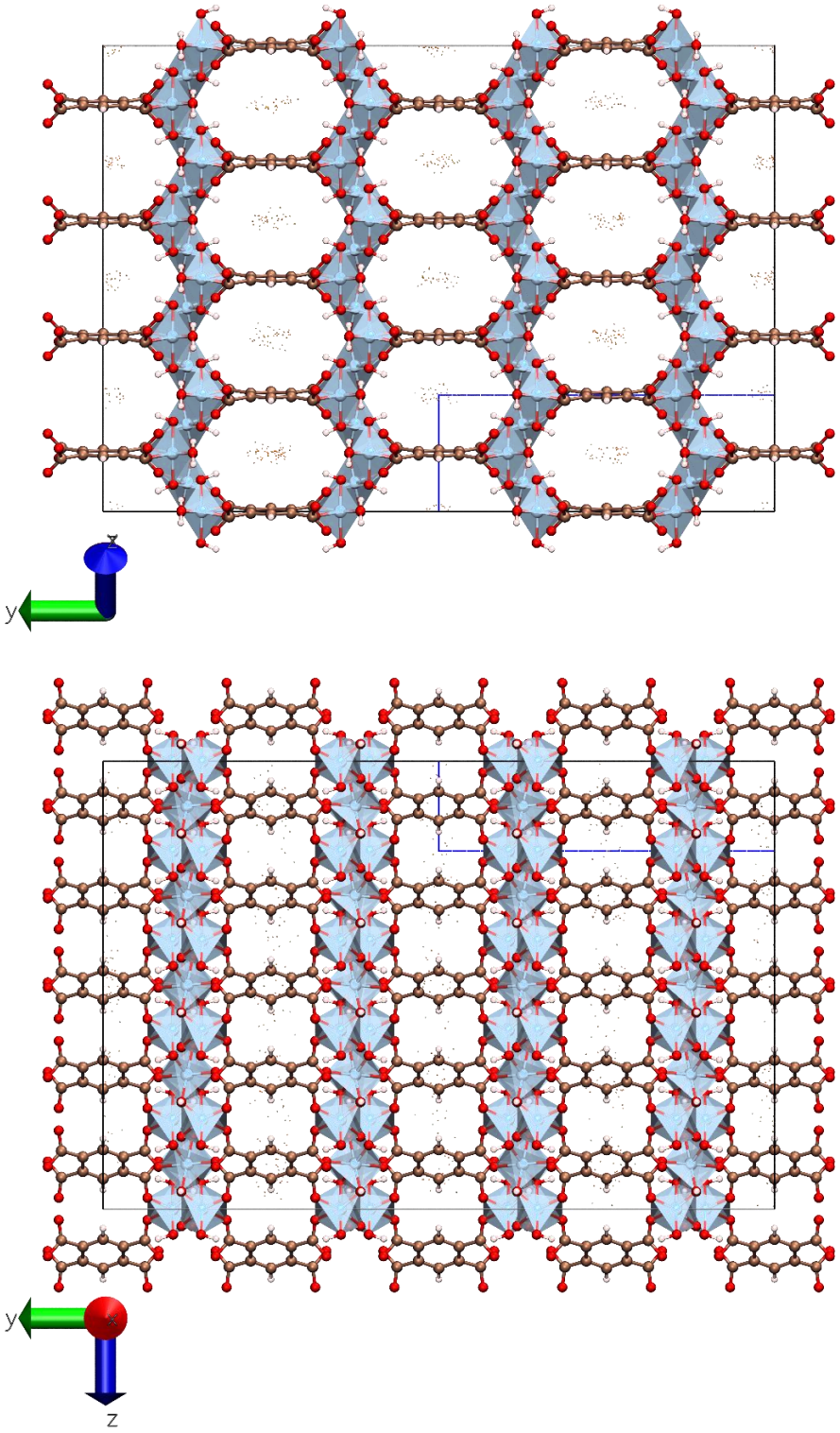

Figure S17. Density map of the single-component adsorption of CH_4 (UA approach) at 0.01 bar and 25 °C obtained for Str2 of MIL-120(Al) from GCMC calculations, as viewed from two directions. The black outer box delimits the SB (4×2×5) and the blue-dashed inner box delimits the UC. The framework atoms outside the SB are only drawn for visual completion of the periodic structure. Colour code for framework atoms: Al (blue); O (red); C (brown); H (white). Colour code for the C atoms from CH_4 (UA): C (orange). CH_4 atoms (UA) are drawn on a 1:8 radii scale relative to framework atoms. Density map generated from the combined snapshots of GCMC simulations collected every 100 cycles of the production run. Structure drawing and density maps produced by VMD 1.9.4[S37].

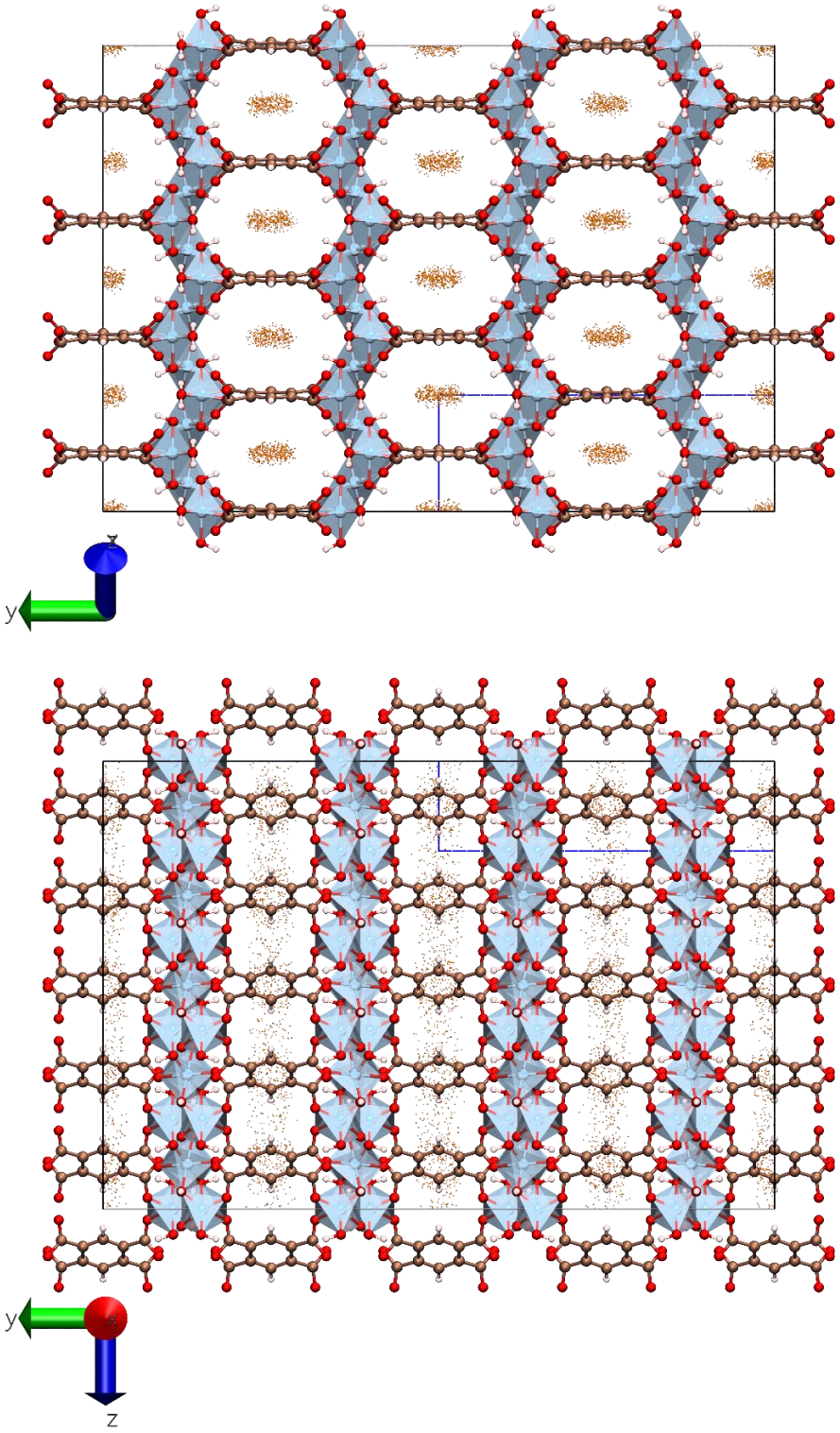

Figure S18. Density map of the single-component adsorption of CH_4 (UA approach) at 0.1 bar and 25 °C obtained for Str2 of MIL-120(Al) from GCMC calculations, as viewed from two directions. The black outer box delimits the SB (4×2×5) and the blue-dashed inner box delimits the UC. The framework atoms outside the SB are only drawn for visual completion of the periodic structure. Colour code for framework atoms: Al (blue); O (red); C (brown); H (white). Colour code for the C atoms from CH_4 (UA): C (orange). CH_4 atoms (UA) are drawn on a 1:8 radii scale relative to framework atoms. Density map generated from the combined snapshots of GCMC simulations collected every 100 cycles of the production run. Structure drawing and density maps produced by VMD 1.9.4[S37].

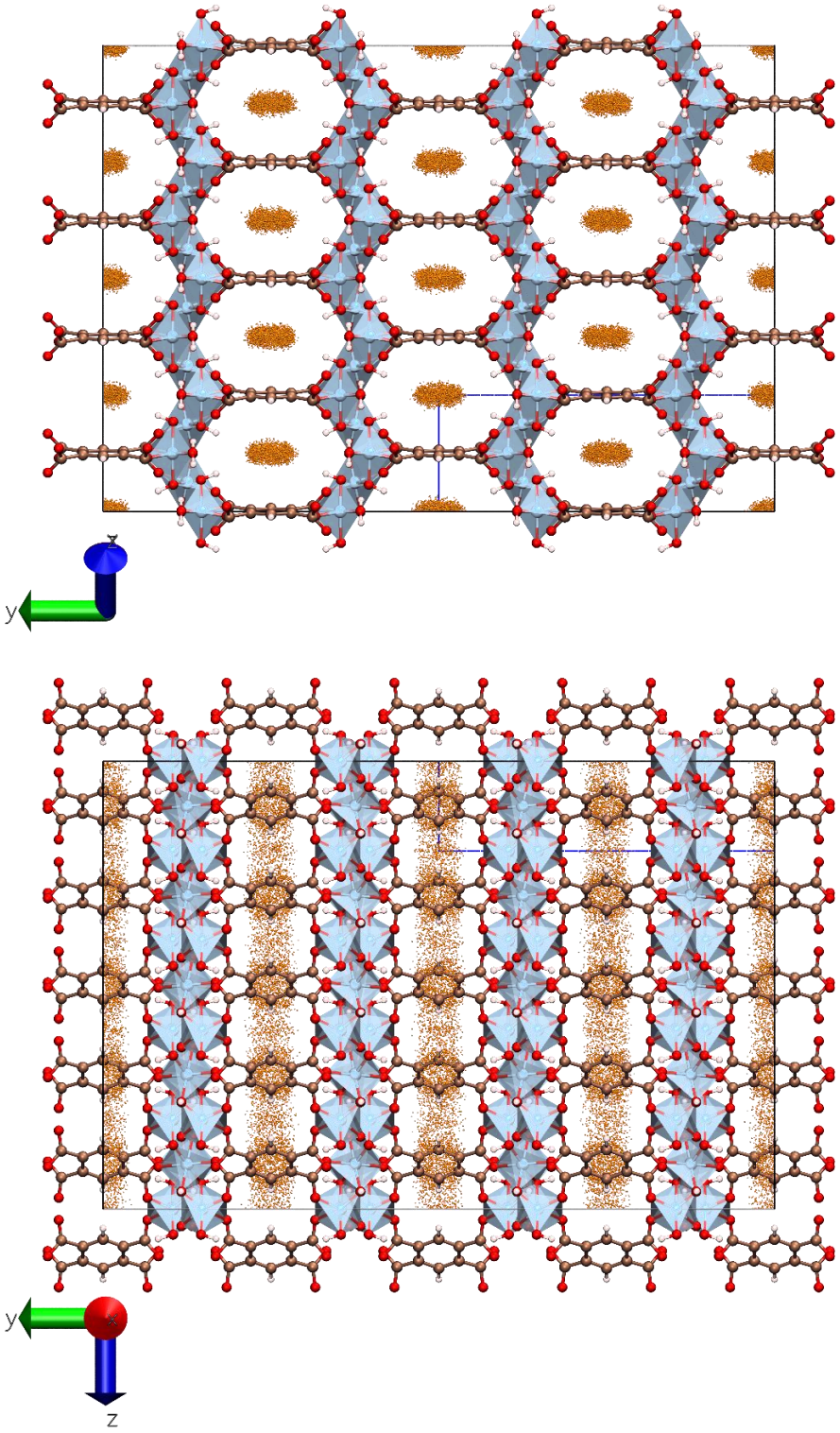

Figure S19. Density map of the single-component adsorption of CH_4 (UA approach) at 1 bar and 25 °C obtained for Str2 of MIL-120(Al) from GCMC calculations, as viewed from two directions. The black outer box delimits the SB (4×2×5) and the blue-dashed inner box delimits the UC. The framework atoms outside the SB are only drawn for visual completion of the periodic structure. Colour code for framework atoms: Al (blue); O (red); C (brown); H (white). Colour code for the C atoms from CH_4 (UA): C (orange). CH_4 atoms (UA) are drawn on a 1:8 radii scale relative to framework atoms. Density map generated from the combined snapshots of GCMC simulations collected every 100 cycles of the production run. Structure drawing and density maps produced by VMD 1.9.4[S37].

MIL-120(Al), Str2, C atoms (CH_4 – UA), 25 °C, 10 bar

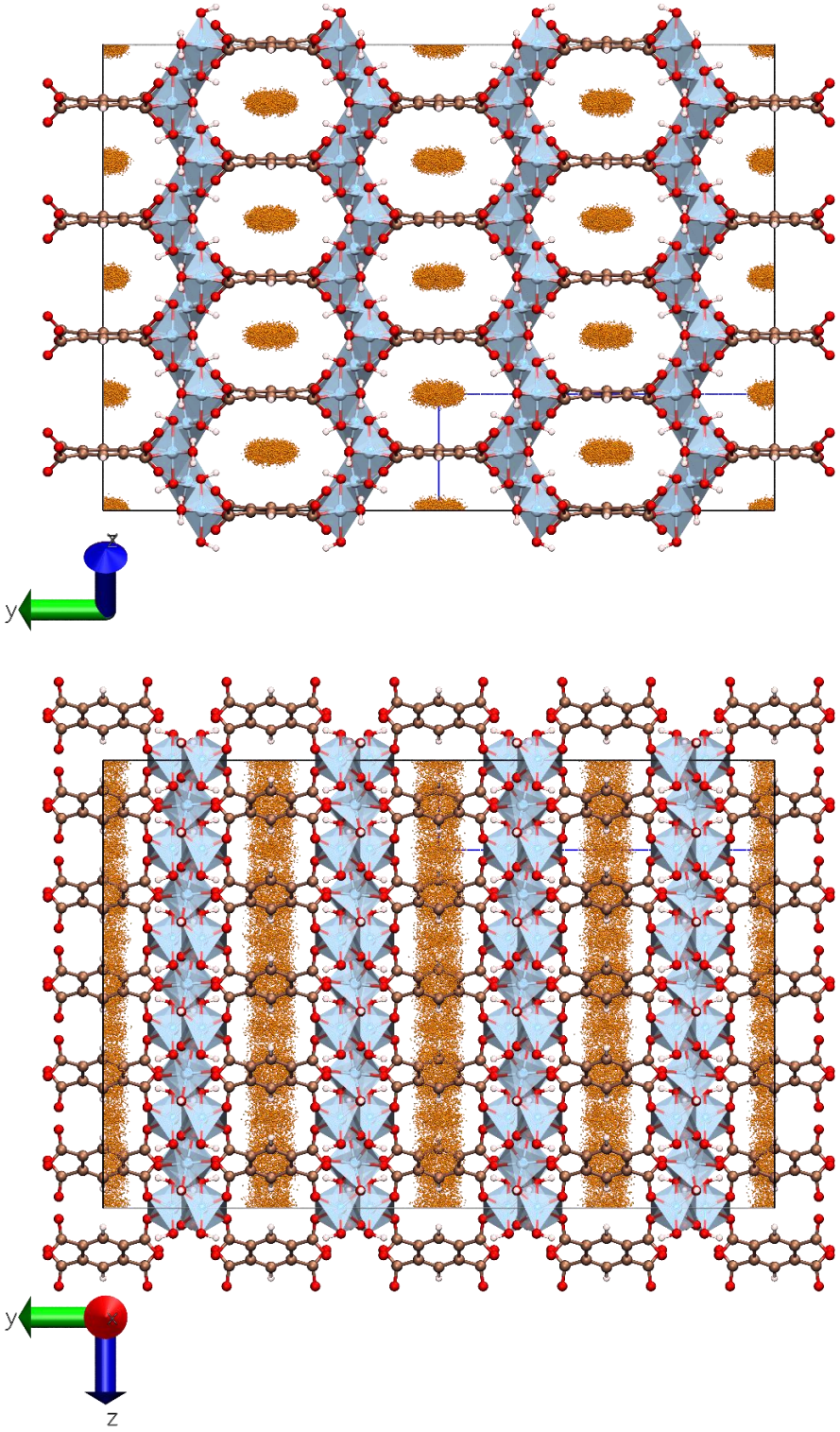

Figure S20. Density map of the single-component adsorption of CH_4 (UA approach) at 10 bar and 25 °C obtained for Str2 of MIL-120(Al) from GCMC calculations, as viewed from two directions. The black outer box delimits the SB (4×2×5) and the blue-dashed inner box delimits the UC. The framework atoms outside the SB are only drawn for visual completion of the periodic structure. Colour code for framework atoms: Al (blue); O (red); C (brown); H (white). Colour code for the C atoms from CH_4 (UA): C (orange). CH_4 atoms (UA) are drawn on a 1:8 radii scale relative to framework atoms. Density map generated from the combined snapshots of GCMC simulations collected every 100 cycles of the production run. Structure drawing and density maps produced by VMD 1.9.4[S37].

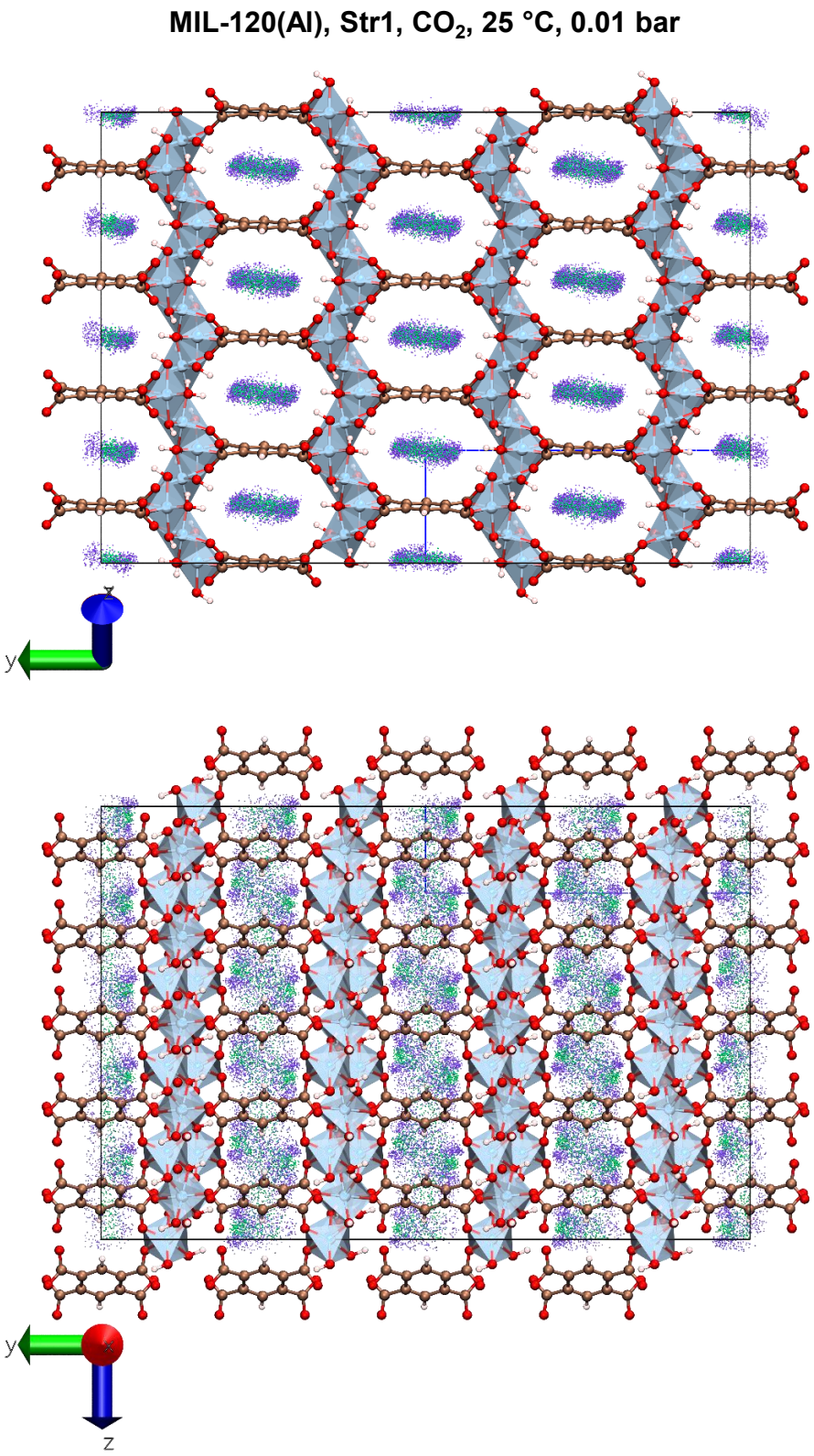

Figure S21. Density map of the single-component adsorption of CO_2 at 0.01 bar and 25 °C obtained for Str1 of MIL-120(Al) from GCMC calculations, as viewed from two directions. The black outer box delimits the SB (4×2×5) and the blue-dashed inner box delimits the UC. The framework atoms outside the SB are only drawn for visual completion of the periodic structure. Colour code for framework atoms: Al (blue); O (red); C (brown); H (white). Colour code for CO_2 atoms: C (green); O (violet). CO_2 atoms are drawn without bonds and on a 1:8 radii scale relative to framework atoms. Density map generated from the combined snapshots of GCMC simulations collected every 100 cycles of the production run. Structure drawing and density maps produced by VMD 1.9.4[S37].

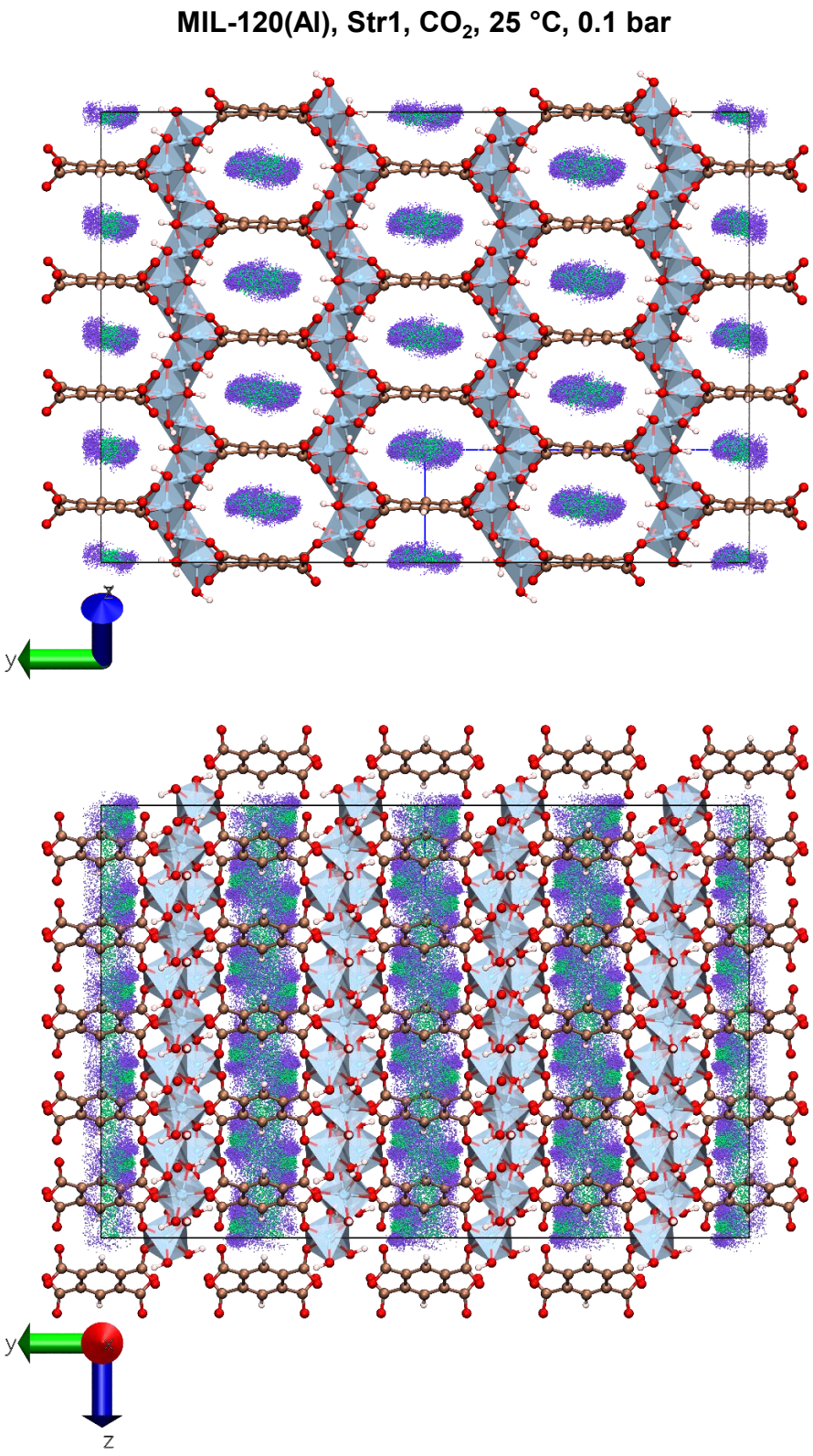

Figure S22. Density map of the single-component adsorption of CO_2 at 0.1 bar and 25 °C obtained for Str1 of MIL-120(Al) from GCMC calculations, as viewed from two directions. The black outer box delimits the SB (4×2×5) and the blue-dashed inner box delimits the UC. The framework atoms outside the SB are only drawn for visual completion of the periodic structure. Colour code for framework atoms: Al (blue); O (red); C (brown); H (white). Colour code for CO_2 atoms: C (green); O (violet). CO_2 atoms are drawn without bonds and on a 1:8 radii scale relative to framework atoms. Density map generated from the combined snapshots of GCMC simulations collected every 100 cycles of the production run. Structure drawing and density maps produced by VMD 1.9.4[S37].

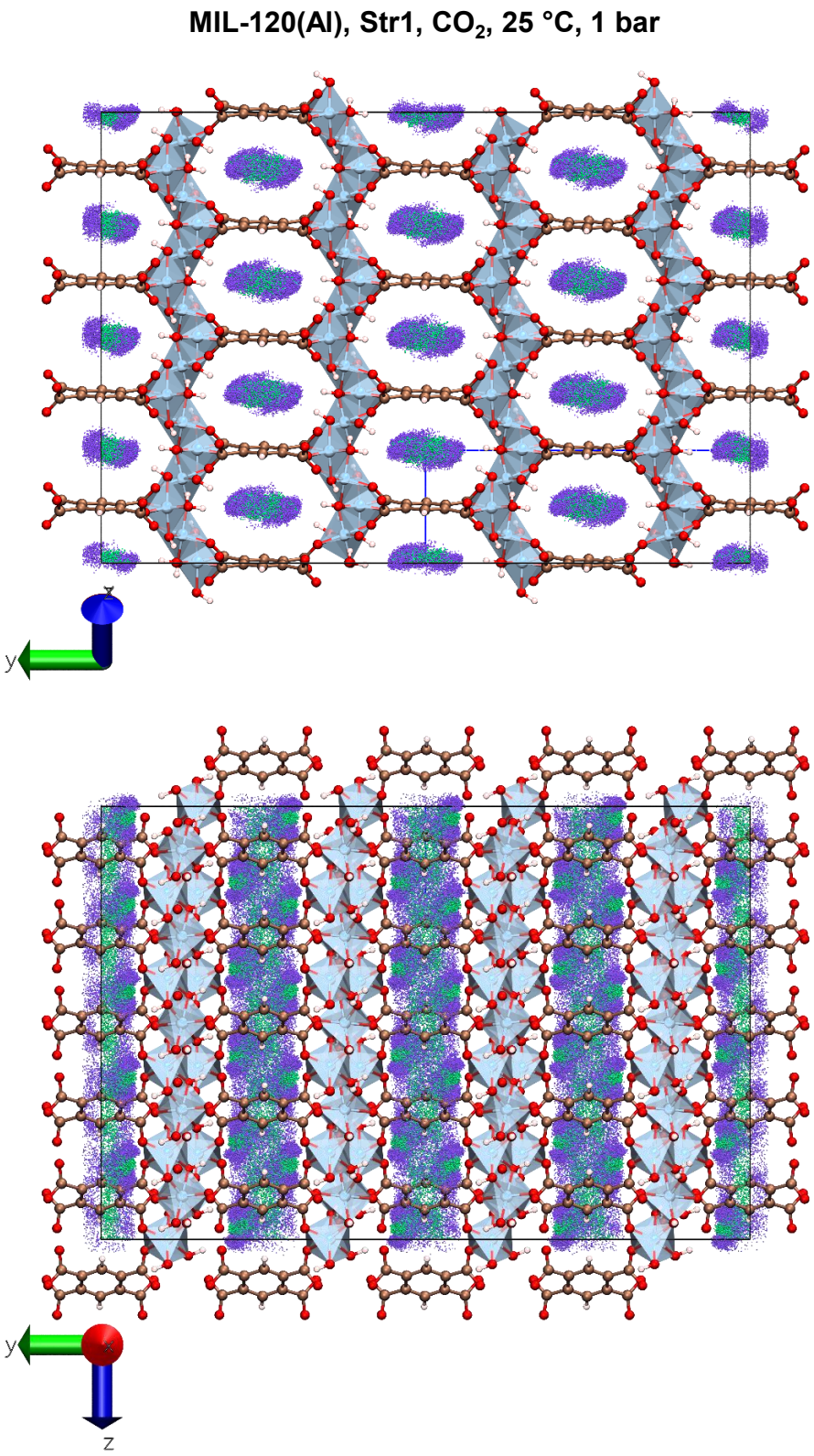

Figure S23. Density map of the single-component adsorption of CO_2 at 1 bar and 25 °C obtained for Str1 of MIL-120(Al) from GCMC calculations, as viewed from two directions. The black outer box delimits the SB (4×2×5) and the blue-dashed inner box delimits the UC. The framework atoms outside the SB are only drawn for visual completion of the periodic structure. Colour code for framework atoms: Al (blue); O (red); C (brown); H (white). Colour code for CO_2 atoms: C (green); O (violet). CO_2 atoms are drawn without bonds and on a 1:8 radii scale relative to framework atoms. Density map generated from the combined snapshots of GCMC simulations collected every 100 cycles of the production run. Structure drawing and density maps produced by VMD 1.9.4[S37].

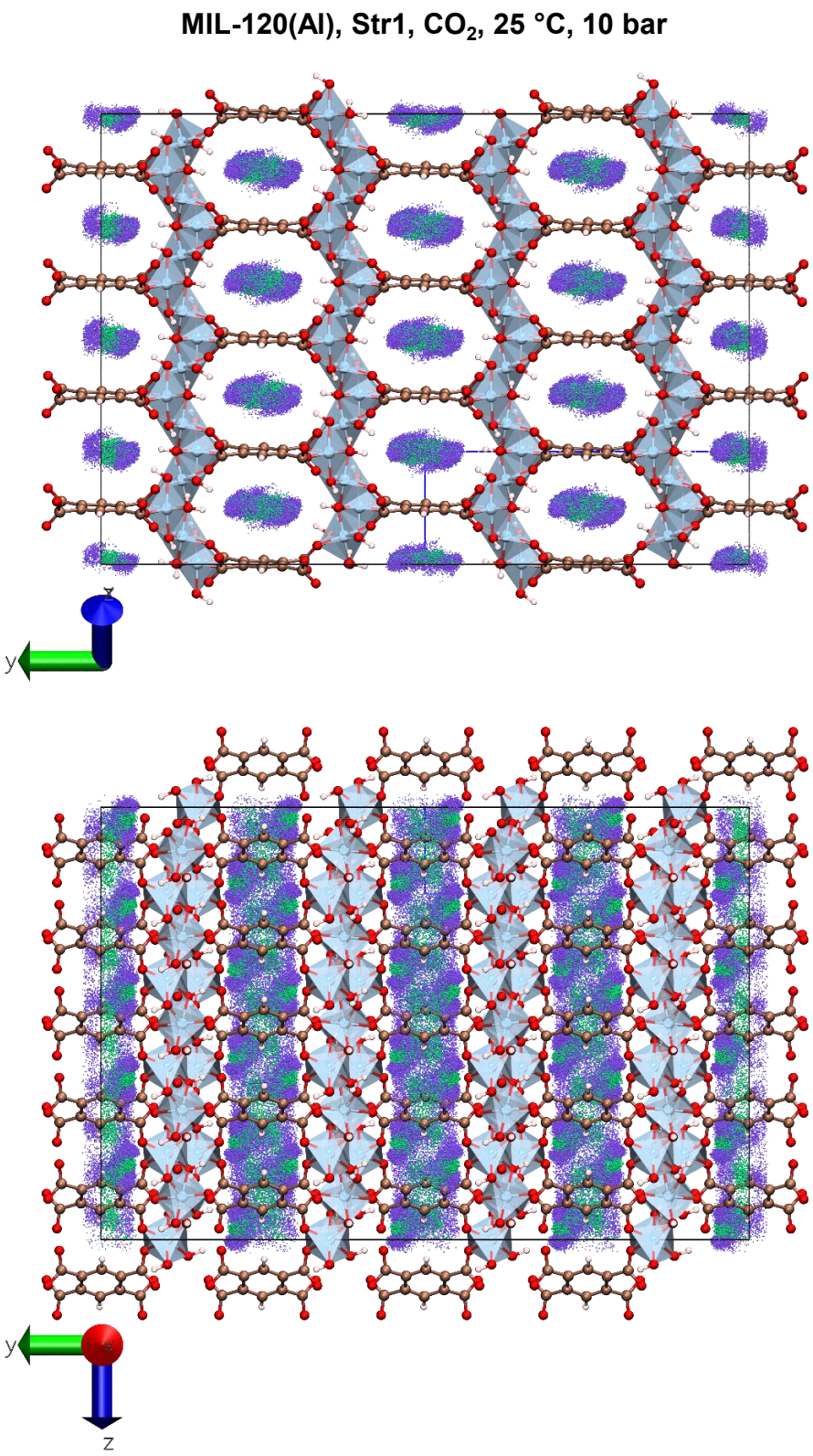

Figure S24. Density map of the single-component adsorption of CO_2 at 10 bar and 25 °C obtained for Str1 of MIL-120(Al) from GCMC calculations, as viewed from two directions. The black outer box delimits the SB (4×2×5) and the blue-dashed inner box delimits the UC. The framework atoms outside the SB are only drawn for visual completion of the periodic structure. Colour code for framework atoms: Al (blue); O (red); C (brown); H (white). Colour code for CO_2 atoms: C (green); O (violet). CO_2 atoms are drawn without bonds and on a 1:8 radii scale relative to framework atoms. Density map generated from the combined snapshots of GCMC simulations collected every 100 cycles of the production run. Structure drawing and density maps produced by VMD 1.9.4[S37].

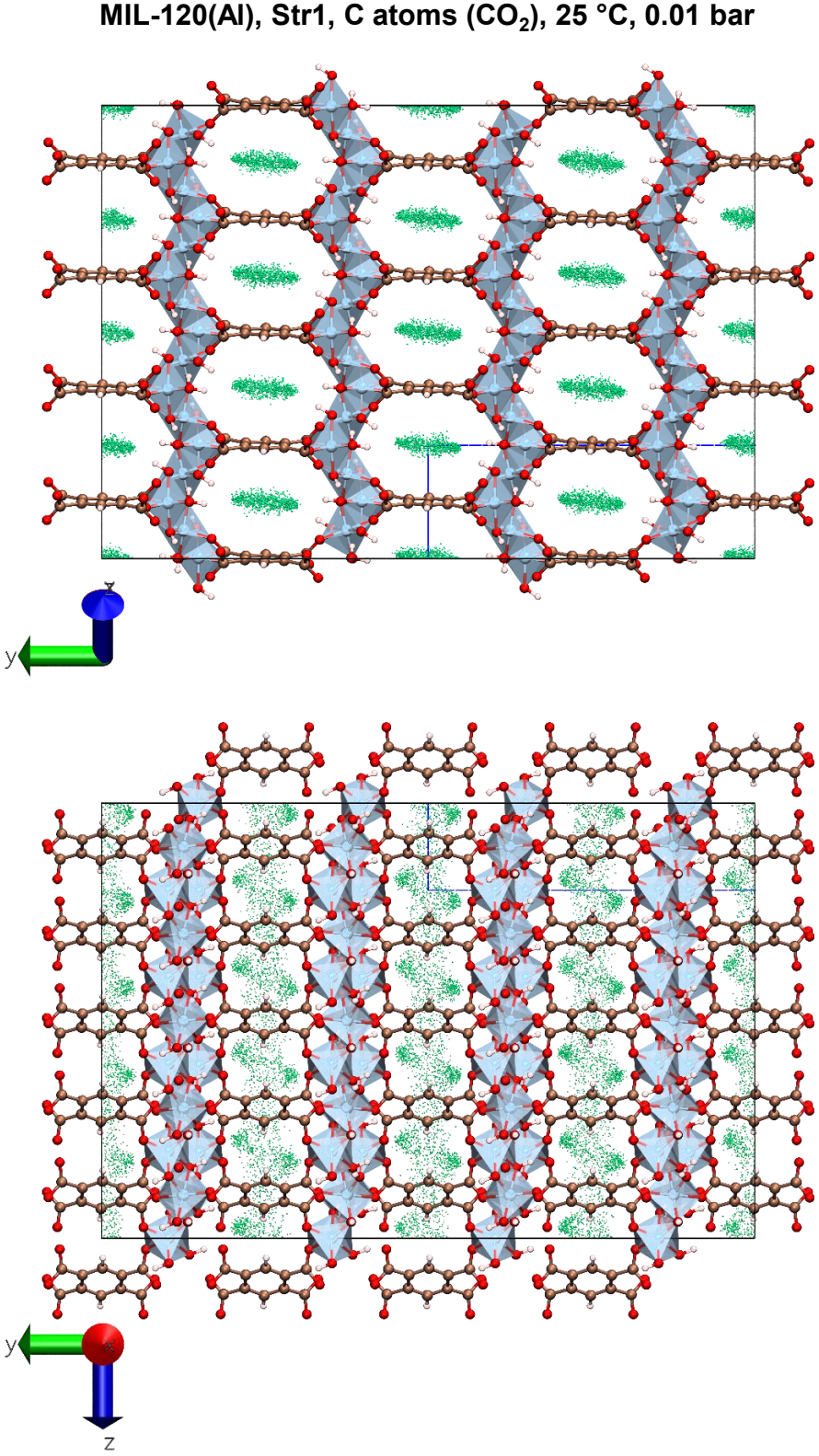

Figure S25. Density map of the single-component adsorption of CO_2 at 0.01 bar and 25 °C obtained for Str1 of MIL-120(Al) from GCMC calculations, showing only the C atoms of CO_2, as viewed from two directions. The black outer box delimits the SB (4×2×5) and the blue-dashed inner box delimits the UC. The framework atoms outside the SB are only drawn for visual completion of the periodic structure. Colour code for framework atoms: Al (blue); O (red); C (brown); H (white). Colour code for the C atoms from CO_2: C (green). C atoms from CO_2 are drawn on a 1:8 radii scale relative to framework atoms. Density map generated from the combined snapshots of GCMC simulations collected every 100 cycles of the production run. Structure drawing and density maps produced by VMD 1.9.4[S37].

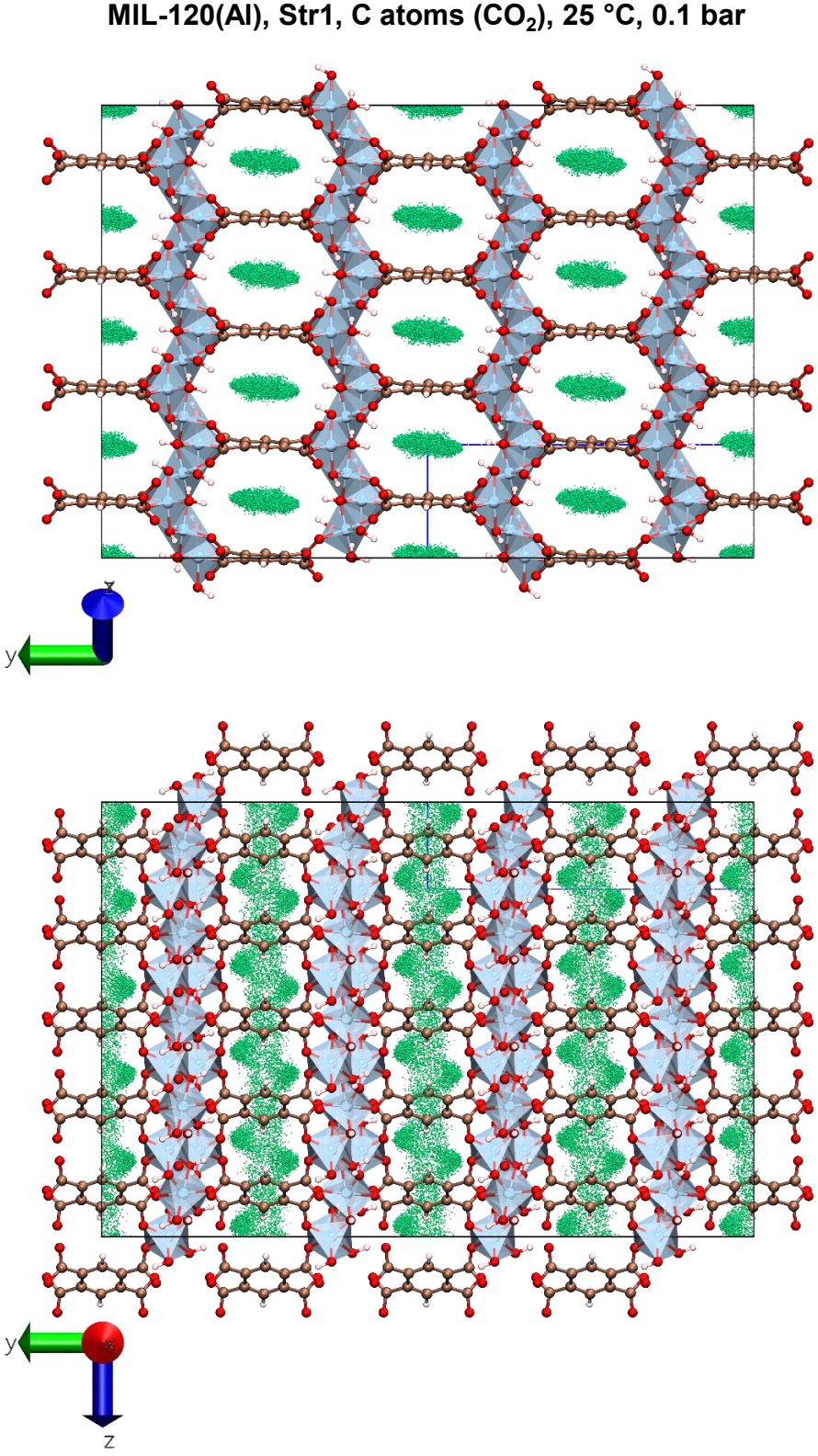

Figure S26. Density map of the single-component adsorption of CO_2 at 0.1 bar and 25 °C obtained for Str1 of MIL-120(Al) from GCMC calculations, showing only the C atoms of CO_2, as viewed from two directions. The black outer box delimits the SB (4×2×5) and the blue-dashed inner box delimits the UC. The framework atoms outside the SB are only drawn for visual completion of the periodic structure. Colour code for framework atoms: Al (blue); O (red); C (brown); H (white). Colour code for the C atoms from CO_2: C (green). C atoms from CO_2 are drawn on a 1:8 radii scale relative to framework atoms. Density map generated from the combined snapshots of GCMC simulations collected every 100 cycles of the production run. Structure drawing and density maps produced by VMD 1.9.4[S37].

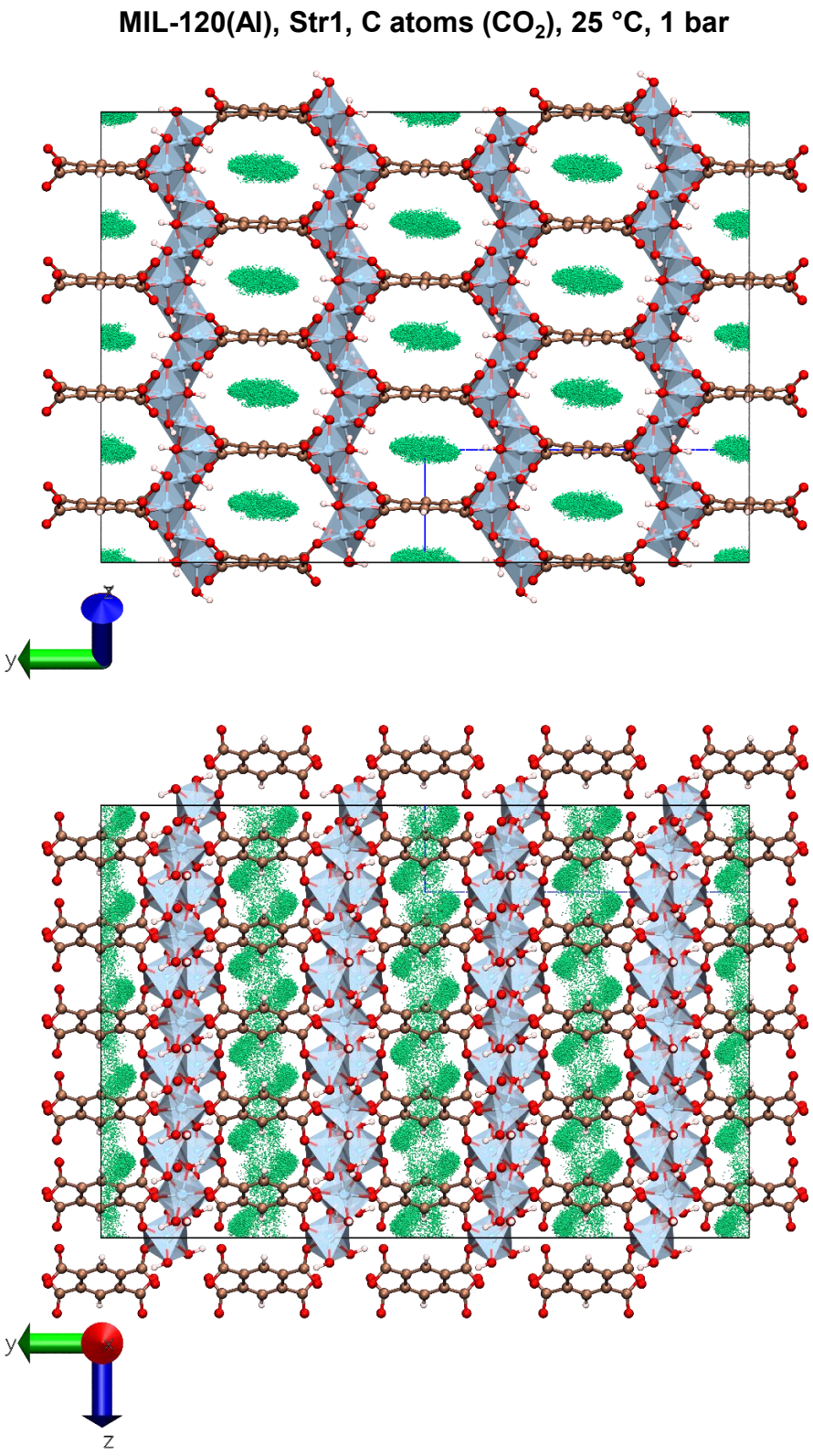

Figure S27. Density map of the single-component adsorption of CO_2 at 1 bar and 25 °C obtained for Str1 of MIL-120(Al) from GCMC calculations, showing only the C atoms of CO_2, as viewed from two directions. The black outer box delimits the SB (4×2×5) and the blue-dashed inner box delimits the UC. The framework atoms outside the SB are only drawn for visual completion of the periodic structure. Colour code for framework atoms: Al (blue); O (red); C (brown); H (white). Colour code for the C atoms from CO_2: C (green). C atoms from CO_2 are drawn on a 1:8 radii scale relative to framework atoms. Density map generated from the combined snapshots of GCMC simulations collected every 100 cycles of the production run. Structure drawing and density maps produced by VMD 1.9.4[S37].

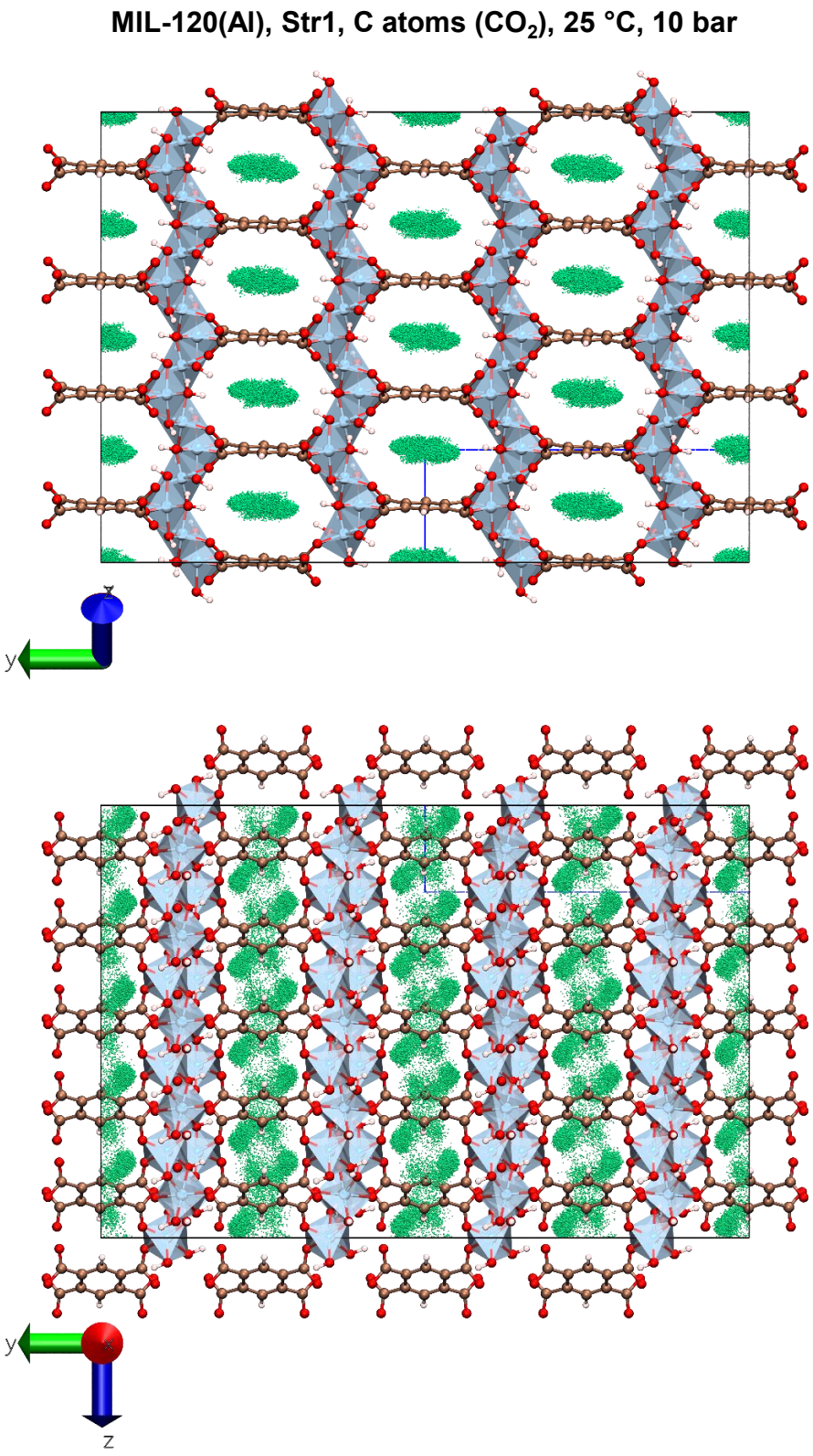

Figure S28. Density map of the single-component adsorption of CO_2 at 10 bar and 25 °C obtained for Str1 of MIL-120(Al) from GCMC calculations, showing only the C atoms of CO_2, as viewed from two directions. The black outer box delimits the SB (4×2×5) and the blue-dashed inner box delimits the UC. The framework atoms outside the SB are only drawn for visual completion of the periodic structure. Colour code for framework atoms: Al (blue); O (red); C (brown); H (white). Colour code for the C atoms from CO_2: C (green). C atoms from CO_2 are drawn on a 1:8 radii scale relative to framework atoms. Density map generated from the combined snapshots of GCMC simulations collected every 100 cycles of the production run. Structure drawing and density maps produced by VMD 1.9.4[S37].

MIL-120(Al), Str1, C atoms (CH_4 – UA), 25 °C, 0.01 bar

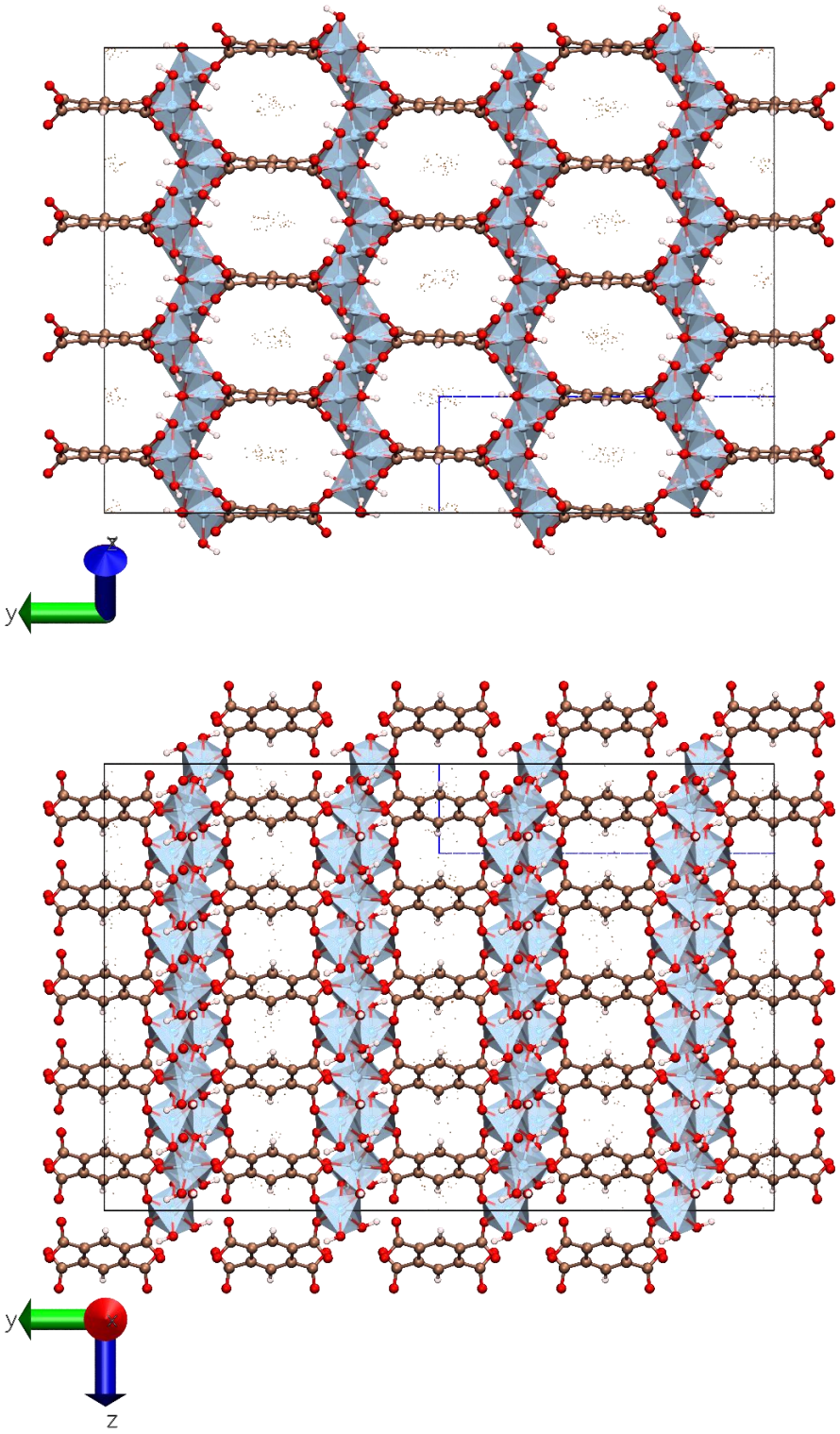

Figure S29. Density map of the single-component adsorption of CH_4 (UA approach) at 0.01 bar and 25 °C obtained for Str1 of MIL-120(Al) from GCMC calculations, as viewed from two directions. The black outer box delimits the SB (4×2×5) and the blue-dashed inner box delimits the UC. The framework atoms outside the SB are only drawn for visual completion of the periodic structure. Colour code for framework atoms: Al (blue); O (red); C (brown); H (white). Colour code for the C atoms from CH_4 (UA): C (orange). CH_4 atoms (UA) are drawn on a 1:8 radii scale relative to framework atoms. Density map generated from the combined snapshots of GCMC simulations collected every 100 cycles of the production run. Structure drawing and density maps produced by VMD 1.9.4[S37].

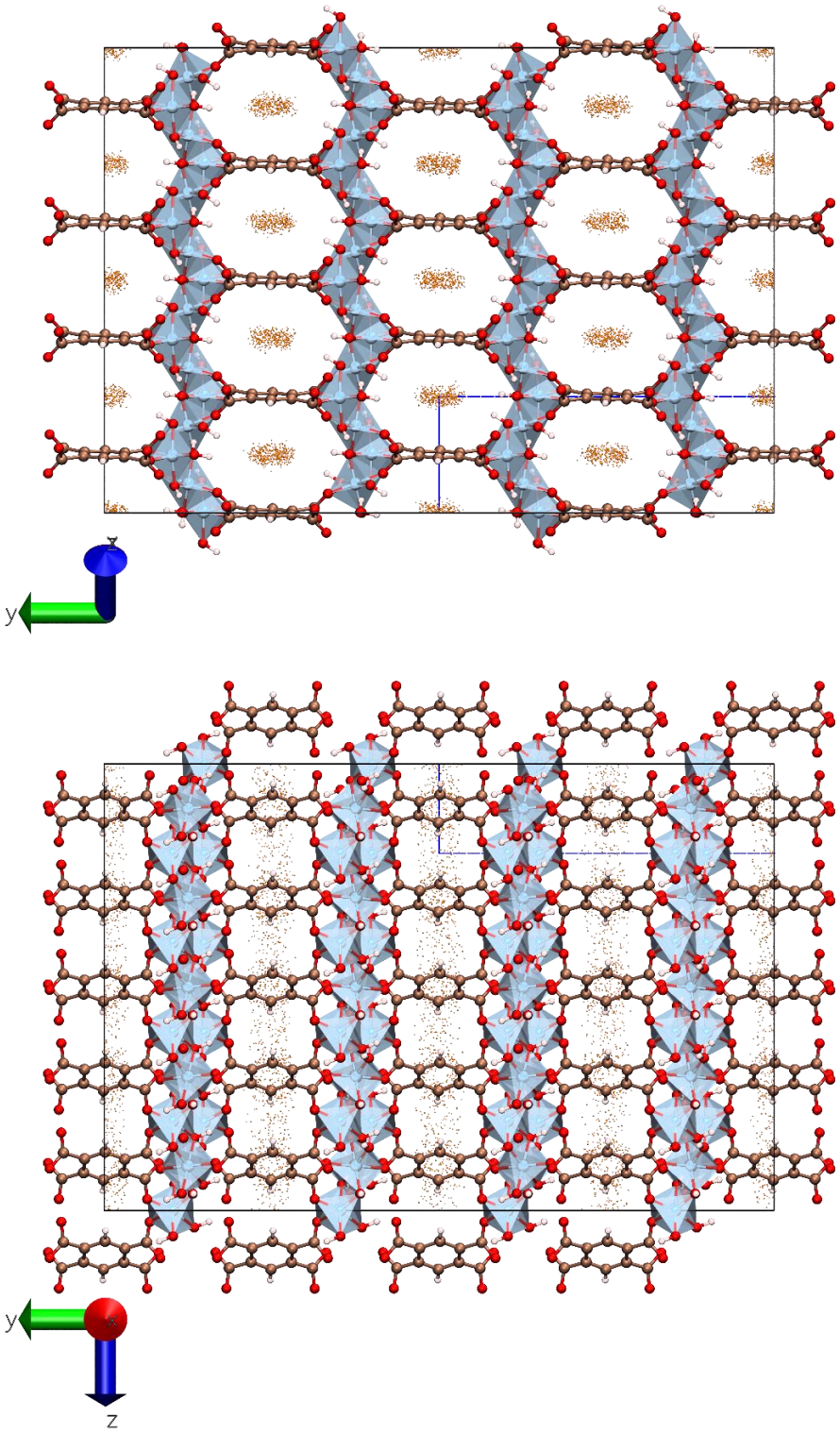

Figure S30. Density map of the single-component adsorption of CH_4 (UA approach) at 0.1 bar and 25 °C obtained for Str1 of MIL-120(Al) from GCMC calculations, as viewed from two directions. The black outer box delimits the SB (4×2×5) and the blue-dashed inner box delimits the UC. The framework atoms outside the SB are only drawn for visual completion of the periodic structure. Colour code for framework atoms: Al (blue); O (red); C (brown); H (white). Colour code for the C atoms from CH_4 (UA): C (orange). CH_4 atoms (UA) are drawn on a 1:8 radii scale relative to framework atoms. Density map generated from the combined snapshots of GCMC simulations collected every 100 cycles of the production run. Structure drawing and density maps produced by VMD 1.9.4[S37].

MIL-120(Al), Str1, C atoms (CH_4 – UA), 25 °C, 1 bar

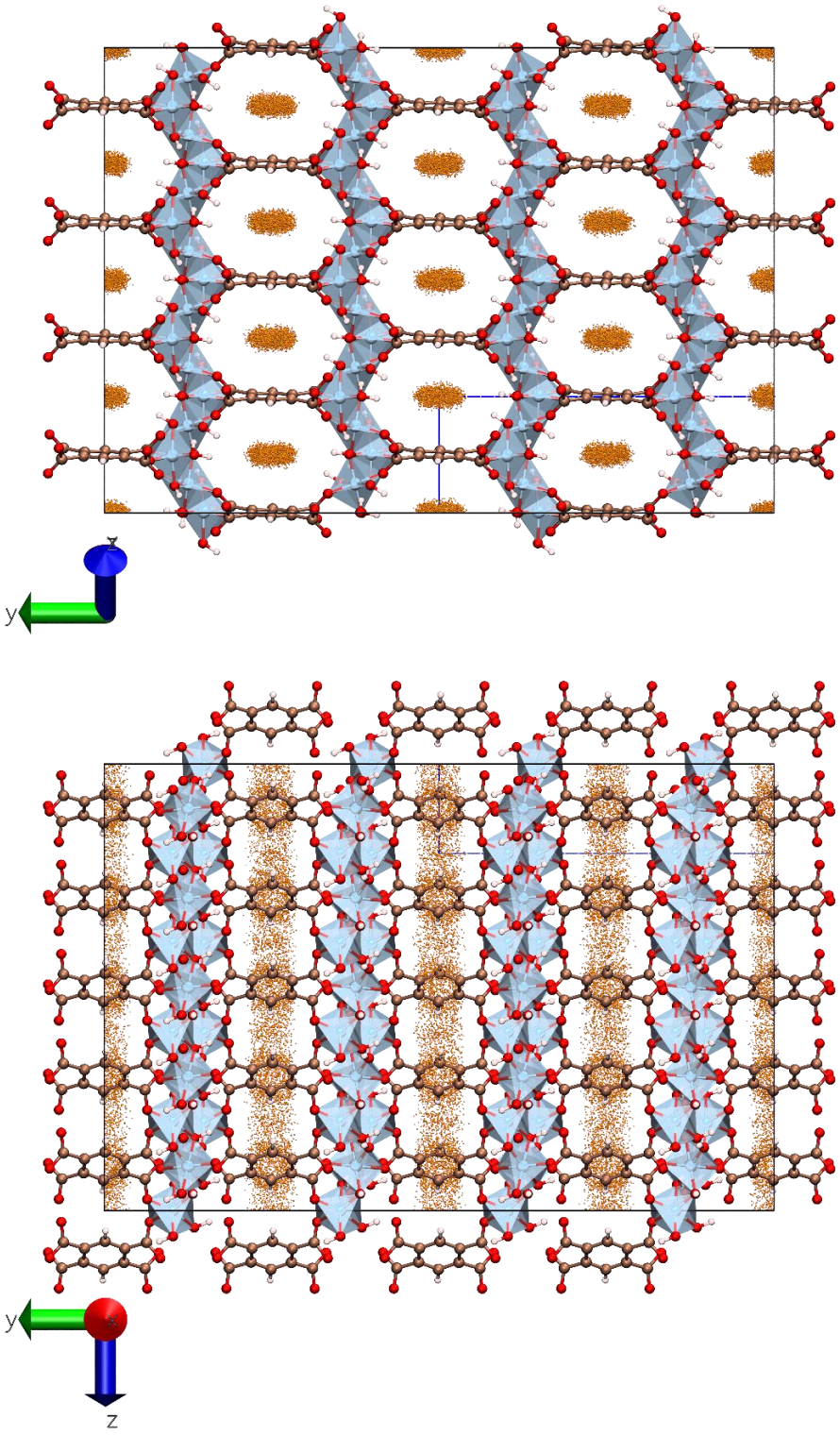

Figure S31. Density map of the single-component adsorption of CH_4 (UA approach) at 1 bar and 25 °C obtained for Str1 of MIL-120(Al) from GCMC calculations, as viewed from two directions. The black outer box delimits the SB (4×2×5) and the blue-dashed inner box delimits the UC. The framework atoms outside the SB are only drawn for visual completion of the periodic structure. Colour code for framework atoms: Al (blue); O (red); C (brown); H (white). Colour code for the C atoms from CH_4 (UA): C (orange). CH_4 atoms (UA) are drawn on a 1:8 radii scale relative to framework atoms. Density map generated from the combined snapshots of GCMC simulations collected every 100 cycles of the production run. Structure drawing and density maps produced by VMD 1.9.4[S37].

MIL-120(Al), Str1, C atoms (CH_4 – UA), 25 °C, 10 bar

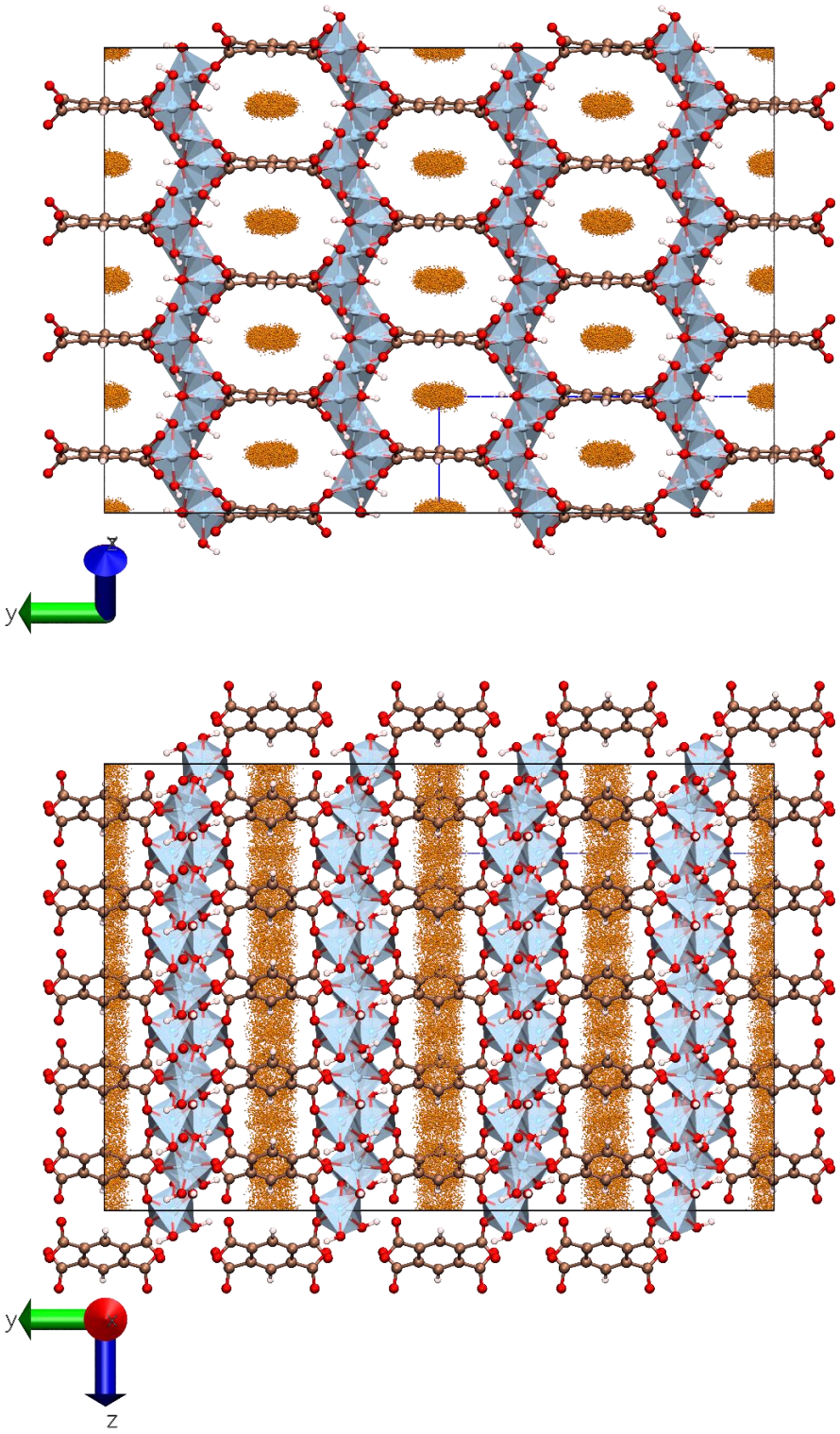

Figure S32. Density map of the single-component adsorption of CH_4 (UA approach) at 10 bar and 25 °C obtained for Str1 of MIL-120(Al) from GCMC calculations, as viewed from two directions. The black outer box delimits the SB (4×2×5) and the blue-dashed inner box delimits the UC. The framework atoms outside the SB are only drawn for visual completion of the periodic structure. Colour code for framework atoms: Al (blue); O (red); C (brown); H (white). Colour code for the C atoms from CH_4 (UA): C (orange). CH_4 atoms (UA) are drawn on a 1:8 radii scale relative to framework atoms. Density map generated from the combined snapshots of GCMC simulations collected every 100 cycles of the production run. Structure drawing and density maps produced by VMD 1.9.4[S37].

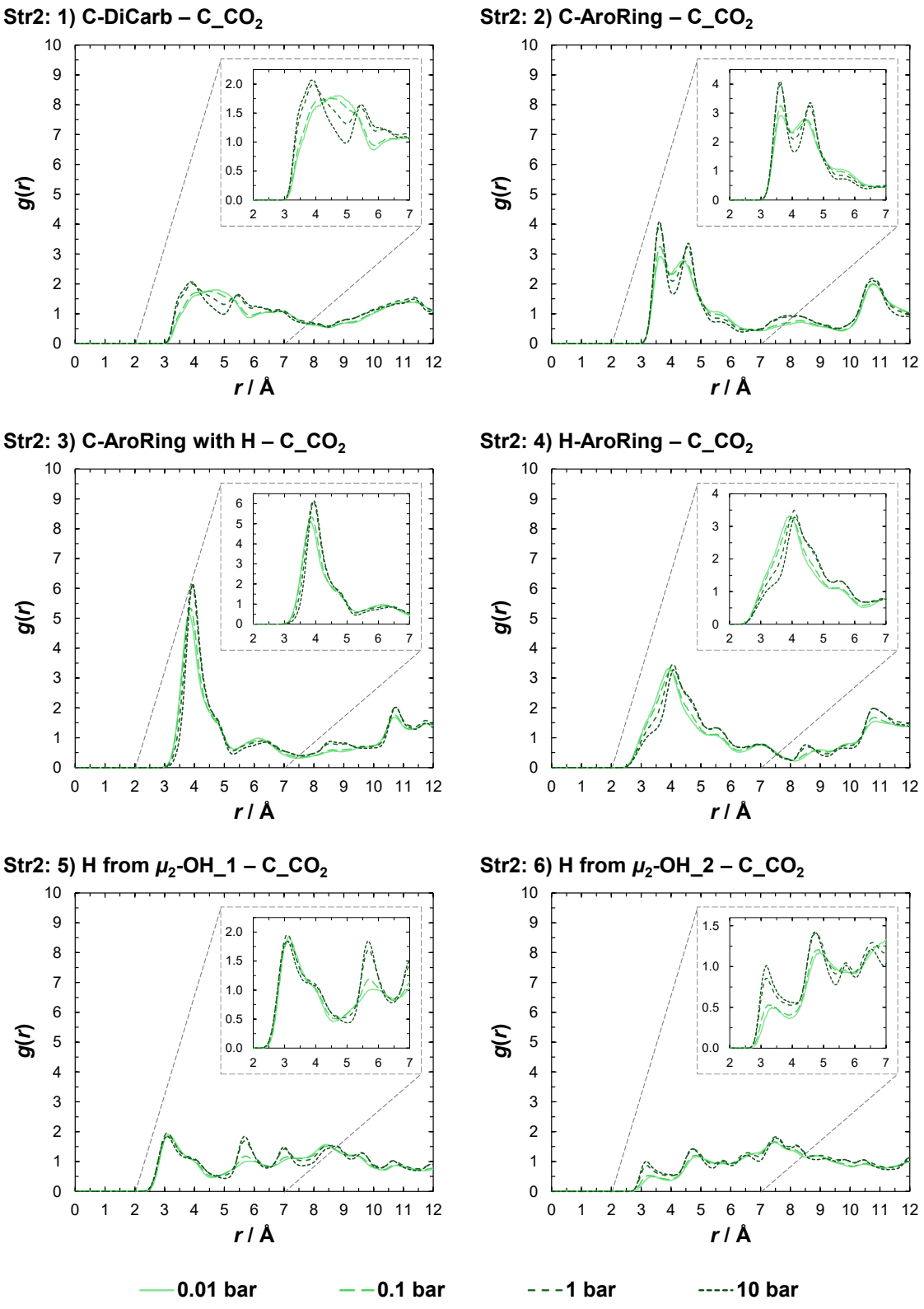

Figure S33. Radial distribution functions (RDFs) of the interaction of atom-types 1 to 6 of structure Str2 of MIL-120(Al) (*cf*. Figure S7 and Table S7) with the C atom of CO_2 in the GCMC-calculated single-component adsorption of CO_2 at 25 °C and 0.01 (full line), 0.1 (long-dashed line), 1 (medium-dashed line) and 10 (short-dashed line) bar. The RDFs have been computed in RASPA[S30] every 100 cycles, with a histogram size of 500 and a range of 12 Å, and represent the average of each atom for the corresponding atom-type.

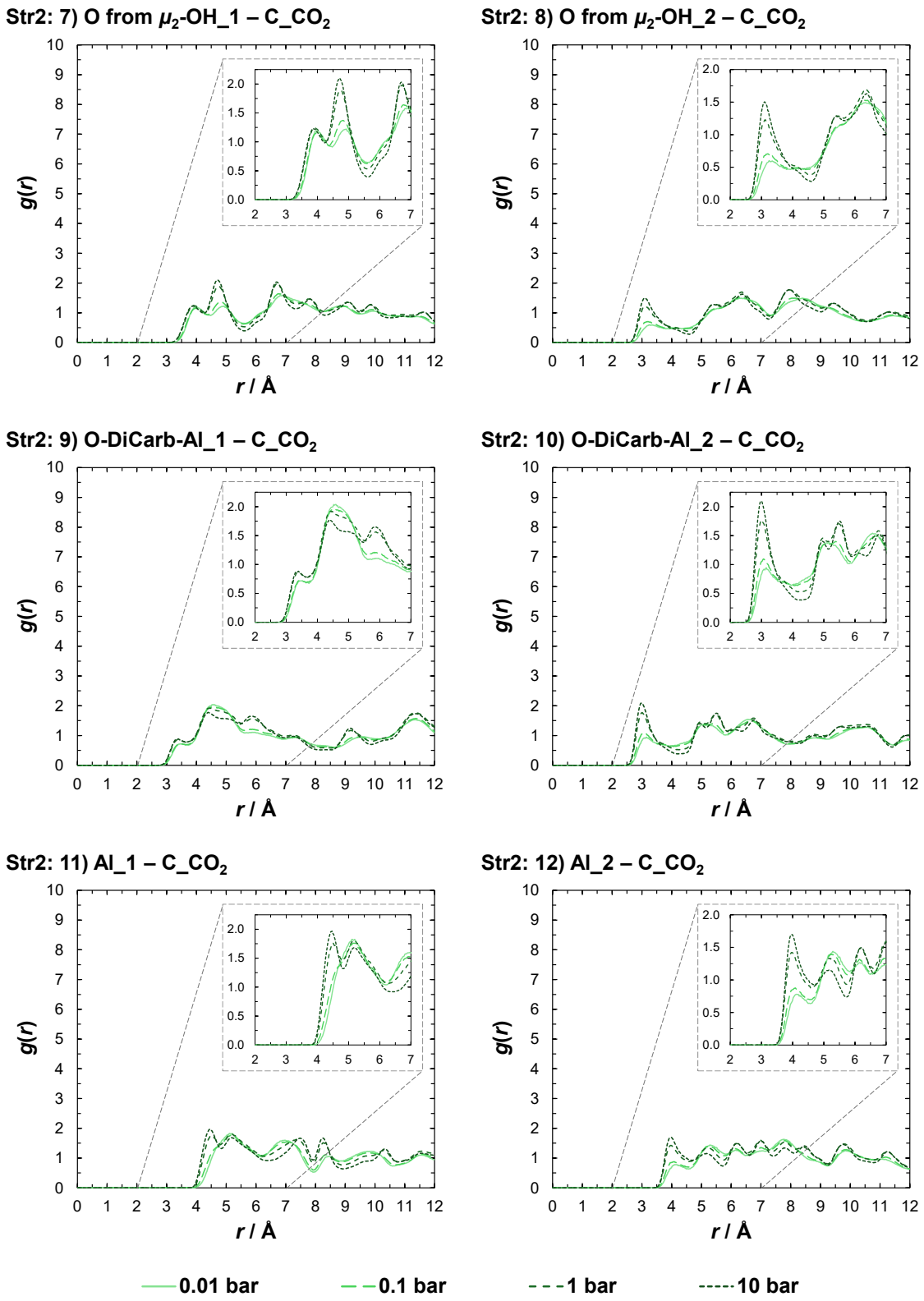

Figure S34. RDFs of the interaction of atom-types 7 to 12 of structure Str2 of MIL-120(Al) (*cf.* Figure S7 and Table S7) with the C atom of CO_2 in the GCMC-calculated single-component adsorption of CO_2 at 25 °C and 0.01 (full line), 0.1 (long-dashed line), 1 (medium-dashed line) and 10 (short-dashed line) bar. The RDFs have been computed in RASPA[S30] every 100 cycles, with a histogram size of 500 and a range of 12 Å, and represent the average of each atom for the corresponding atom-type.

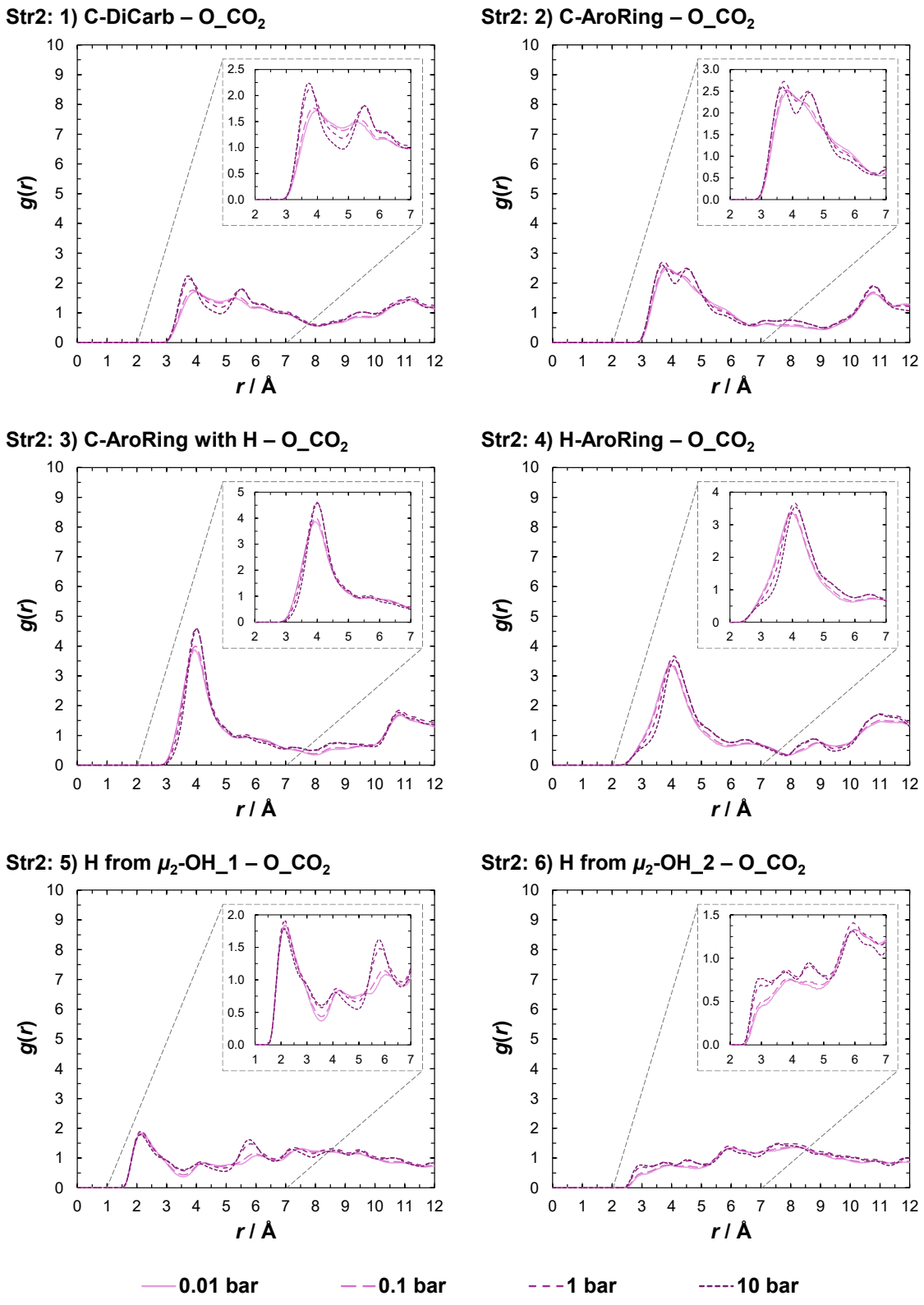

Figure S35. RDFs of the interaction of atom-types 1 to 6 of structure Str2 of MIL-120(Al) (*cf.* Figure S7 and Table S7) with the O atom of CO_2 in the GCMC-calculated single-component adsorption of CO_2 at 25 °C and 0.01 (full line), 0.1 (long-dashed line), 1 (medium-dashed line) and 10 (short-dashed line) bar. The RDFs have been computed in RASPA[S30] every 100 cycles, with a histogram size of 500 and a range of 12 Å, and represent the average of each atom for the corresponding atom-type.

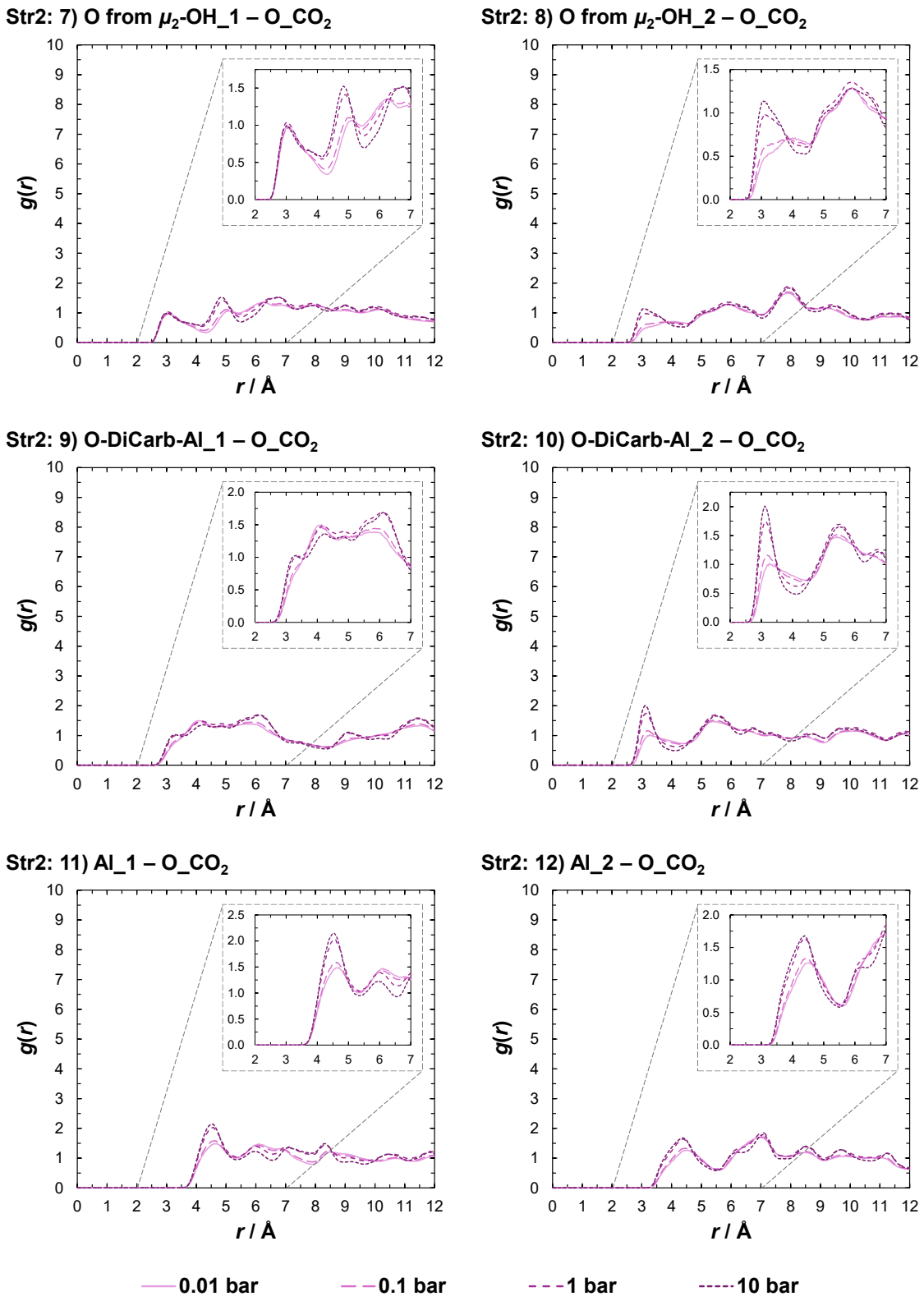

Figure S36. RDFs of the interaction of atom-types 7 to 12 of structure Str2 of MIL-120(Al) (*cf.* Figure S7 and Table S7) with the O atom of CO_2 in the GCMC-calculated single-component adsorption of CO_2 at 25 °C and 0.01 (full line), 0.1 (long-dashed line), 1 (medium-dashed line) and 10 (short-dashed line) bar. The RDFs have been computed in RASPA[S30] every 100 cycles, with a histogram size of 500 and a range of 12 Å, and represent the average of each atom for the corresponding atom-type.

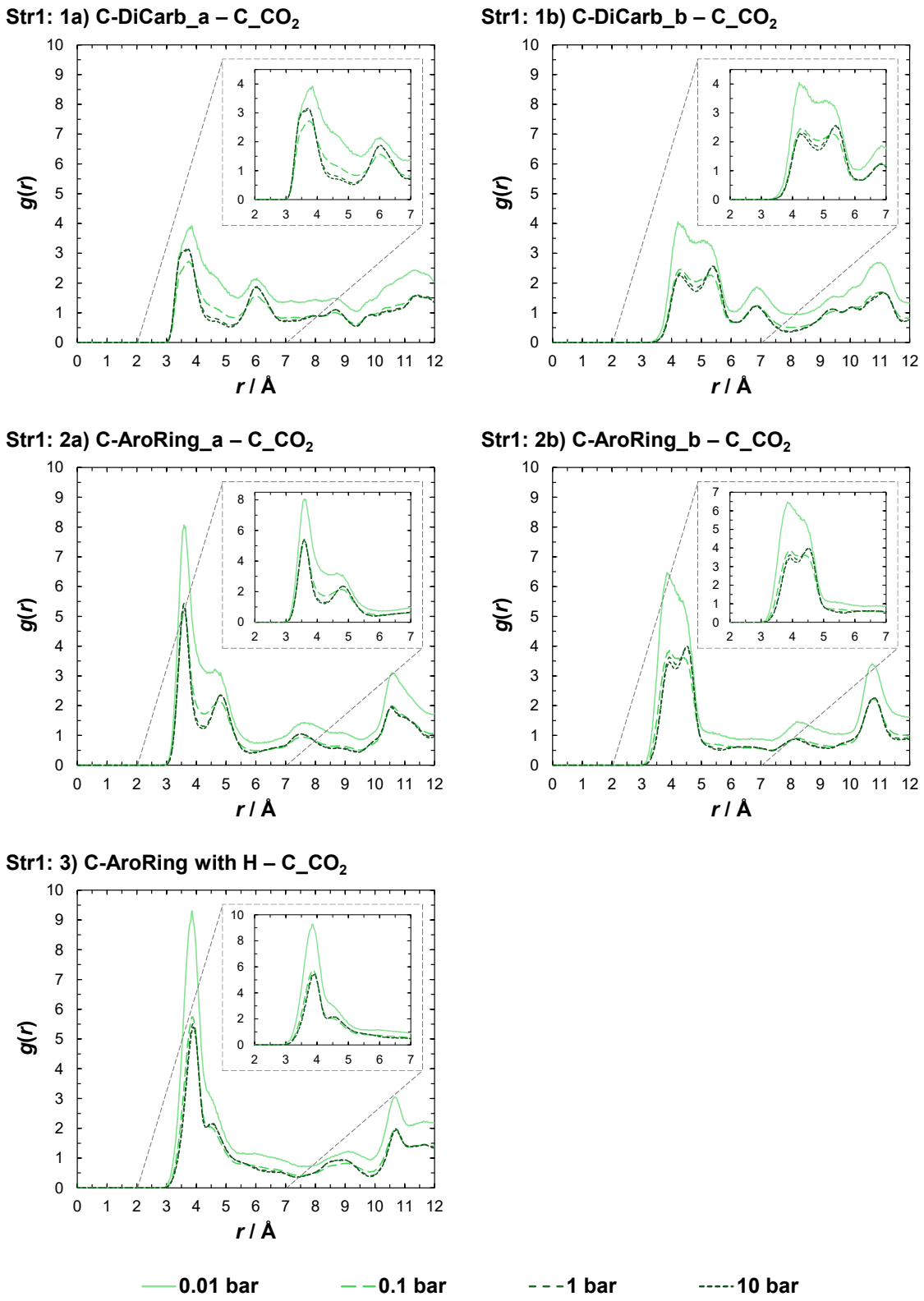

Figure S37. RDFs of the interaction of atom-types 1 to 3 of structure Str1 of MIL-120(Al) (*cf.* Figure S8 and Table S8) with the C atom of CO_2 in the GCMC-calculated single-component adsorption of CO_2 at 25 °C and 0.01 (full line), 0.1 (long-dashed line), 1 (medium-dashed line) and 10 (short-dashed line) bar. The RDFs have been computed in RASPA[S30] every 100 cycles, with a histogram size of 500 and a range of 12 Å, and represent the average of each atom for the corresponding atom-type.

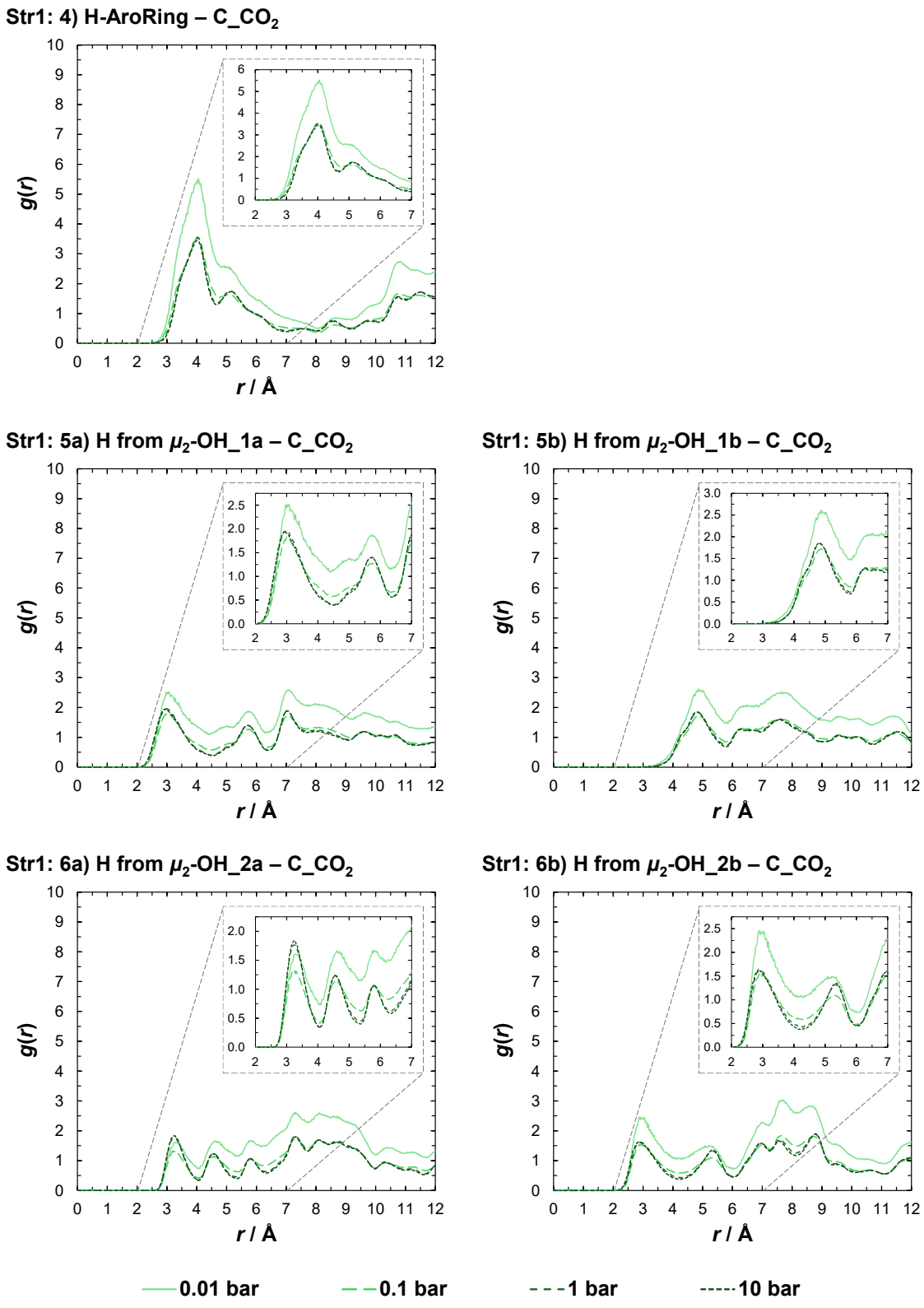

Figure S38. RDFs of the interaction of atom-types 4 to 6 of structure Str1 of MIL-120(Al) (*cf.* Figure S8 and Table S8) with the C atom of CO_2 in the GCMC-calculated single-component adsorption of CO_2 at 25 °C and 0.01 (full line), 0.1 (long-dashed line), 1 (medium-dashed line) and 10 (short-dashed line) bar. The RDFs have been computed in RASPA[S30] every 100 cycles, with a histogram size of 500 and a range of 12 Å, and represent the average of each atom for the corresponding atom-type.

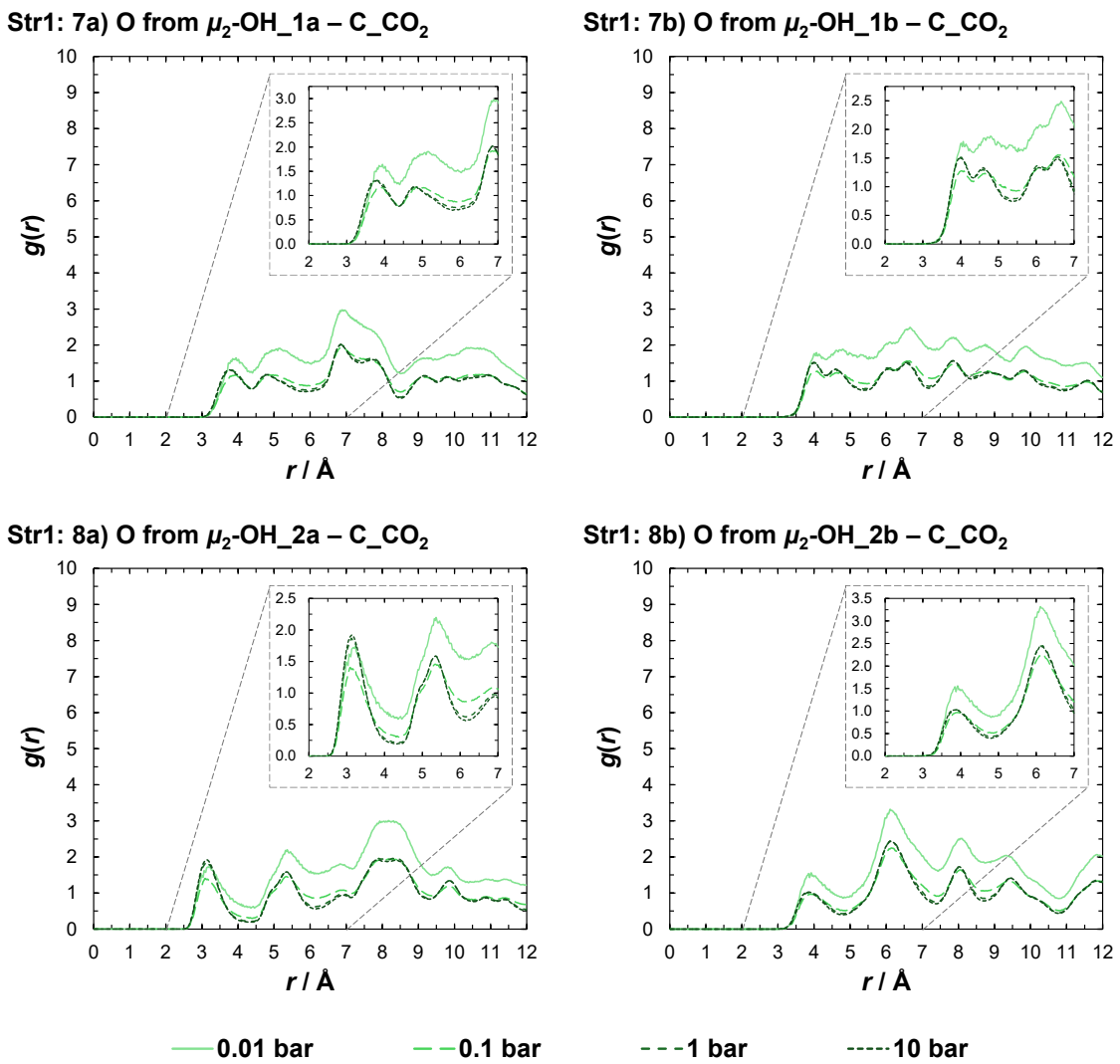

Figure S39. RDFs of the interaction of atom-types 7 and 8 of structure Str1 of MIL-120(Al) (*cf.* Figure S8 and Table S8) with the C atom of CO_2 in the GCMC-calculated single-component adsorption of CO_2 at 25 °C and 0.01 (full line), 0.1 (long-dashed line), 1 (medium-dashed line) and 10 (short-dashed line) bar. The RDFs have been computed in RASPA[S30] every 100 cycles, with a histogram size of 500 and a range of 12 Å, and represent the average of each atom for the corresponding atom-type.

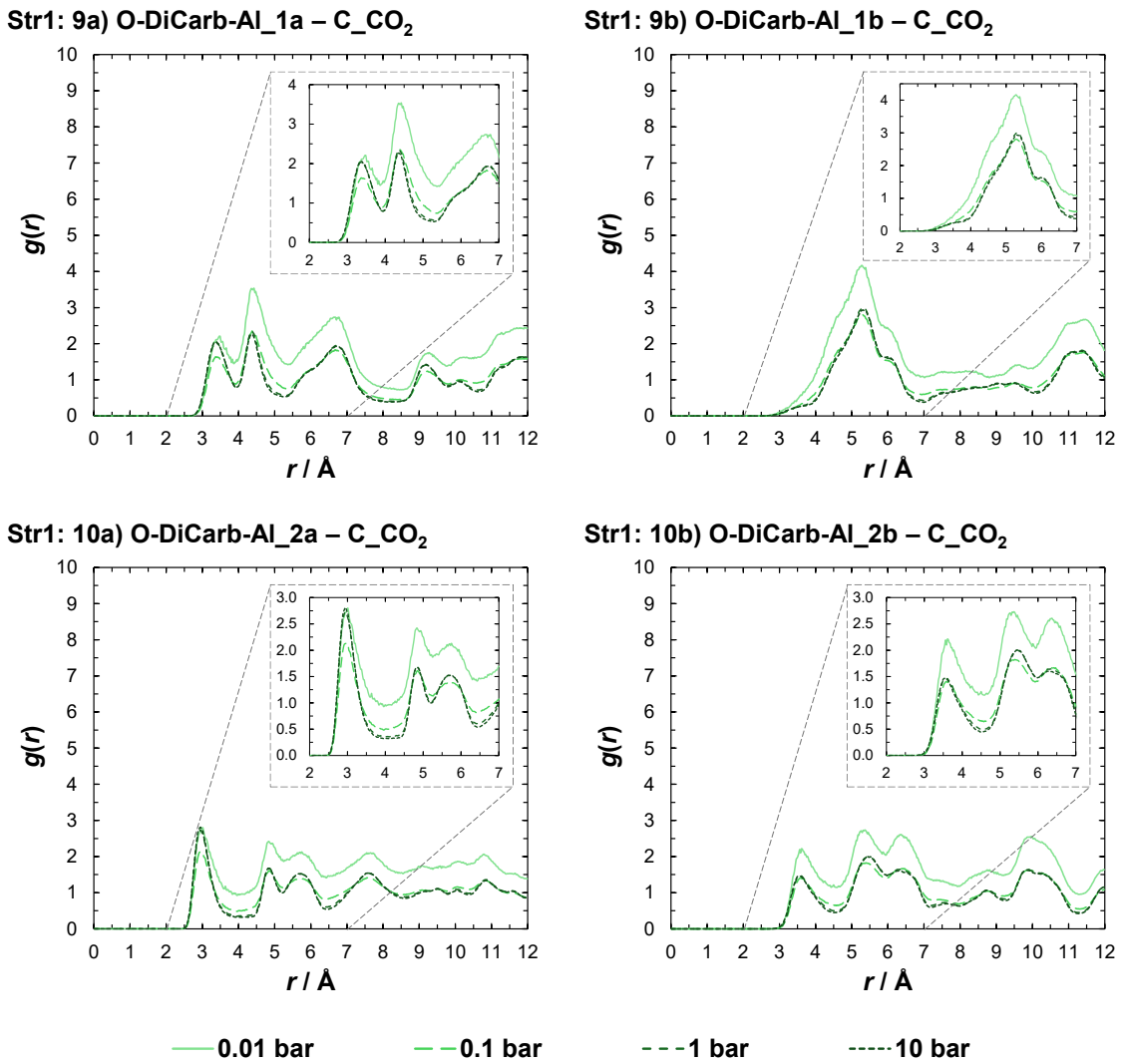

Figure S40. RDFs of the interaction of atom-types 9 and 10 of structure Str1 of MIL-120(Al) (*cf.* Figure S8 and Table S8) with the C atom of CO_2 in the GCMC-calculated single-component adsorption of CO_2 at 25 °C and 0.01 (full line), 0.1 (long-dashed line), 1 (medium-dashed line) and 10 (short-dashed line) bar. The RDFs have been computed in RASPA[S30] every 100 cycles, with a histogram size of 500 and a range of 12 Å, and represent the average of each atom for the corresponding atom-type.

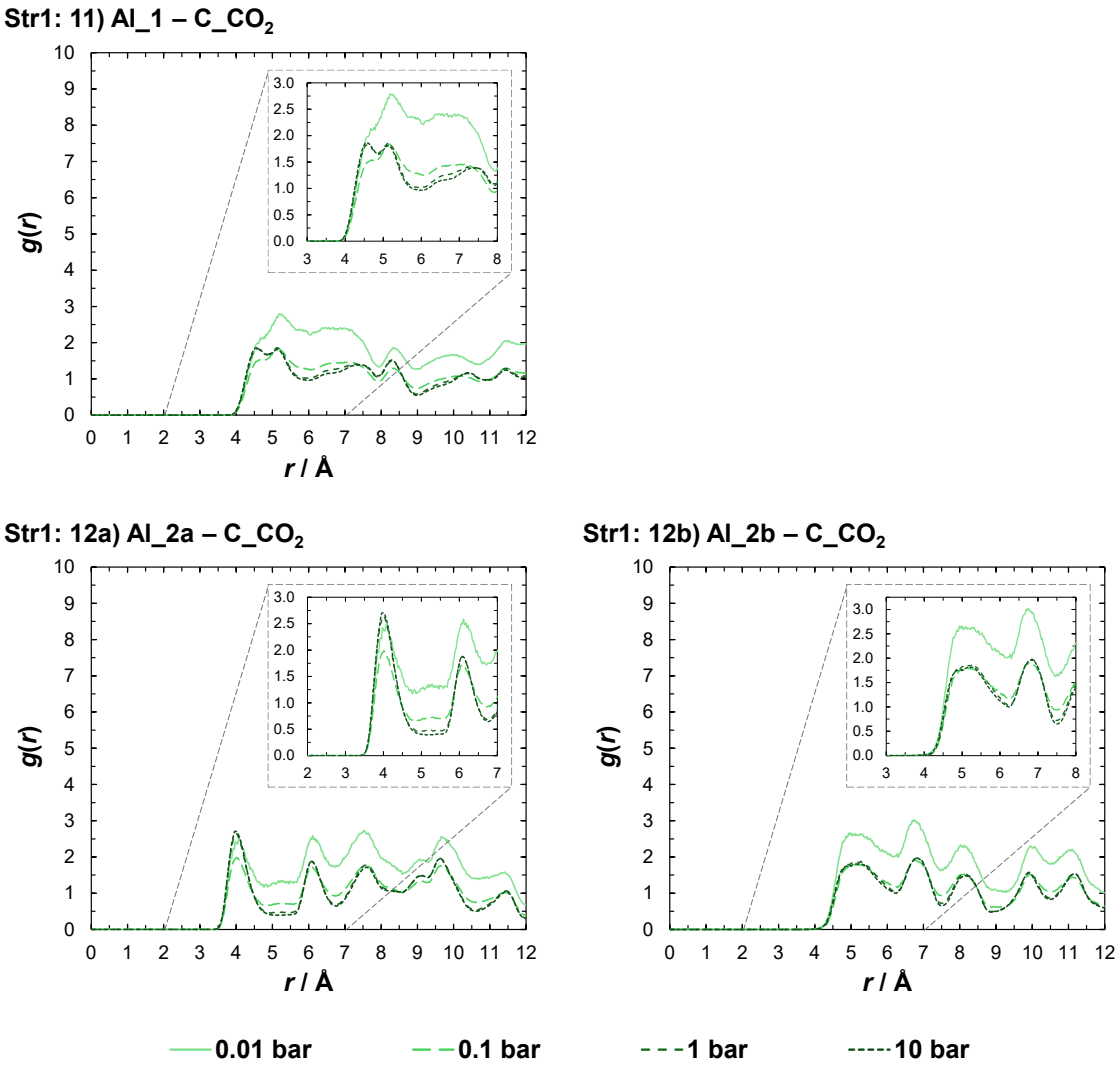

Figure S41. RDFs of the interaction of atom-types 11 and 12 of structure Str1 of MIL-120(Al) (*cf.* Figure S8 and Table S8) with the C atom of CO_2 in the GCMC-calculated single-component adsorption of CO_2 at 25 °C and 0.01 (full line), 0.1 (long-dashed line), 1 (medium-dashed line) and 10 (short-dashed line) bar. The RDFs have been computed in RASPA[S30] every 100 cycles, with a histogram size of 500 and a range of 12 Å, and represent the average of each atom for the corresponding atom-type.

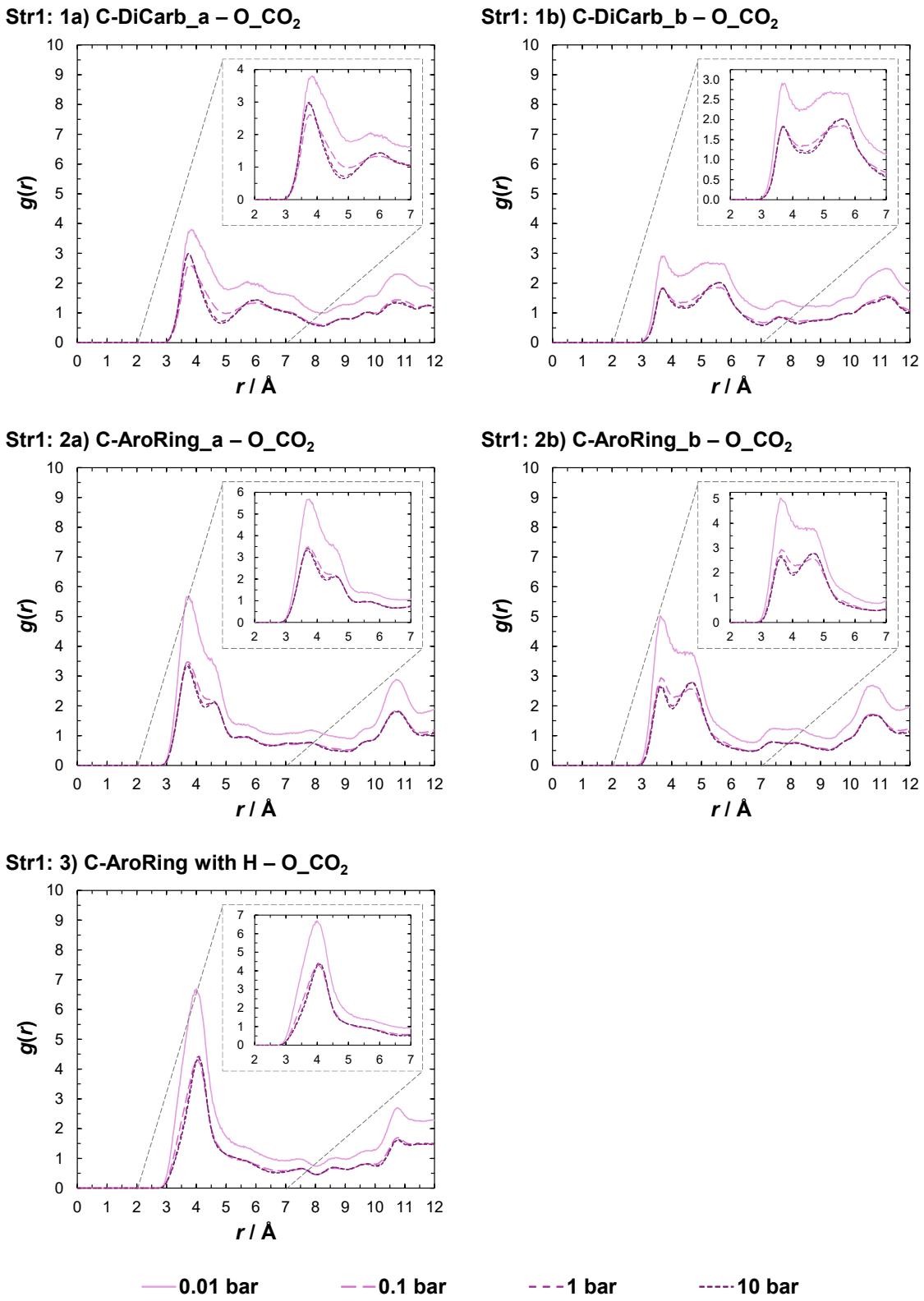

Figure S42. RDFs of the interaction of atom-types 1 to 3 of structure Str1 of MIL-120(Al) (*cf.* Figure S8 and Table S8) with the O atom of CO_2 in the GCMC-calculated single-component adsorption of CO_2 at 25 °C and 0.01 (full line), 0.1 (long-dashed line), 1 (medium-dashed line) and 10 (short-dashed line) bar. The RDFs have been computed in RASPA[S30] every 100 cycles, with a histogram size of 500 and a range of 12 Å, and represent the average of each atom for the corresponding atom-type.

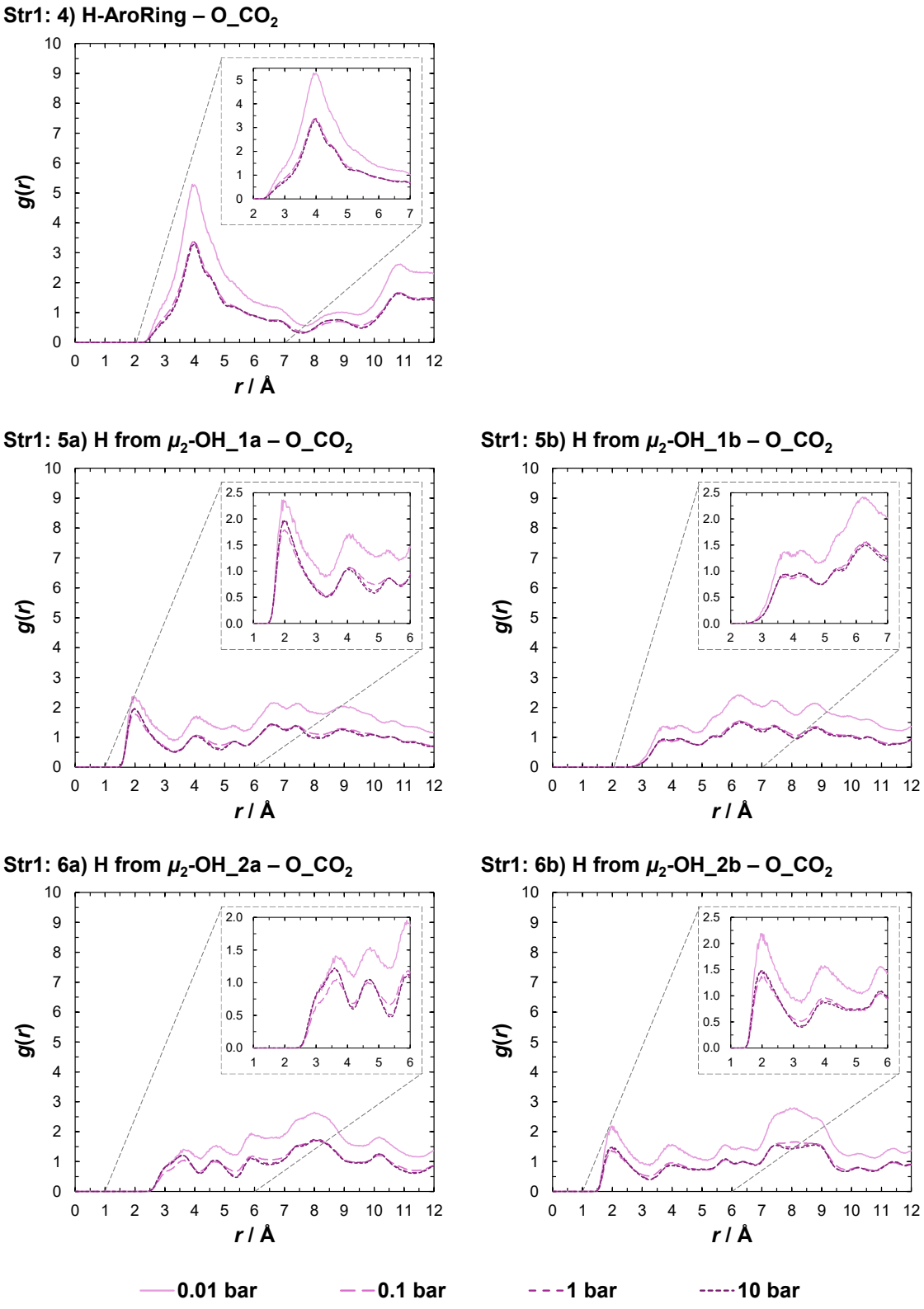

Figure S43. RDFs of the interaction of atom-types 4 to 6 of structure Str1 of MIL-120(Al) (*cf.* Figure S8 and Table S8) with the O atom of CO_2 in the GCMC-calculated single-component adsorption of CO_2 at 25 °C and 0.01 (full line), 0.1 (long-dashed line), 1 (medium-dashed line) and 10 (short-dashed line) bar. The RDFs have been computed in RASPA[S30] every 100 cycles, with a histogram size of 500 and a range of 12 Å, and represent the average of each atom for the corresponding atom-type.

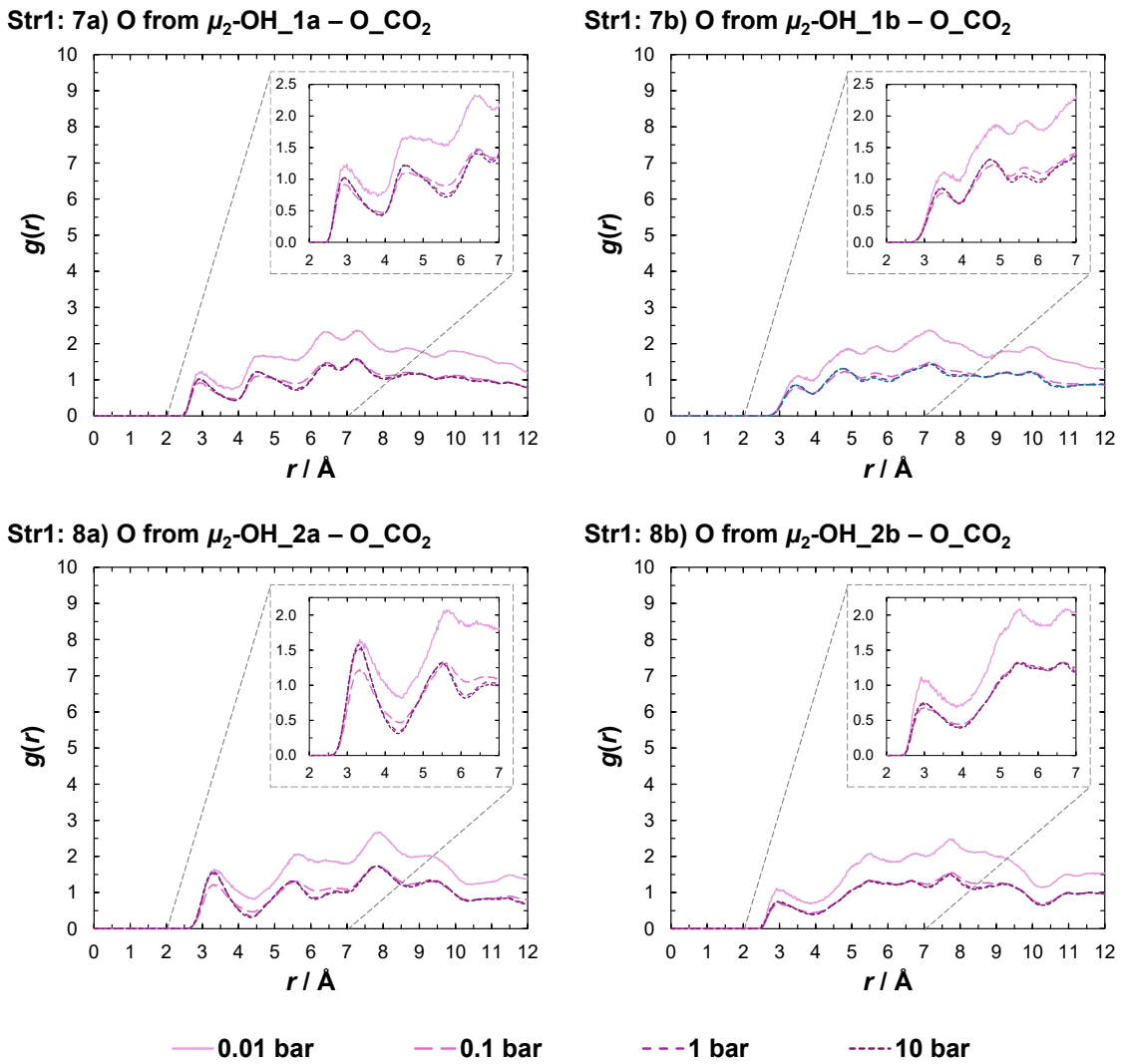

Figure S44. RDFs of the interaction of atom-types 7 and 8 of structure Str1 of MIL-120(Al) (*cf.* Figure S8 and Table S8) with the O atom of CO_2 in the GCMC-calculated single-component adsorption of CO_2 at 25 °C and 0.01 (full line), 0.1 (long-dashed line), 1 (medium-dashed line) and 10 (short-dashed line) bar. The RDFs have been computed in RASPA[S30] every 100 cycles, with a histogram size of 500 and a range of 12 Å, and represent the average of each atom for the corresponding atom-type.

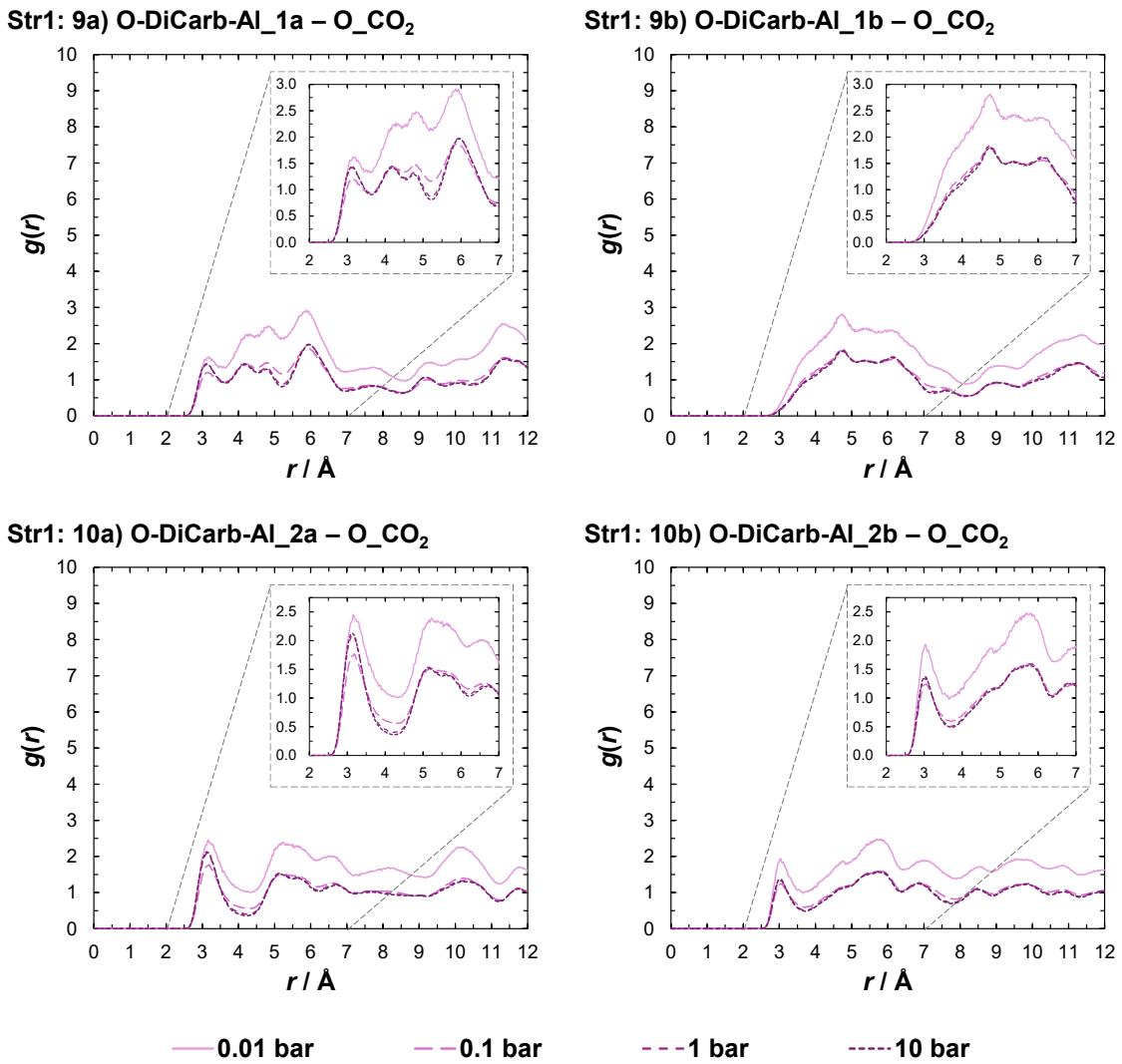

Figure S45. RDFs of the interaction of atom-types 9 and 10 of structure Str1 of MIL-120(Al) (*cf.* Figure S8 and Table S8) with the O atom of CO_2 in the GCMC-calculated single-component adsorption of CO_2 at 25 °C and 0.01 (full line), 0.1 (long-dashed line), 1 (medium-dashed line) and 10 (short-dashed line) bar. The RDFs have been computed in RASPA[S30] every 100 cycles, with a histogram size of 500 and a range of 12 Å, and represent the average of each atom for the corresponding atom-type.

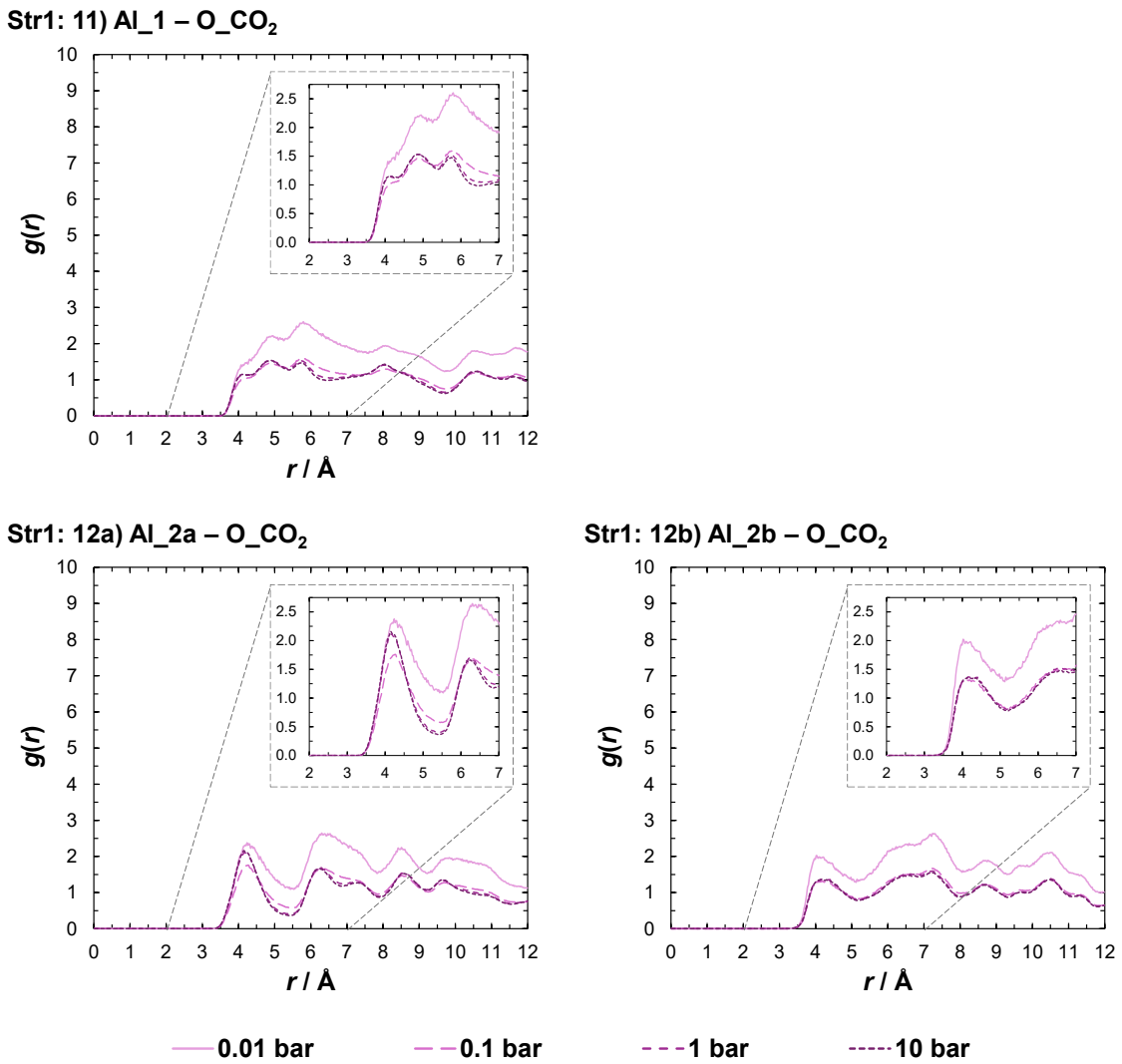

Figure S46. RDFs of the interaction of atom-types 11 and 12 of structure Str1 of MIL-120(Al) (*cf.* Figure S8 and Table S8) with the O atom of CO_2 in the GCMC-calculated single-component adsorption of CO_2 at 25 °C and 0.01 (full line), 0.1 (long-dashed line), 1 (medium-dashed line) and 10 (short-dashed line) bar. The RDFs have been computed in RASPA[S30] every 100 cycles, with a histogram size of 500 and a range of 12 Å, and represent the average of each atom for the corresponding atom-type.

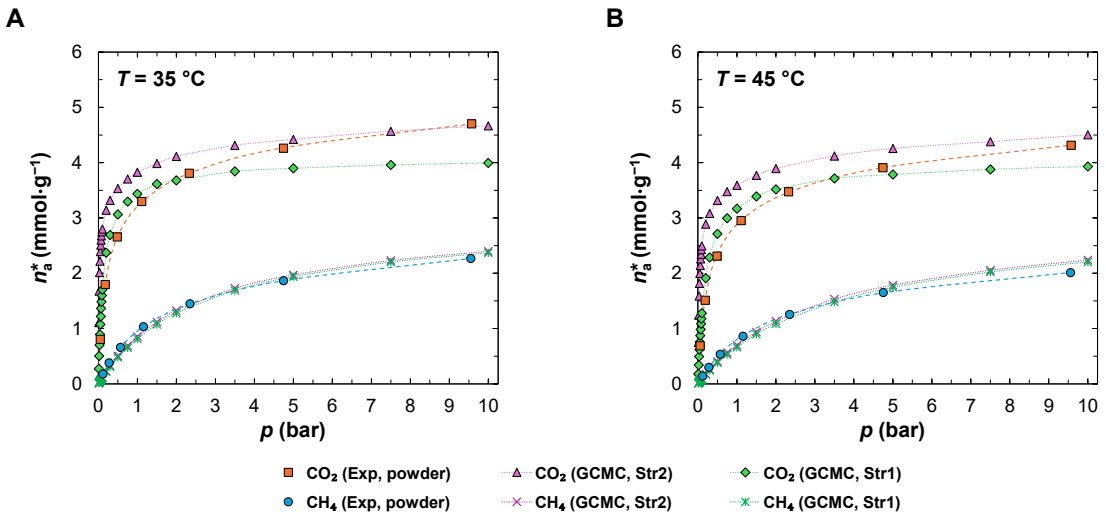

Figure S47. Comparison of the single-component adsorption isotherms of CO_2 and CH_4 at **A**) 35 and **B**) 45 °C, measured for the powder form of MIL-120(Al) (*cf*. Table S2) and calculated by GCMC for Str2 (*cf*. Figure S7 and Table S7) and Str1 (*cf*. Figure S8 and Table S8). The dashed lines represent the non-linear least-squares fit of the Virial isotherm model to the experimental data (*cf*. Table S3). The dotted lines in GCMC-calculated isotherms serve only as a visual guide of the data trends to the reader.

S2.C. Experimental multi-component adsorption studies

Binary breakthrough (BT) experiments of CO_2 and CH_4 (CO_2, 99.998 %, Air Liquide and CH_4, 99.995 %, Air Liquide) mixtures have been conducted on the shaped MIL-120(Al) beads (particle size with d_p [1.4–2[mm) under dry and wet (with pre-adsorbed water vapour) conditions at 25 °C and *ca*. 1 bar, in a lab-made fixed-bed dynamic adsorption system, illustrated on a diagram in Figure S48. In this setup, the gases are controlled individually via mass flow controllers (MFC) (McMillan, model 80SD), and the column outlet composition is registered via an inline mass spectrometer (MS) (Pfeiffer Vacuum, QMG 220 PrismaPlus), with a precision variable leak valve (VAT, 59024-GE01) set before the MS inlet. The adsorption column is submerged in a thermostatic water bath (VWR, VWB2 12, 0.1 °C of accuracy) for temperature control, and the system pressure is monitored in a two-channel digital power supply and readout (MKS, PDR2000A) onto which pressure transducers (MKS, Micro-Baratron AA08A12PCA2GA1) are connected. The column pressure is adjusted using a back-pressure regulator (Swagelok, KBP1F0A4A5A20000) set up after the column. Before going into the MS, the column outlet stream is diluted in *ca*. 80 ml·min^{-1} (reference state (RS): 25 °C, 1 atm) of helium (He, Air Liquide, Alphagaz 1) for an adequate concentration quantification.[S38,S39] The calibration of the MFCs has been checked prior to running the experiments using a bubble flowmeter.[S40] The MS measurements have been run in the multiple ion detection (MID) mode using the secondary electron multiplier (SEM). In a typical MS run, the scans are collected with a SEM voltage of 915 V, 100 ms of dwell time, the resolution set to 30, and ion fragments for CO_2, CH_4 and He with mass-to-charge ratios (*m*/*z*) of 44, 15 and 4, respectively. Additional details can be found in a previous work.[S41]

For the binary breakthrough experiments, a 50:50 (% *V*/*V*) CO_2:CH_4 gas mixture with a total flowrate of *ca*. 20 ml·min^{-1} (RS: 25 °C, 1 atm) was passed in a column filled with *ca*. 3.2 g of MIL-120(Al) beads (with $L_{bed,ads}$ ≈ 7.8 cm and $D_{col,int.}$ = 0.77 cm). Before the first binary breakthrough experiment under dry conditions, a blank experiment, using an empty column of the same dimensions, was run under the same experimental conditions to determine the dead volume of the system and calibrate the MS signals. The adsorbed amounts have been calculated from the integration of the experimental breakthrough curves after discounting the dead volume determined from the integration of the blank run curves, as described in detail in a previous work.[S41] After the blank experiment, the packed column was activated *in situ* for 8 h (following overnight vacuum) at 150 °C (heating rate (HR): 5 °C·min^{-1}) under a He flow of *ca*. 51 ml·min^{-1} (RS: 25 °C, 1 atm), with vacuum applied at the outlet of the column (*cf*. Figure S48). The cyclability of the material has been evaluated by running ten consecutive adsorption/desorption cycles. The adsorption and desorption branches of each experiment were run for 30 min, using a He flow of *ca*. 20 ml·min^{-1} (RS: 25 °C, 1 atm) to clean the material during the desorption branches.

The influence of the presence of pre-adsorbed water vapour on the separation of a 50:50 (% *V*/*V*) CO_2:CH_4 gas mixture with a total flowrate of *ca*. 20 ml·min^{-1} (RS: 25 °C, 1 atm) has also been studied. For these experiments under humid conditions, a pre-loading of water vapour

at a known relative humidity (RH) was performed, by exposing the material to a flow of He of *ca*. 20 ml·min^{-1} (RS: 25 °C, 1 atm) carrying the water vapour from a bubbler. Before the first experiment under humid conditions, the packed column was activated *in situ* for 1 h (following overnight vacuum) at 150 °C (HR: 5 °C·min^{-1}) under a He flow of *ca*. 52 ml·min^{-1} (RS: 25 °C, 1 atm), with vacuum applied at the outlet of the column (*cf*. Figure S48). The packed bed was pre-loaded with water vapour at RH ≈ 50 %. The pre-loading was achieved by passing He at *ca*. 20 ml·min^{-1} (RS: 25 °C, 1 atm) through a water bubbler submerged in a thermostatic water bath (VWR, VWB2 2, 0.1 °C of accuracy) set at the desired temperature (13.9 °C)[S2], before passing the He+H_2O_{vapour} mix through the packed bed. The exposure time of the He+H_2O_{vapour} mix in the packed bed was *ca*. 3 h and 30 min. A second experiment under humid conditions was performed at a higher RH and exposure time. Before this second experiment, the packed column was activated *in situ* for 8 h (following overnight vacuum) at 150 °C (HR: 5 °C·min^{-1}) under a He flow of *ca*. 52 ml·min^{-1} (RS: 25 °C, 1 atm) , with vacuum applied at the outlet of the column (*cf*. Figure S48). The packed bed was then pre-loaded with water vapour at RH ≈ 80 % ($T_{bubbler}$ = 21.3 °C)[S2]. The pre-loading was done as in the previous experiment. The exposure time of the He+H_2O_{vapour} mix in the packed bed was *ca*. 48 h.

Following the experiments carried under humid conditions, a final binary breakthrough experiment under dry conditions was conducted with a 50:50 (% *V*/*V*) CO_2:CH_4 gas mixture with a total flowrate of *ca*. 20 ml·min^{-1} (RS: 25 °C, 1 atm), to assess if the experiments performed under wet conditions affected the adsorption properties of the material permanently. Prior to the experiment, the packed column was activated *in situ* for 12 h (following overnight vacuum) at 150 °C (HR: 5 °C·min^{-1}) under a He flow of *ca*. 52 ml·min^{-1} (RS: 25 °C, 1 atm) , with vacuum applied at the outlet of the column (*cf*. Figure S48).

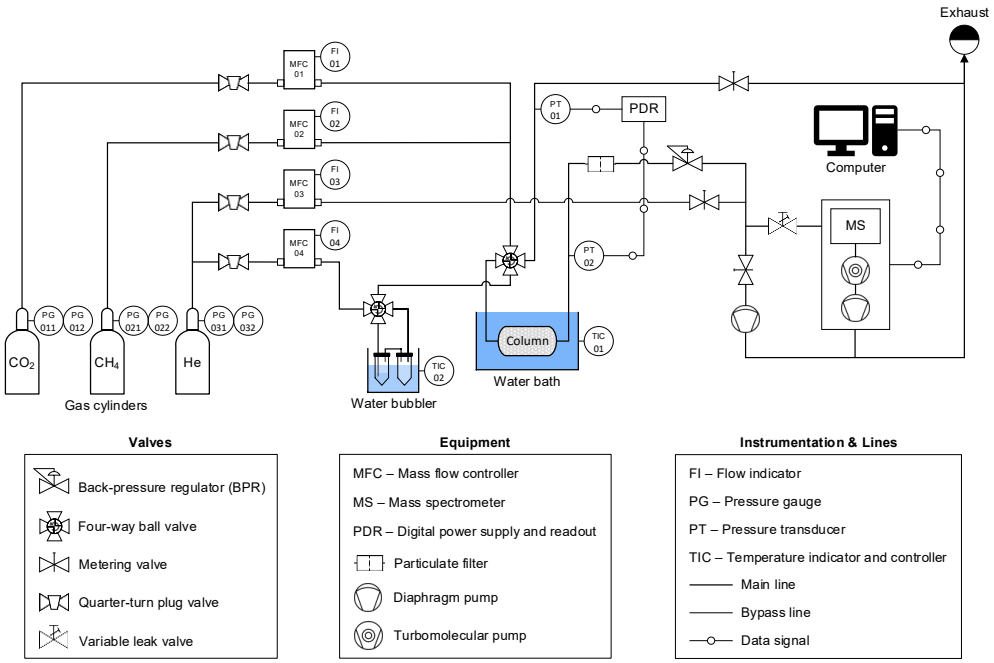

Figure S48. Diagram of the lab-made fixed-bed dynamic adsorption system used in the multi-component adsorption studies with the shaped MIL-120(Al) beads (d_p [1.4–2[mm).

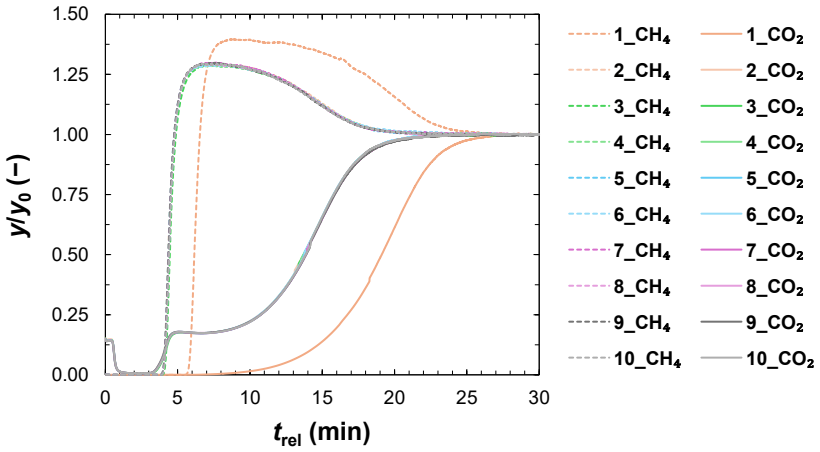

Figure S49. Overlap of the adsorption branches of the CH_4 and CO_2 breakthrough curves of experimental BT runs 1 through 10 (*cf.* Figure 5 in the main text). In the *x*-axis, t_{rel} is the time relative to the beginning of each BT experiment.

Table S9. CO_2 and CH_4 uptakes calculated from the experimental breakthrough (BT) curves and predicted from IAST from the single-component experimental data for the shaped MIL-120(Al) beads (d_p [1.4–2[mm) (*cf.* Table S3).

Run	n_{CO_2} (mmol·g^{-1})		n_{CH_4} (mmol·g^{-1})	
	Exp. (BT)	IAST	Exp. (BT)	IAST
1 (Dry)	2.7536	2.8244	0.0308	0.0954
2 (Dry)	1.7839	2.8229	0.0312	0.0954
3 (Dry)	1.7869	2.8248	0.0342	0.0951
4 (Dry)	1.7753	2.8220	0.0324	0.0957
5 (Dry)	1.7874	2.8251	0.0322	0.0951
6 (Dry)	1.7745	2.8238	0.0334	0.0954
7 (Dry)	1.7854	2.8262	0.0322	0.0950
8 (Dry)	1.7797	2.8229	0.0348	0.0957
9 (Dry)	1.7819	2.8251	0.0311	0.0952
10 (Dry)	1.7723	2.8248	0.0349	0.0952
1_H_2O (RH 50 %, exposure 3h30min)	2.6939	–	0.0382	–
2_H_2O (RH 80 %, exposure 48h)	1.3104	–	0.0033	–
11 (Dry)	2.7095	2.8256	0.0397	0.0954

S2.D. Comparison with other adsorbent materials

A literature survey has been conducted to compare the performance of MIL-120(Al) for the adsorptive separation of CO_2 and CH_4 with other adsorbent materials. The types of materials surveyed have been activated carbons (AC), carbon molecular sieves (CMS), other metal-organic frameworks (MOF), pillared clays (PILC), periodic mesoporous organosilicas (PMO), silicas and zeolites. The temperatures have been considered in the range of 25±5 °C. The parameters chosen for the comparison have been the uptake of CO_2, n_{CO_2}, at 1 bar, the selectivity for CO_2, S_{CO_2/CH_4}, calculated from IAST[S7,S12] as the mean selectivity or the composition-dependent selectivity for CO_2:CH_4 = (50±10):(50∓10) %(*V*/*V*), or obtained from binary gas mixture breakthrough experiments with CO_2:CH_4 = (50±10):(50∓10) %(*V*/*V*), and the isosteric enthalpy of adsorption, $\Delta H_{ads,CO_2}$. Whenever possible, the data are presented as written in the cited works. Otherwise, the data presented have been determined from the fitting parameters reported in the cited literature, or from visual or digital inspection of graphs presented in the cited literature using the Graph Suchi Yomitori System (GSYS2.4)[S42], a graphical data point digitizer software.

Table S10. Performance of MIL-120(Al) for CO_2/CH_4 separation *vs*. other adsorbent materials.

Type	Material	Form	*T* (°C)	$n_{CO_2,\ 1\ bar}$ (mmol·g^{-1})	S_{CO_2/CH_4} (–)	$-\Delta H_{ads,CO_2}$ (kJ·mol^{-1})	Reference
AC	Maxsorb [a]	n.s.	25	1.92	–	19.7–24	S43
	Pine-sawdust AC [b]	Pellets	30	2.5	5.23	24.2	S44
	CS-CO_2 [c]	n.s.	30	2.32	3.9	20.3–23.5	S45
	CS-H_2O [c]			2.30	4.1	22.4–25.7	
	Calgon BPL [d]	n.s.	30	1.7	3.6	–	S46
CMS	Takeda 5A [e]	n.s.	30	2.28	–	26–35	S47
	CMS-1 [f]	Cylinder	25	1.94	1.67	23.5–25	S48
	CMS-2 [f]			0.94	1.28	–	
	CMS-3 [f]			0.83	1.37		
MOF	**MIL-120(Al) [g]**	**Powder**	**25**	**3.56**	**30.57 (i)**	**36.7–43.1**	**This work**
		Beads		**3.33**	**30.68 (i)** **89.3 (ii)**	–	
	MIL-53(Al) [h]	Powder	25	2.58	14.42	23.27	S49
		Beads		2.13	11.41	21.48	
	MIL-101(Cr) [h]	Powder		1.54	4.09	26.23	
		Beads		1.12	3.7	22.62	
	NH_2-MIL-53(Al) [i]	Powder + pellets	30	1.96	207	32	S50
	MIL-160(Al) [j]	Powder	25	3.89	10.09 (i)	33	S41,S51
		Beads		2.81	10.51 (i) 18.4 (ii)	–	
	CuBTC [k]	n.s.	30	4.55	–	30	S47
	UiO-66(Zr) [k]			1.34	–	27	
	UiO-66(Zr)-NH_2 [k]			2.69	–	31–35	
	MIL-125(Ti) [k]			1.79	–	26	
	MIL-125(Ti)-NH_2 [k]			2.64	–	30	
	MIL-100(Fe) [k]			3.15	–	22–37	
	MIL-100(Cr) [k]			3.50	–	22–59	

Table S10 (*cont.*). Performance of MIL-120(Al) for CO_2/CH_4 separation *vs*. other adsorbent materials.

Type	Material	Form	T (°C)	$n_{CO_2,\ 1\ bar}$ (mmol·g^{-1})	S_{CO_2/CH_4} (–)	$-\Delta H_{ads,CO_2}$ (kJ·mol^{-1})	Reference
MOF	CAU-10-H [l]	Powder	30	2.30	4.9 (1 bar) 5.8 (10 bar)	–	S52
	CAU-10-OH [l]			1.07	3.5 (1 bar) 3.6 (10 bar)		
	CAU-10-NH_2 [l]			1.82	4.4 (1 bar) 6.6 (10 bar)		
	CAU-10-NO_2 [l]			1.95	8.0 (1 bar) 13.8 (10 bar)		
	CAU-10-OCH_3 [l]			0.81	1.7 (1 bar) 3.5 (10 bar)		
	CAU-10-CH_3 [l]			1.21	3.0 (1 bar) 3.6 (10 bar)		
	MOF-808@N [m]	Powder	25	1.30	7.8 (1 bar) 9.2 (10 bar)	29.1	S53
	MOF-808 [m]			1.21	8.5 (1 bar) 7.9 (10 bar)	31.3	
	DUT-67@N [m]			1.28	6.4 (1 bar) 5.6 (10 bar)	25	
	DUT-67 [m]			1.23	5.7 (1 bar) 5.8 (10 bar)	32.5	
PILC	$(Al_2O_3)_B$ [n]	Powder	25	0.36	7.3	–	S14
	$(Al_2O_3)_W$ [n]			0.42	8.5		
	$(ZrO_2)_B$ [n]			0.27	5.1		
	$(ZrO_2)_W$ [n]			0.41	16.0		
PMO	Ph-PMO [o]	Powder	25	0.37	5.5	–	S54
	NH_2-Ph-PMO [o]			0.40	5.4		
	APTMS@Ph-PMO [o]			0.71	12.8		
	APTMS@NH_2-Ph-PMO [o]			0.50	12.1		
Silica	SBA-15 [p]	Powder	25	0.64	8.8	–	S55
	N-3@SBA-15 [p]			1.39	14498		
	TMMAP@SBA-15 [p]			1.03	1119		
	APTES@SBA-15 [q]	Powder	25	0.57	9.8	–	S15
	3-DEAPTES@SBA-15 [q]			0.34	5.0		
	MCM-41 [r]	Powder	25	0.68	5.1	21.6	S56,S57
Zeolite	Silicalite-1 [s]	Powder	25	1.61	2.9	26–30	S58
	Beta [s]			1.96	4.6	19–58	
	DDR [s]			1.01	4.6	28–42	
	13X [t]	Shaped	25	4.7	88	37.2	S50,S59
	NaX [u]	n.s.	30	4.82	–	38–49	S47
	4A [v]	Powder	25	4.2917	–	36.2 ± 1.6 42.9	S60
	5A [w]	Beads	30	3.0608	–	24-46	S61
	NaY [x]	Powder	25	5.5	65.7 (1 bar) 55.8 (5 bar)	33.4	S62
	0.5%PEPO-NaY [x]			4.1	70.84 (1 bar) 95.34 (5 bar)	32.6	
	1%PEPO-NaY [x]			3.2	45.83 (1 bar) 70.74 (5 bar)	31.4	
	2%PEPO-NaY [x]			2.2	38.27 (1 bar) 56.06 (5 bar)	29.9	
	Na-ZSM-5 [y]	Pellets	20	1.39	–	26.5–29.5	S63

Notes from Table S10:

n.s. – not specified

a n_{CO_2} calculated for 25 °C and 1 bar from the fitting parameters of the Sips model provided in Table 6 in ref. [S43]; $-\Delta H_{ads,CO_2}$ (from the Clausius-Clapeyron equation) range obtained from Figure 6 in ref. [S43].

b n_{CO_2} at 30 °C and 1 bar obtained from the isotherm in Figure 1 in ref. [S44]; S_{CO_2/CH_4} from a breakthrough experiment of CO_2:CH_4=50:50 %(*V*/*V*), at 30 °C and 1.2 bar, as reported in Table 2 in ref. [S44]; $-\Delta H_{ads,CO_2}$ (from the Clausius-Clapeyron equation) is the average value as reported in ref. [S44].

c n_{CO_2} calculated for 30 °C and 1 bar from the fitting parameters of the Tóth model provided in Table 2 in ref. [S45]; S_{CO_2/CH_4} from IAST for CO_2:CH_4=50:50 %(*V*/*V*), at 30 °C and 5 bar, obtained from Figure 4 in ref. [S45]; $-\Delta H_{ads,CO_2}$ (from the Clausius-Clapeyron equation) range obtained from Figure 3 in ref. [S45].

d n_{CO_2} at 30 °C and 1 bar obtained from the isotherm in Figure 3 in ref. [S46]; S_{CO_2/CH_4} calculated from the CO_2 and CH_4 uptakes from a breakthrough experiment of CO_2:CH_4=50:50 %(*V*/*V*), at 30 °C and 1 bar, reported in Table 3 in ref. [S46].

e n_{CO_2} calculated for 30 °C and 1 bar from the fitting parameters of the Tóth model provided in Table S2 in ref. [S47]; $-\Delta H_{ads,CO_2}$ (from microcalorimetry experiments at 30 °C) range/value as reported in Table 4 in ref. [S47].

f n_{CO_2} calculated for 25 °C and 1 bar from the fitting parameters of the Langmuir model provided in Table 3 in ref. [S48]; S_{CO_2/CH_4} from IAST for CO_2:CH_4=50:50 %(*V*/*V*), at 25 °C and 10 bar as reported in ref. [S48]; $-\Delta H_{ads,CO_2}$ (from the Clausius-Clapeyron equation) range for CMS-1 obtained from Figure 5 in ref. [S48].

g n_{CO_2} calculated at 25 °C and 1 bar from the fitting parameters of the Virial model (*cf.* Table S3); S_{CO_2/CH_4} calculated from (i) IAST as the mean selectivity at 25 °C and 5 bar from the fitting parameters of the Virial model (*cf.* Table S3) and (ii) the CO_2 and CH_4 uptakes from a breakthrough experiment of CO_2:CH_4=50:50 %(*V*/*V*), at 25 °C and *ca.* 1 bar (*cf.* Table S9); $-\Delta H_{ads,CO_2}$ (from the Clausius-Clapeyron equation) range represented in Figure 2C in the main text.

h n_{CO_2} at 25 °C and 1 bar as reported in Table 2 in ref. [S49]; S_{CO_2/CH_4} from IAST for CO_2:CH_4=50:50 %(*V*/*V*), at 25 °C and 1 bar as reported in Table 5 in ref. [S49]; $-\Delta H_{ads,CO_2}$ (from the Clausius-Clapeyron equation) as reported in Table 2 in ref. [S49].

i n_{CO_2} at 30 °C and 1 bar as reported in ref. [S50]; S_{CO_2/CH_4} from the CO_2 and CH_4 uptakes from a breakthrough experiment of CO_2:CH_4=40:60 %(*V*/*V*), at 30 °C and 1 bar, as reported in Table 3 in ref. [S50]; $-\Delta H_{ads,CO_2}$ (from the Clausius-Clapeyron equation) as reported in ref. [S50].

j n_{CO_2} calculated at 25 °C and 1 bar from the fitting parameters of the Virial model in Table S16 in ref. [S41]; S_{CO_2/CH_4} calculated from (i) IAST as the mean selectivity at 25 °C and 5 bar from the fitting parameters of the Virial model for the powder and for the beads with d_p [1-1.4[mm in Table S16 and (ii) the CO_2 and CH_4 uptakes from a breakthrough experiment of CO_2:CH_4=50:50 %(*V*/*V*), at 25 °C and *ca.* 1.15 bar, reported in Table 4 in ref. [S41]; $-\Delta H_{ads,CO_2}$ (from the Clausius-Clapeyron equation) value as reported for low coverage in ref. [S51].

k n_{CO_2} calculated for 30 °C and 1 bar from the fitting parameters of the Tóth model provided in Table S2 in ref. [S47]; $-\Delta H_{ads,CO_2}$ (from microcalorimetry experiments at 30 °C) range/value as reported in Table 4 in ref. [S47].

l n_{CO_2} calculated for 30 °C and 1 bar from the fitting parameters of the Triple-Site Langmuir model provided in Table S2 in ref. [S52]; S_{CO_2/CH_4} from IAST for CO_2:CH_4=50:50 %(*V*/*V*), at 30 °C and 1 and 10 bar as reported Table 2 in ref. [S52].

m n_{CO_2} at 25 °C and 1 bar as reported in Table 2 in ref. [S53]; S_{CO_2/CH_4} from IAST for CO_2:CH_4=50:50 %(*V*/*V*), at 25 °C and 1 and 10 bar as reported Table 2 in ref. [S53]; $-\Delta H_{ads,CO_2}$ (from the Clausius-Clapeyron equation) as reported for the lowest CO_2 uptake in Table 2 ref. [S53].

n n_{CO_2} calculated for 25 °C and 1 bar from the fitting parameters of the Virial model provided in Table SI-S2 in ref. [S14]; S_{CO_2/CH_4} calculated from IAST as the mean selectivity at 25 °C and 5 bar from the fitting parameters of the Virial model provided in Table SI-S2 in ref. [S14].

o n_{CO_2} calculated for 25 °C and 1 bar from the fitting parameters of the Virial model provided in Table 1 in ref. [S54]; S_{CO_2/CH_4} calculated from IAST as the mean selectivity at 25 °C and 5 bar from the fitting parameters of the Virial model provided in Table 1 in ref. [S54].

p n_{CO_2} calculated for 25 °C and 1 bar from the fitting parameters of the Virial model provided in Table 2 in ref. [S55]; S_{CO_2/CH_4} calculated from IAST as the mean selectivity at 25 °C and 5 bar from the fitting parameters of the Virial model provided in Table 2 in ref. [S55].

q n_{CO_2} calculated at 25 °C and 1 bar from the fitting parameters of the Langmuir-Virial model provided in Table 2 in ref. [S15]; S_{CO_2/CH_4} calculated from IAST as the mean selectivity at 25 °C and 5 bar from the fitting parameters of the Virial model provided in Table 2 in ref. [S15].

r n_{CO_2} calculated for 25 °C and 1 bar from the fitting parameters of the Tóth model provided in Table 1 in ref. [S56]; S_{CO_2/CH_4} from IAST for CO_2:CH_4=50:50 %(*V*/*V*), at 25 °C and 1 bar obtained from Figure 6 in ref. [S56]; $-\Delta H_{ads,CO_2}$ (from the Clausius-Clapeyron equation) as reported for the lowest CO_2 uptake in Table 3 ref. [S57].

s n_{CO_2} at 25 °C and 1 bar, and converted to mmol·g^{-1} from the values reported in Table S2 in ref. [S58]; S_{CO_2/CH_4} from IAST for CO_2:CH_4=50:50 %(*V*/*V*), at 25 °C and 1 bar obtained from Figure 6 in ref. [S58]; $-\Delta H_{ads,CO_2}$ (from the Clausius-Clapeyron equation) range obtained from Figure 8 in ref. [S58].

t Material used as pellets in ref. [S59] and granules in ref. [S50]; n_{CO_2} at 25 °C and 1 bar obtained from Figure 5 in ref. [S59]; S_{CO_2/CH_4} from the CO_2 and CH_4 uptakes from a breakthrough experiment of CO_2:CH_4=40:60 %(*V*/*V*), at 30 °C and 1 bar, as reported in Table 3 in ref. [S50]; $-\Delta H_{ads,CO_2}$ value from low pressures as reported in ref. [S59].

u n_{CO_2} calculated for 30 °C and 1 bar from the fitting parameters of the Tóth model provided in Table S2 in ref. [S47]; $-\Delta H_{ads,CO_2}$ (from microcalorimetry experiments at 30 °C) range as reported in Table 4 in ref. [S47].

v n_{CO_2} at 25 °C and 1.0784 bar as reported in Online resource 6 in ref. [S60]; $-\Delta H_{ads,CO_2}$ values as reported in Table 2 in ref. [S60].

w n_{CO_2} at 30 °C and 0.9758 bar as reported in Table A1 in ref. [S61]; $-\Delta H_{ads,CO_2}$ (from the Clausius-Clapeyron equation) range obtained from Figure 4 in ref. [S61].

x n_{CO_2} at 25 °C and 1 bar obtained from Figure 6 in ref. [S62]; S_{CO_2/CH_4} from IAST for CO_2:CH_4=50:50 %(*V*/*V*), at 25 °C and 1 and 5 bar as reported in Table 3 in ref. [S62]; $-\Delta H_{ads,CO_2}$ (from the Clausius-Clapeyron equation) values as reported in Table 2 in ref. [S62].

y n_{CO_2} calculated for 20 °C and 1 bar from the fitting parameters of the Tóth model provided in Table 1 in ref. [S63]; $-\Delta H_{ads,CO_2}$ (from the Clausius-Clapeyron equation) range obtained from Figure 9 in ref. [S63].

Nomenclature

Abbreviation	Description
3-DEAPTES	[3-(Diethylamino)propyl]trimethoxysilane
Ac	Acetate
AC	Activated carbon
AP	Ambient pressure
APTES	(3-Aminopropyl)triethoxysilane
APTMS	(3-Aminopropyl)trimethoxysilane
AroRing	Aromatic ring
BET	Brunauer–Emmett–Teller
BPR	Back-pressure regulator
BT	Breakthrough runs in the fixed-bed dynamic adsorption system
ca.	*circa*
CAU	*Christian-Albrechts-Universität*
cf.	*confer*
CMS	Carbon molecular sieves
CS	Cherry stone
CuBTC	Copper(II) benzene-1,3,5-tricarboxylate
DDR	Deca-dodecasil 3R
DFT	Density functional theory
DI	Dionised
DiCarb	Dicarboxylate
DUT	Dresden University of Technology
e.g.	*exempli gratia*
ESP	Electrostatic potential
et al.	*et alii*
EXAFS	Extended X-ray absorption fine structure
Exp	Experimental
GCMC	Grand-canonical Monte Carlo
GGA	Generalised gradient approximation (DFT)
HR	Heating rate
i.e.	*id est*
IAST	Ideal Adsorbed Solution theory
LJ	Lennard-Jones
MCM	Mobil Composition of Matter
MFC(s)	Mass flow controller(s)
MID	Multiple ion detection (MS)
MIL	*Matériaux de l'Institut Lavoisier*
MOF(s)	Metal-organic framework(s)
MS	Mass spectrometer
PAW	Projector augmented wave (DFT)
PBE	Perdew, Burke, and Ernzerhof (DFT)
PDR	Digital power supply and readout
PEPO	Polyether polyols
PG	Pressure gauge
Ph	Phenylene
PILC	Pillared clays

(Continued from the previous page)

Abbreviation	Description
PMO	Periodic mesoporous organosilicas
PT	Pressure transducer
PSA	Pressure swing adsorption
PXRD	Powder X-ray diffraction
RDF(s)	Radial distribution function(s)
REPEAT	Repeating Electrostatic Potential Extracted Atomic
RH	Relative humidity
rpm	Revolutions per minute (unit of rotational speed)
RS	Reference state
SB	Simulation box
SBA	Santa Barbara Amorphous
SEM	Scanning electron microscopy; Secondary electron multiplier (MS)
SI	Supporting Information
ssNMR	Solid-state nuclear magnetic resonance
STY	Space-time yield
TGA	Thermogravimetric analysis
TIC	Temperature indicator and controller
TMMAP	Ttrimethoxy[3-(methylamino) propyl]silane
TraPPE	Transferable Potentials for Phase Equilibria (force field)
UA	United atoms
UC	Unit cell
UFF	Universal force field
VASP	Vienna Ab initio Simulation Package
VESTA	Visualization for Electronic and Structural Analysis
VMD	Visual Molecular Dynamics
vs.	*versus*
ZSM	Zeolite Socony Mobil

Latin symbol	Description
a	Crystal lattice length parameter
Å	Angstrom (unit of length)
Al	Aluminium (chemical symbol)
atm	Standard atmosphere (unit of pressure)
b	Crystal lattice length parameter
bar	Unit of pressure
c	Centi- (metric prefix)
c	Crystal lattice length parameter
C	Carbon (atomic symbol)
cal	Calorie (unit of energy)
CH_4	Methane (chemical formula)
C_i	*i*-th coefficient of the Virial isotherm series expansion
CO_2	Carbon dioxide (chemical formula)
Cu K_α	Copper K_α X-ray radiation
$D_{col,int}$	Internal column diameter (BT studies)
D_l	van der Waals well depth (UFF force field)
d_p	Particle size (diameter)

(Continued from the previous page)

Latin symbol	Description
e^-	Atomic charge unit
eV	Electronvolt (unit of energy)
g	gram (unit of mass)
h	hour (unit of time)
H	Hydrogen (atomic symbol)
H_2O	Water (chemical formula)
H_2S	Hydrogen sulphide
He	Helium (atomic symbol)
J	Joule (unit of energy)
k	Kilo- (metric prefix)
K	Kelvin (unit of temperature)
K	Henry constant (Virial and Langmuir-Virial isotherm)
k_B	Boltzmann constant
$L_{bed,ads}$	Adsorbent bed length (BT studies)
m	Saturation capacity (Langmuir-Virial isotherm)
m	Meter (unit of length); Milli- (metric prefix)
m/z	Mass-to-charge ratio (MS)
min	Minute (unit of time)
mol	Mole (unit of the amount of substance)
N	Number of molecules in the system (GCMC)
N_2	Nitrogen (molecular, chemical formula)
n_a^*	Absolute adsorbed amount
n_e^*	Excess adsorbed amount
NO_x	Nitrogen oxides
O	Oxygen (atomic symbol)
p	Pressure (physical quantity)
P	Probability (GCMC)
$p°$	Saturation pressure (physical quantity)
q	Atom partial charge
R	Universal gas constant
R^2_{adj}	Adjusted correlation coefficient (from non-linear least-squares fittings)
r_{ij}	Distance between atoms *i* and *j*
S_{BET}	BET surface area
S_{CO_2,CH_4}	Selectivity of CO_2 relative to CH_4
SO_x	Sulphur oxides
t	Time (physical quantity)
T	Temperature (physical quantity)
t_{rel}	Relative time
$U_{C,ij}$	Coulomb potential between atoms *i* and *j*
U_{ij}	Total interaction energy between atoms *i* and *j*
$U_{LJ,ij}$	Lennard-Jones potential between atoms *i* and *j*
V	Volume (physical quantity)
V	Volt (unit of electric potential)
V_{pore}	Pore volume
V_{micro}	Micropore volume
w	weight (physical quantity)

(Continued from the previous page)

Latin symbol	Description
$\bar{W}_{micro}$	Median micropore width
x	Adsorbed-phase molar composition; Fractional coordinate
x_l	van der Waals bond length (UFF force field)
y	Gas-phase molar composition; Fractional coordinate
y_0	Inlet gas-phase molar composition
z	Compressibility factor; Axial direction; Fractional coordinate

Greek symbol	Description
α	Crystal lattice angle parameter
β	Crystal lattice angle parameter
γ	Crystal lattice angle parameter
ΔH_{ads}	Isosteric enthalpy of adsorption
ε_0	Vacuum permittivity
ε_{ij}	Dispersion energy (well depth of the potential) between atoms *i* and *j*
λ	Wavelength
μ	Micro- (metric prefix)
μ_2-OH	Bridging OH ligand (MIL-120(Al) structure)
ρ_g	Molar density of the gas phase
σ_{ij}	Distance at which the potential energy between particles *i* and *j* is zero

Miscellaneous	Description
°	Degree (unit of angle)
°C	Degree Celsius (unit of temperature)
%	Percentage
$	United States dollar (currency)

Subscript	Description
0	Initial
a	Absolute (adsorbed amount)
ads	Adsorption
C	Coulomb (GCMC)
i	*i*-th parameter (in a series of elements); Atom/component *i*;
j	Atom *j*
LJ	Lennard-Jones
micro	Relating to micropore
p	Relating to particle
pore	Relating to pore
rel	Relative

Superscript	Description
*	Property at equilibrium
°	Saturation state (pressure)
i	*i*-th parameter (in a series of elements)

References

S1 Micromeritics Instrument Corporation, 2024, 7.00.

S2 B. Chen, D. Fan, R. V. Pinto, I. Dovgaliuk, S. Nandi, D. Chakraborty, N. García-Moncada, A. Vimont, C. J. McMonagle, M. Bordonhos, A. Al Mohtar, I. Cornu, P. Florian, N. Heymans, M. Daturi, G. De Weireld, M. Pinto, F. Nouar, G. Maurin, G. Mouchaham and C. Serre, *Adv. Sci.*, 2024, **11**, 2401070.

S3 D. M. Ruthven, *Principles of Adsorption and Adsorption Processes*, John Wiley & Sons, 1984.

S4 F. J. Wilkins, *Proc. R. Soc. London. Ser. A - Math. Phys. Sci.*, 1938, **164**, 496–509.

S5 R. M. Barrer and R. M. Gibbons, *Trans. Faraday Soc.*, 1963, **59**, 2875–2887.

S6 A. V. Kiselev, *J. Colloid Interface Sci.*, 1968, **28**, 430–442.

S7 A. L. Myers, *Adsorption*, 2003, **9**, 9–16.

S8 A. L. Myers and P. A. Monson, *Langmuir*, 2002, **18**, 10261–10273.

S9 J. C. Holste, K. R. Hall, P. T. Eubank, G. Esper, M. Q. Watson, W. Warowny, D. M. Bailey, J. G. Young and M. T. Bellomy, *J. Chem. Thermodyn.*, 1987, **19**, 1233–1250.

S10 D. R. Douslin, R. H. Harrison, R. T. Moore and J. P. Mccullough, *J. Chem. Eng. Data*, 1964, **9**, 358–363.

S11 J. H. Dymond, R. C. Wilhoit, K. N. Marsh and K. C. Wong, *Virial Coefficients of Pure Gases*, Springer-Verlag Berlin Heidelberg, 2002.

S12 A. L. Myers and J. M. Prausnitz, *AIChE J.*, 1965, **11**, 121–127.

S13 M. L. Pinto, J. Pires and J. Rocha, *J. Phys. Chem. C*, 2008, **112**, 14394–14402.

S14 J. Pires, V. K. Saini and M. L. Pinto, *Environ. Sci. Technol.*, 2008, **42**, 8727–8732.

S15 M. Pacheco, M. Bordonhos, M. Sardo, R. Afonso, J. R. B. Gomes, L. Mafra and M. L. Pinto, *Chem. Eng. J.*, 2022, **443**, 136271.

S16 R. W. Hyland and E. A. Mason, *J. Res. Natl. Bur. Stand. Sect. A Phys. Chem.*, 1967, **71A**, 219.

S17 F. G. Keyes, *J. Chem. Phys.*, 1947, **15**, 602–612.

S18 A. Nuhnen and C. Janiak, *Dalt. Trans.*, 2020, **49**, 10295–10307.

S19 G. Kresse and J. Hafner, *Phys. Rev. B*, 1993, **47**, 558–561.

S20 G. Kresse and J. Hafner, *Phys. Rev. B*, 1994, **49**, 14251–14269.

S21 G. Kresse and J. Furthmüller, *Comput. Mater. Sci.*, 1996, **6**, 15–50.

S22 G. Kresse and J. Furthmüller, *Phys. Rev. B - Condens. Matter Mater. Phys.*, 1996, **54**, 11169–11186.

S23 C. Volkringer, T. Loiseau, M. Haouas, F. Taulelle, D. Popov, M. Burghammer, C. Riekel, C. Zlotea, F. Cuevas, M. Latroche, D. Phanon, C. Knöfelv, P. L. Llewellyn and G. Férey, *Chem. Mater.*, 2009, **21**, 5783–5791.

S24 Avogadro Chemistry, 2022, https://avogadro.cc/.

S25 M. D. Hanwell, D. E. Curtis, D. C. Lonie, T. Vandermeerschd, E. Zurek and G. R. Hutchison, *J. Cheminform.*, 2012, **4**, 1–17.

S26 S. Grimme, S. Ehrlich and L. Goerigk, *J. Comput. Chem.*, 2011, **32**, 1456–1465.

S27 P. E. Blöchl, *J. Chem. Phys.*, 1995, **103**, 7422–7428.

S28 G. Kresse and D. Joubert, *Phys. Rev. B - Condens. Matter Mater. Phys.*, 1999, **59**, 1758–1775.

S29 C. Campañá, B. Mussard and T. K. Woo, *J. Chem. Theory Comput.*, 2009, **5**, 2866–2878.

S30 D. Dubbeldam, S. Calero, D. E. Ellis and R. Q. Snurr, *Mol. Simul.*, 2015, **42**, 81–101.

S31 D. Dubbeldam, A. Torres-Knoop and K. S. Walton, *Mol. Simul.*, 2013, **39**, 1253–1292.

S32 A. H. Farmahini, S. Krishnamurthy, D. Friedrich, S. Brandani and L. Sarkisov, *Chem. Rev.*, 2021, **121**, 10666–10741.

S33 A. K. Rappé, C. J. Casewit, K. S. Colwell, W. A. Goddard and W. M. Skiff, *J. Am. Chem. Soc.*, 1992, **114**, 10024–10035.

S34 J. J. Potoff and J. I. Siepmann, *AIChE J.*, 2001, **47**, 1676–1682.

S35 M. G. Martin and J. I. Siepmann, *J. Phys. Chem. B*, 1998, **102**, 2569–2577.

S36 K. Momma and F. Izumi, *J. Appl. Crystallogr.*, 2011, **44**, 1272–1276.

S37 W. Humphrey, A. Dalke and K. Schulten, *J. Mol. Graph.*, 1996, **14**, 33–38.

S38 E. J. García, J. Pérez-Pellitero, G. D. Pirngruber, C. Jallut, M. Palomino, F. Rey and S. Valencia, *Ind. Eng. Chem. Res.*, 2014, **53**, 9860–9874.

S39 P. Serra-Crespo, R. Berger, W. Yang, J. Gascon and F. Kapteijn, *Chem. Eng. Sci.*, 2015, **124**, 96–108.

S40 N. S. Wilkins, A. Rajendran and S. Farooq, *Adsorption*, 2021, **27**, 397–422.

S41 M. Bordonhos, M. I. S. Neves, A. Marandi, F. Nouar, M. Jorge, J. R. B. Gomes, C. Serre and M. L. Pinto, *Chem. Eng. J.*, 2025, **524**, 169276.

S42 Japan Charged-Particle Nuclear Reaction Data Group (JCPRG), Graph Suchi Yomitori System (GSYS2.4), https://www.jcprg.org/gsys/2.4/.

S43 C. A. Grande, R. Blom, A. Möller and J. Möllmer, *Chem. Eng. Sci.*, 2013, **89**, 10–20.

S44 I. Durán, N. Álvarez-Gutiérrez, F. Rubiera and C. Pevida, *Chem. Eng. J.*, 2018, **353**, 197–207.

S45 N. Álvarez-Gutiérrez, M. V. Gil, F. Rubiera and C. Pevida, *Fuel Process. Technol.*, 2016, **142**, 361–369.

S46 N. Álvarez-Gutiérrez, S. García, M. V. Gil, F. Rubiera and C. Pevida, *Energy and Fuels*, 2016, **30**, 5005–5015.

S47 A. D. Wiersum, J. S. Chang, C. Serre and P. L. Llewellyn, *Langmuir*, 2013, **29**, 3301–3309.

S48 X. Song, L. Wang, X. Ma and Y. Zeng, *Appl. Surf. Sci.*, 2017, **396**, 870–878.

S49 N. Singh, S. Dalakoti, A. Sharma, R. Chauhan, R. S. Murali, S. Divekar, S. Dasgupta and Aarti, *Sep. Purif. Technol.*, 2024, **341**, 012072.

S50 S. A. Peter, G. V. Baron, J. Gascon, F. Kapteijn and J. F. M. Denayer, *Adsorption*, 2013, **19**, 1235–1244.

S51 D. Damasceno Borges, P. Normand, A. Permiakova, R. Babarao, N. Heymans, D. S. Galvao, C. Serre, G. De Weireld and G. Maurin, *J. Phys. Chem. C*, 2017, **121**, 26822–26832.

S52 A. D. Wiersum, C. Giovannangeli, D. Vincent, E. Bloch, H. Reinsch, N. Stock, J. S. Lee, J. S. Chang and P. L. Llewellyn, *ACS Comb. Sci.*, 2013, **15**, 111–119.

S53 H. N. Wamba, S. Dalakoti, N. Singh, S. Divekar, J. Ngoune, A. Arya and S. Dasgupta, *Ind. Eng. Chem. Res.*, 2023, **62**, 19773–19783.

S54 M. A. O. Lourenço, C. Siquet, M. Sardo, L. Mafra, J. Pires, M. Jorge, M. L. Pinto, P. Ferreira and J. R. B. Gomes, *J. Phys. Chem.*, 2016, **120**, 3863–3875.

S55 L. Mafra, T. Čendak, S. Schneider, P. V. Wiper, J. Pires, J. R. B. Gomes and M. L. Pinto, *Chem. Eng. J.*, 2018, **336**, 612–621.

S56 Y. Belmabkhout and A. Sayari, *Chem. Eng. Sci.*, 2009, **64**, 3729–3735.

S57 Y. Belmabkhout, R. Serna-Guerrero and A. Sayari, *Chem. Eng. Sci.*, 2009, **64**, 3721–3728.

S58 J. Yang, J. Li, W. Wang, L. Li and J. Li, *Ind. Eng. Chem. Res.*, 2013, **52**, 17856–17864.

S59 S. Cavenati, C. A. Grande and A. E. Rodrigues, *J. Chem. Eng. Data*, 2004, **49**, 1095–1101.

S60 K. G. Wynnyk, B. Hojjati, P. Pirzadeh and R. A. Marriott, *Adsorption*, 2017, **23**, 149–162.

S61 M. Mofarahi and F. Gholipour, *Microporous Mesoporous Mater.*, 2014, **200**, 1–10.

S62 A. Sharma, A. Verma, U. Kumar, N. Singh, S. Dalakoti, R. Chauhan, S. Bhandari, S. Divekar, S. Dasgupta and Aarti, *Microporous Mesoporous Mater.*, 2024, **367**, 112984.

S63 M. Rahmani, B. Mokhtarani, M. Mafi and N. Rahmanian, *Ind. Eng. Chem. Res.*, 2022, **61**, 6600–6610.